Universidade Estadual de Campinas
Instituto de Química

Rafael Pires de Oliveira

Copolímeros de poli[metacrilato de (oligoetileno glicol) metil éter] (POEGMA): agregação em solução aquosa e formação de hidrogéis com celulose nanocristalina

Campinas
2021

RAFAEL PIRES DE OLIVEIRA

COPOLÍMEROS DE POLI[METACRILATO DE (OLIGOETILENO GLICOL) METIL ÉTER] (POEGMA): AGREGAÇÃO EM SOLUÇÃO AQUOSA E FORMAÇÃO DE HIDROGÉIS COM CELULOSE NANOCRISTALINA

Tese de Doutorado apresentada ao Instituto de Química da Universidade Estadual de Campinas como parte dos requisitos exigidos para a obtenção do título de Doutor em Ciências.

Orientador: Prof. Dr. Watson Loh
Coorientador: Prof. Dr. Michael Kam Chiu Tam

O arquivo digital corresponde à versão final da Tese defendida pelo aluno Rafael Pires de Oliveira e orientada pelo Prof. Dr. Watson Loh.

CAMPINAS
2021

Ficha catalográfica
Universidade Estadual de Campinas
Biblioteca do Instituto de Química
Simone Luiz Alves - CRB 8/9094

Pires-Oliveira, Rafael, 1985-
P665c Copolímeros de poli[metacrilato de (oligoetileno glicol) metil éter] (POEGMA) : agregação em solução aquosa e formação de hidrogeis com celulose nanocristalina / Rafael Pires-Oliveira. – Campinas, SP : [s.n.], 2021.

Orientador: Watson Loh.
Coorientador: Michael Kam Chiu Tam.
Tese (doutorado) – Universidade Estadual de Campinas, Instituto de Química.

1. Colóides. 2. ATRP. 3. Nanomateriais. I. Loh, Watson, 1965-. II. Tam, Michael Kam Chiu. III. Universidade Estadual de Campinas. Instituto de Química. IV. Título.

Informações para Biblioteca Digital

Título em outro idioma: Poly(oligo(ethylene glycol) methyl ether methacrylate) (POEGMA) copolymers : aggregation in aqueous solution and hydrogel formation with celulose nanocrystals
Palavras-chave em inglês:
Colloids
ATRP
Nanomaterials
Área de concentração: Físico-Química
Titulação: Doutor em Ciências
Banca examinadora:
Watson Loh [Orientador]
Maria Isabel Felisberti
Juliana da Silva Bernardes
Edvani Curti Muniz
Nádya Pesce da Silveira
Data de defesa: 26-11-2021
Programa de Pós-Graduação: Química

Identificação e informações acadêmicas do(a) aluno(a)
- ORCID do autor: https://orcid.org/0000-0003-1855-5322
- Currículo Lattes do autor: http://lattes.cnpq.br/8345333120198170

Banca Examinadora

Prof. Dr. Watson Loh (Orientador)

Profa. Dra. Maria Isabel Felisberti (UNICAMP)

Dra. Juliana da Silva Bernardes (LNNano/CNPEM)

Prof. Dr. Edvani Curti Muniz (UFPI)

Profa. Dra. Nádya Pesce da Silveira (UFRGS)

A Ata da defesa assinada pelos membros da Comissão Examinadora consta no SIGA/Sistema de Fluxo de Dissertação/Tese e na Secretaria do Programa da Unidade.

Este exemplar corresponde à redação final da Tese de Doutorado defendida pelo aluno Rafael Pires de Oliveira, aprovada pela Comissão Julgadora em 26 de novembro de 2021.

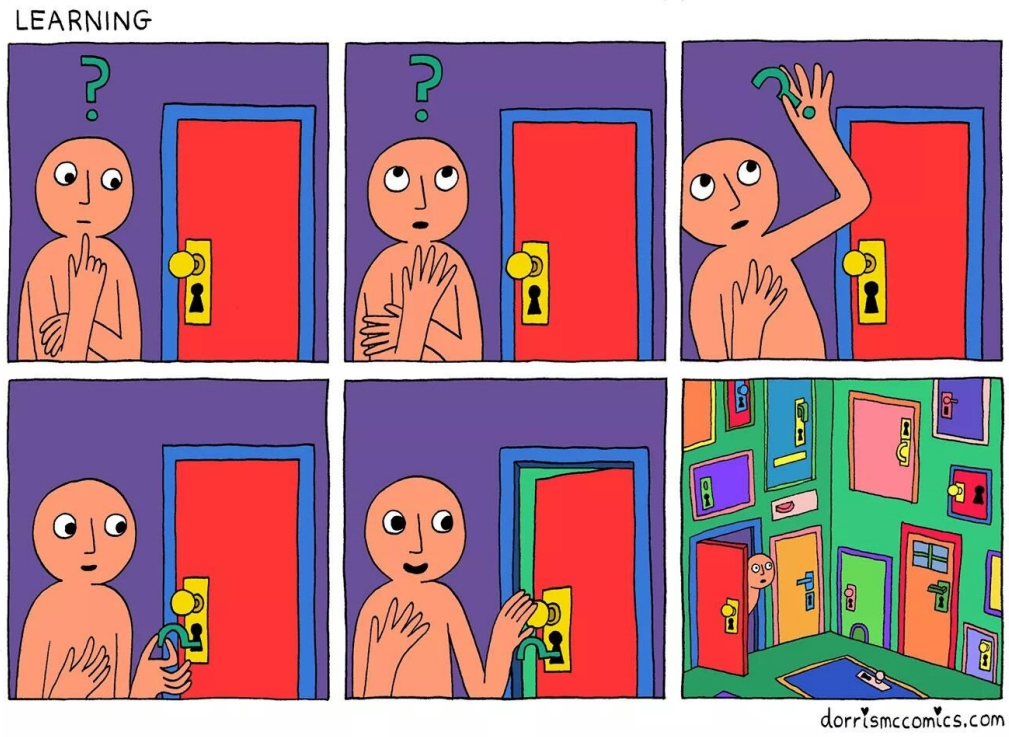

“The problem with the world is
that the intelligent people are full of doubts,
while the stupid ones are full of confidence.”
— Charles Bukowski

Dedico...

Aos meus avós Ariovaldo, Cida (in memoriam) e Henriqueta que sempre se orgulhavam previamente de ter um neto Doutor.

À minha sobrinha entusiasta da natureza e ciência das coisas, Beatriz; e ao meu recém-chegado sobrinho Guilherme, que tem uma vida e um mundo todo a explorar e conhecer!

Agradecimentos

Primeiramente, agradeço ao Professor Watson Loh pelo aceite de orientação, após o falecimento da Profa. Inés Joekes, a qual era a minha orientadora inicial. Agradeço as inúmeras oportunidades, ensinamentos e insistências para que este trabalho fosse concluído.

Agradeço aos meus pais pelo incentivo, paciência e carinho em toda a jornada. Ao Patrick pela companhia, compreensão e apoio ao longo desta jornada de noites viradas. Aos meus irmãos pela ajuda e suporte sempre que necessários.

I am very thankful to Prof. Michael Tam for the formal orientation and welcoming me in his lab at University of Waterloo. I am especially grateful to Prof. Emily Cranston who also welcomed me in her research group at the McMaster University.

Aos Professores Edvaldo Sabadini e Marcelo Ganzarolli e aos colegas de laboratório Lab B-145 pela sempre agradável companhia, mesmo com os problemas de lab: Ana Maria, Bruno, Caio, Caroline, Cesar, Fernandinha, Flávia, Guilherme, Ito, Juliana Sá, Lia, Lívia, Manazael, Marta, Mathilde, Monique, Nathalia, Oigres, Parinaz, Dra. Patricia, Piva, Renato, Rogerio, Scheila e Victor.

My colleagues at Prof. Tam's lab, in particular: Juntao, Yang Song, Nishil, Nate, Patrick, Kiyoshi, and Juliana (again).

Alguns colegas viraram amigos e inspiração, discutindo o sentido da vida, ciência, o meu projeto, os projetos deles, política ou uma receita culinária que fosse, mas sempre de maneira inspiradora. A eles tenho uma enorme gratidão: Juntao Tang, Victor Baldim, Rafael Kashima, Scheila Alves, Juliana Sá e Oigres Bernadinelli.

Ao Luis, que participou de parte deste período com curiosidade, apoio e companhia.

À professora Maria Isabel Felisberti pelas ricas discussões de resultados, disponibilizar um espaço no laboratório, reagentes e todo o apoio dado.

Ao professor Cesar L. Petzhold por me ensinar técnicas de polimerização e caracterização e dividir a bancada do laboratório comigo, mesmo aos finais de semana.

À Claudia Martelli, responsável pelo laboratório de UV-vis, pela liberdade dada para trabalhar em seu lab, e pela disposição contínua em ajudar e alegria contagiante.

Aos professores e funcionários do IQ pelos ensinamentos, orientações indiretas e todo o suporte e apoio prestado todos esses anos.

Aos amigos e colegas que ajudaram realizando, discutindo os resultados e ajudando a entender melhor os sistemas, em especial, à Lia Beraldo pelos ajustes nas curvas de SAXS, à

Carol Ezequiel com os resultados de XPS, ao Renato Nunes pelas medidas de reologia, e ao Juntao Tang pelas imagens de AFM e TEM realizadas no Canadá.

À doutoranda Júlia B. Sabadini pelo espírito colaborativo realizando as recentes preciosas medidas de DLS e DSC, uma vez que eu não tenho disponibilidade para acessar os laboratórios.

À Bianca Andrade de Campos pelo contínuo estímulo e por compartilhar o conhecimento em relação à importante pesquisa e avaliação de propriedade intelectual.

Agradeço ao CNPEM pelo uso das instalações e ajuda dos excelentes profissionais, contribuindo para as medidas de SAXS, MEV, XPS e microtomografia de raios-X (microCT).

À Bruna Mendonça e ao André Conde, ambos entusiastas do meu estudo e meus líderes enquanto eu trabalhava para a Oxiteno, pelo apoio e grande incentivo para concluir este trabalho.

À CelluForce por gentilmente fornecer as amostras de celulose nanocristalina. À Fapesp projeto temático 2015/25406-5 pelo financiamento ao laboratório e ao projeto.

"O presente trabalho foi realizado com apoio do Conselho Nacional de Desenvolvimento Científico e Tecnológico (CNPq) – Código de Financiamento 159080/2013-4".

"O presente trabalho foi realizado com apoio da Coordenação de Aperfeiçoamento de Pessoal de Nível Superior - Brasil (CAPES) – Código de Financiamento 001".

"O presente trabalho foi realizado com apoio da Coordenação de Aperfeiçoamento de Pessoal de Nível Superior - Brasil (CAPES) – Projeto A128/2013".

Muito obrigado !

Resumo

Polímeros são amplamente utilizados em diversos setores do mercado em variadas aplicações e o conhecimento de suas propriedades permite a geração de materiais funcionais mais otimizados. O POEGMA, poli[metacrilato de (oligoetileno glicol) metil éter], é um copolímero randômico do tipo *graft* que é biocompatível e apresenta transição de fase em uma temperatura crítica inferior, podendo formar micelas ou agregados macroscópicos. Esta propriedade é dependente de sua arquitetura molecular, constituída por um esqueleto hidrofóbico e cadeias laterais hidrofílicas de óxido de etileno (EO). Neste trabalho, copolímeros POEGMA foram sintetizados utilizando-se polimerização radicalar por desativação reversível variando-se o comprimento e a quantidade da cadeia lateral enxertada no esqueleto. Os copolímeros foram caracterizados por cromatografia de permeação em gel (GPC) e ressonância magnética nuclear (RMN) e o seu comportamento em solução aquosa em função da temperatura foi avaliado pelas técnicas espalhamento de luz dinâmico (DLS), turbidimetria, microcalorimetria de varredura (HSDSC), espalhamento de raios-X a baixo ângulo (SAXS) e espectrofotometria no UV-vis. A quantidade de grupos EO presentes no copolímero afeta a temperatura de transição de fases, enquanto o comprimento das cadeias laterais induz às diferentes estruturas formadas acima da temperatura crítica.

A celulose nanocristalina (CNC) é um material composto por partículas de dimensão nanométrica obtidas de plantas ou microorganismos e com potencial para reduzir a quantidade de produtos derivados do petróleo. O enxerto de copolímeros POEGMA na sua superfície possibilita a formação reversível de hidrogéis responsivos à temperatura e/ou à presença de íons. Neste estudo, foram preparados materiais de CNC enxertado com POEGMA de diferentes composições através de uma reação em meio aquoso e em temperatura ambiente. Os produtos obtidos foram caracterizados por microscopia eletrônica de transmissão e de força atômica (AFM), espectroscopia no infravermelho com transformada de Fourier (FT-IR), análise termogravimétrica (TGA), espectroscopia de fotoelétrons excitados por raios-X (XPS), e HSDSC. O comportamento térmico e a formação de hidrogéis foram determinados por turbidimetria, reologia, análise termomecânica e microtomografia de raios-X. Apesar da comprovação de enxerto do copolímero na superfície da CNC, a sua quantificação não foi possível pelas metodologias habituais, e os resultados de microcalorimetria abriram uma nova possibilidade para estimar a quantidade de copolímero POEGMA enxertado na superfície das nanopartículas. A adição de eletrólitos e/ou o aumento da temperatura induz de forma reversível

a formação de hidrogel. Além disso, a CNC melhora as propriedades mecânicas do hidrogel e diminui a quantidade necessária de polímero para formar gel.

Outra maneira de formação de hidrogéis foi inicialmente explorada através da reticulação supramolecular por meio da inclusão da cadeia de oligoetileno glicol no macrociclo da α-ciclodextrina. Este tipo de reticulação física é também reversível e pode ser refeita após rompida, caracterizando um material auto-curável, excelente para aplicações biomédicas. A formação dos complexos de inclusão foi inicialmente determinada por titulação calorimétrica isotérmica (ITC) e DLS e foi posteriormente estudada no grupo de pesquisa por técnicas complementares. O entendimento individual e em conjunto destes sistemas permitiu a elaboração de sistemas poliméricos funcionais otimizados, beneficiando aplicações em diversas áreas da ciência e possibilitando aumentar a eficiência e racionalização no uso dos materiais poliméricos.

Abstract

Polymers are widely used in several industrial sectors in a variety of applications and building knowledge of their properties allows the generation of more advanced functional materials. POEGMA, poly[(ethylene glycol) methyl ether methacrylate], is a biocompatible random graft copolymer that displays a phase transition at a lower critical temperature, forming micelles or macroscopic aggregates. This feature is dependent of its molecular architecture, consisting of a hydrophobic backbone and hydrophilic ethylene oxide (EO) side chains. In this study, POEGMA copolymers were synthesized using reversible-deactivation radical polymerization varying the length and content of the side chain grafted to the backbone. The copolymers were characterized by gel permeation chromatography (GPC) and nuclear magnetic resonance (NMR), and their aqueous behavior as a function of temperature was assessed by dynamic light scattering (DLS), turbidimetry, high sensitivity differential scanning calorimetry (HSDSC), small-angle X-ray scattering (SAXS) and UV-vis spectrophotometry. The amount of EO groups present in the copolymer affects the phase transition temperature, while the length of the side chains induces the formation of different structures above the critical temperature.

Nanocrystalline cellulose (CNC) is a material comprising particles of nanometric-size obtained from plants or microorganisms with the potential to reduce the number of petroleum-derived products. Grafting POEGMA copolymers onto CNC surface enables the reversible formation of hydrogels responsive to temperature and/or to the presence of ions. In this study, CNC grafted with POEGMA of different compositions were generated through a reaction in an aqueous medium and at room temperature. The products were characterized by transmission electron microscopy and atomic force microscopy (AFM), Fourier-transform infrared spectroscopy (FT-IR), thermogravimetric analysis (TGA), X-ray photoelectron spectroscopy (XPS), and high sensitivity differential scanning calorimetry (HSDSC). The thermal behavior and hydrogel formation were characterized by turbidimetry, rheology, thermomechanical analysis, and X-ray microtomography. Although copolymer grafting onto the CNC surface was proved, its quantification was not possible by the usual methodologies, and the microcalorimetry results opened a new possibility to estimate the amount of POEGMA grafted onto the surface of nanoparticles. The addition of electrolytes and/or the increase in temperature reversibly induces hydrogel formation. In addition, CNC improves the mechanical properties of the hydrogel and reduces the amount of polymer needed to form a gel.

Another method of forming hydrogels was initially explored through supramolecular crosslinking by the inclusion of an oligoethylene glycol chain into the α-cyclodextrin macrocycle. This type of physical crosslinking is also reversible and can be redone after breaking, featuring a self-healing material, excellent for biomedical applications. The formation of inclusion complexes was initially determined by isothermal calorimetric titration (ITC) and DLS, and it was later studied in the research group using complementary techniques. The individual and holistic understanding of these systems unlocks the elaboration of advanced functional polymeric systems, benefiting applications in several areas of science and making it possible to increase efficiency, rationalization in the use of polymeric materials.

Lista de Figuras

Lista de Tabelas

Sumário

1. Introdução geral

1.1. Estruturação da Tese

Os resultados deste trabalho serão apresentados em três tópicos: (a) caracterização das propriedades térmicas em solução aquosa dos copolímeros da família POEGMA, (b) caracterização do POEGMA enxertado sobre a CNC, e (c) investigação da formação de hidrogel físico.

1.2. Conceitos gerais

Polímeros

Polímeros são macromoléculas constituídas por unidades químicas repetidas ligadas covalentemente, denominadas monômeros. Polímeros podem ter sua origem natural ou sintética – amido, celulose, látex, lã, e proteínas são exemplos de polímeros naturais, enquanto que polietileno (PE), polipropileno (PP), poliestireno (PS), policarbonato (PC), poli(etileno tereftalato) (PET) e Nylon são alguns exemplos de polímeros sintéticos mais conhecidos e que são processados para formar plásticos[1] [1, 2]. Polímeros, naturais ou sintéticos, são amplamente utilizados na indústria e estão presentes no cotidiano de todas as pessoas em qualquer lugar do mundo. Os primeiros entendimentos e desenvolvimentos de polímeros, realizados pelo químico alemão Hermann Staudinger, levou-o a ser laureado com o Prêmio Nobel de Química em 1953 por suas descobertas no campo da química macromolecular [3] e continuam até os dias de hoje um campo relevante de desenvolvimentos constante nos meios acadêmico e industrial, como comprovado por uma pesquisa de artigos científicos e patentes.

Esta pesquisa foi realizada utilizando-se o termo "*Polymer*", buscando-se por referências na plataforma SciFinder^n (*American Chemical Society*) [4], obtendo-se mais de 2,7 milhões de resultados de artigos científicos. Através da plataforma de busca e análises de propriedade intelectual PatSnap *IP intelligence platform* [5] foi pesquisado o mesmo termo "polymer" nos campos de título, resumo e quadro reivindicatório (termo original e traduzidos automaticamente) em 116 bases de dados, resultando em aproximadamente 1,5 milhões de famílias de patentes desde 1922 até os dias atuais e cerca de um milhão de famílias de patentes

[1] Os termos "polímeros" e "plásticos" são frequentemente utilizados erroneamente como sinônimos; plásticos são materiais formados após o processamento dos polímeros [1].

publicadas apenas nos últimos 20 anos. Famílias de patentes consideram apenas um documento representativo relacionado à mesma única invenção que foi depositada em mais de um território, evitando assim a multiplicidade equivocada na contagem de uma única invenção. A Figura 1 mostra a quantidade crescente de publicações anuais relacionados ao desenvolvimento de polímeros, notando-se um aumento ainda mais pronunciado nos artigos científicos. Em geral, artigos científicos são relacionados aos desenvolvimentos iniciais da tecnologia, associados à pesquisa acadêmica, ao passo que as patentes demonstram um grau mais avançado do desenvolvimento da tecnologia, com uma aplicação prática comprovada e são associadas majoritariamente às indústrias.

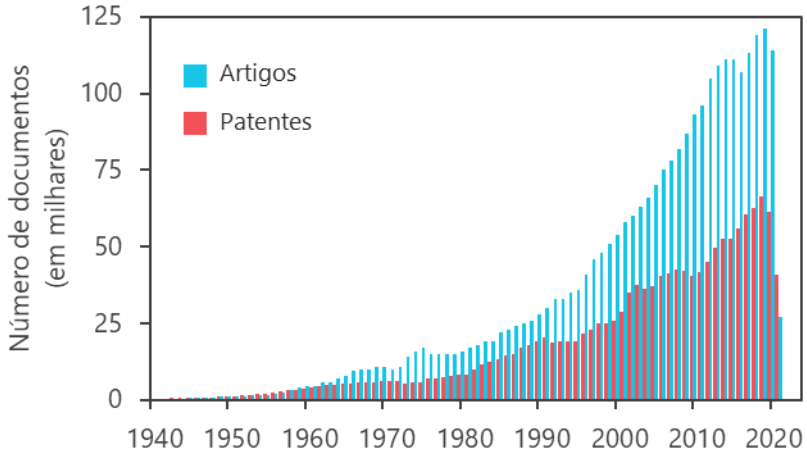

Figura 1: Número de artigos científicos e patentes publicados ao longo dos anos referente ao tema de polímeros.

A tecnologia de polímeros apresenta patentes depositadas em todos os continentes (Figura 2-A) e, curiosamente, é um dos raros casos em que o número de documentos depositados na China não é o maior da lista, sendo neste caso os Estados Unidos o território líder. A análise de territórios em que as patentes são depositadas mostra quais os mercados mais potenciais para aquela tecnologia. Dentre os titulares majoritários dos últimos 20 anos (Figura 2-B) estão grandes e conhecidas empresas de diferentes setores, desde a Fujifilm, que atua principalmente no setor de fotografia, ótica, e dispositivos médico-eletrônicos, até empresas cosméticas, como a L'Oréal e a Procter & Gamble (P&G), além das empresas que atuam na área de materiais e insumos químicos, como a BASF, LG Chemicals, 3M, Toray, Sumitomo Chemical, Dow Chemical e a petroquímica Sinopec.

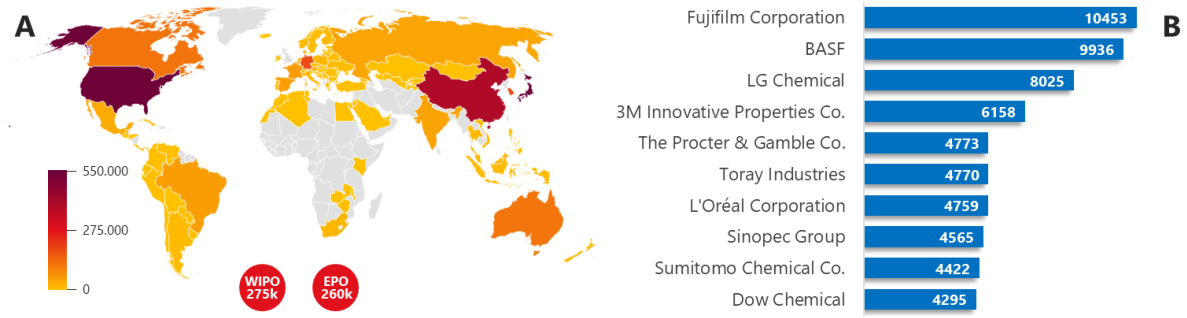

Figura 2: Patentes relacionadas ao tema de polímeros: (A) distribuição de depósitos ao redor do mundo indicando principais mercados-alvo e (B) principais titulares das patentes depositadas nos últimos 20 anos.

A partir da análise de categoria de Classificação Internacional de Patentes (IPC) [6] das patentes obtidas na busca, pode-se identificar a tecnologia central da invenção. Na Figura 3 vê-se que os polímeros são utilizados em diversas aplicações, por exemplo em fibras têxteis, formulações cosméticas e farmacêuticas, tintas e adesivos, materiais para baterias, materiais óticos e, obviamente, plásticos. Combinando as duas análises podemos avaliar qual a principal tecnologia desenvolvida por cada empresa titular das patentes.

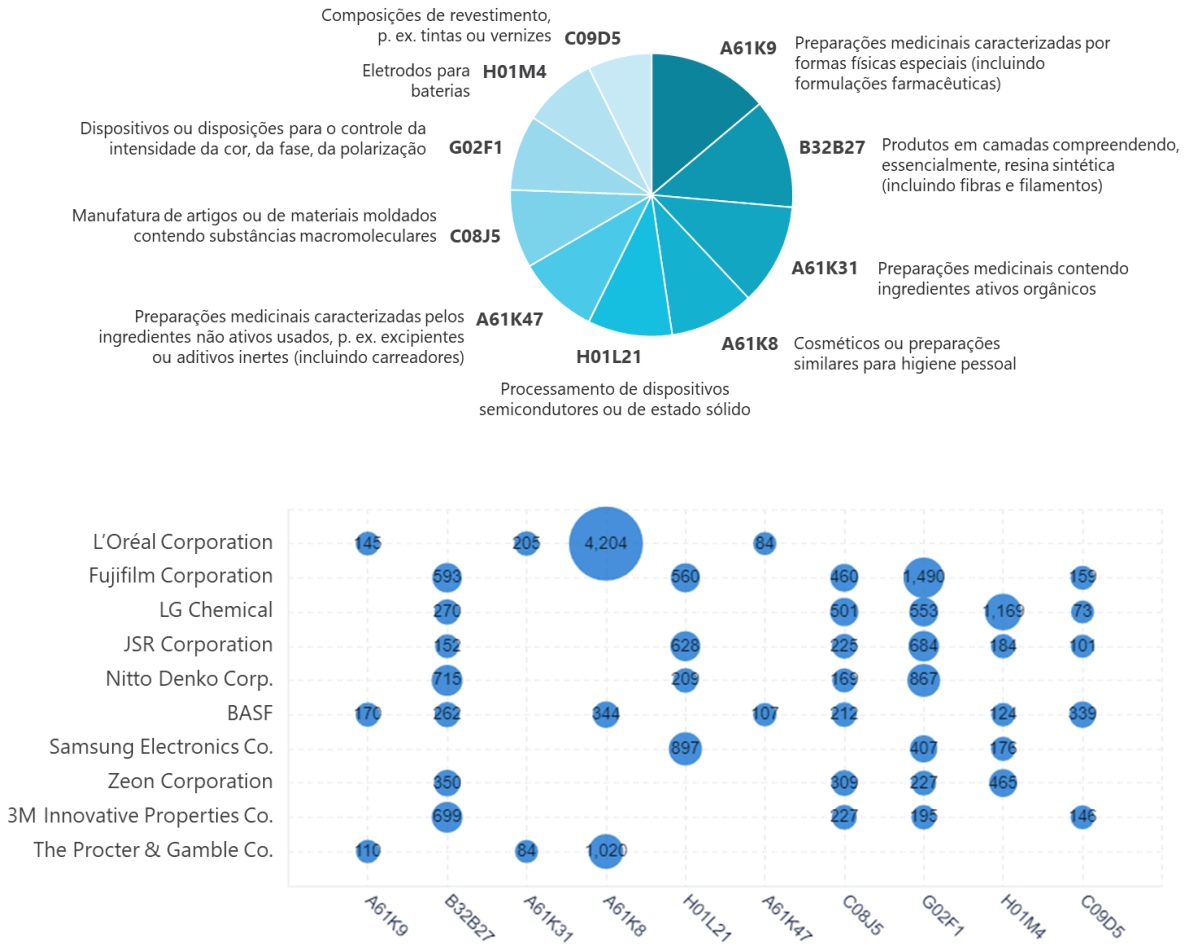

Figura 3: Principais categorias de Classificação Internacional de Patentes (IPC) presentes nas patentes de polímeros depositadas nos últimos 20 anos mostrando quais são as principais tecnologias associadas (acima) e quais são as principais tecnologias patenteadas pelos maiores titulares (abaixo). Para identificação detalhada de cada categoria, verifique a referência [6]. Gráficos gerados pela plataforma PatSnap [5].

Através de análises de inteligência artificial (disponível na plataforma PatSnap) pelos termos e frases encontrados nos documentos de patente, pode-se obter a denominada roda de inovação (Figura 4), que identifica e detalha como a tecnologia central da busca (polímeros, neste caso) se relaciona com as tecnologias de aplicação (segundo e mais externo nível da roda da inovação). Vê-se, por exemplo, que os polímeros podem ser utilizados na forma de resinas como matriz, compósitos ou em solução, podem ser utilizados em composições cosméticas como agentes adesivos ou de recobrimento (que pode estar associado à tecnologia de encapsulamento), podem ser utilizados em sistemas de baterias de lítio, em sistemas eletrônicos de telas e de dispositivos de imagem, entre outros. Esta análise é útil ainda para, quando necessário, enriquecer e afunilar a busca por mais aplicações específicas de uma determinada tecnologia.

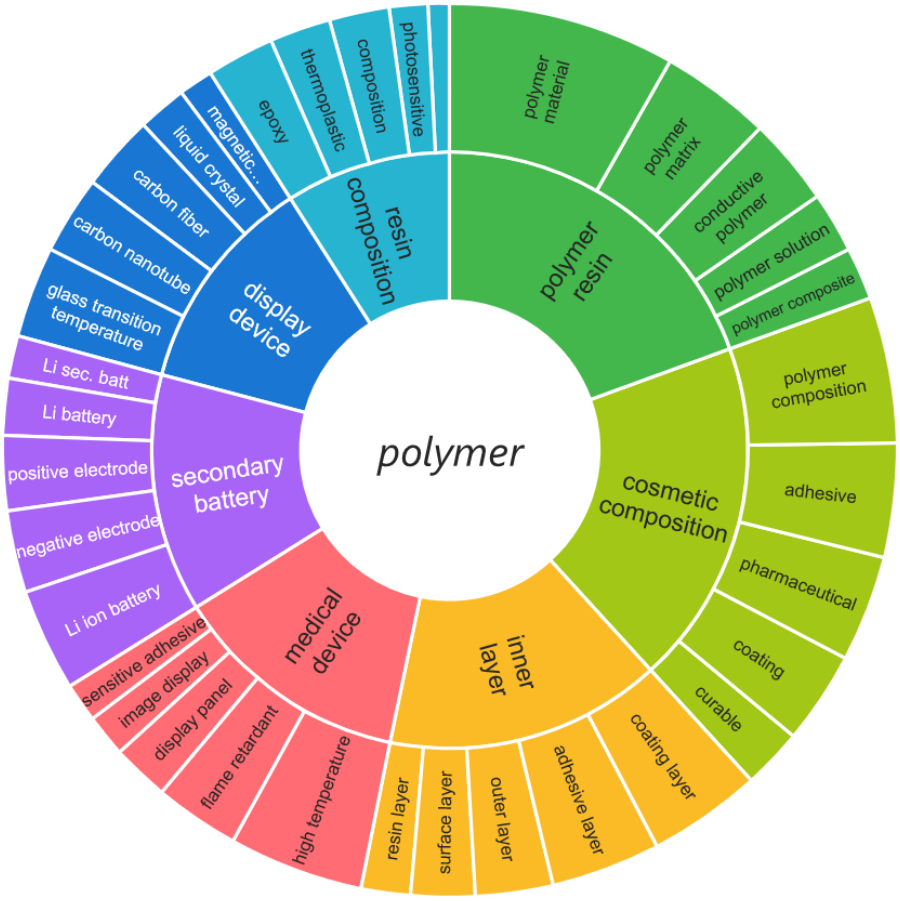

Figura 4: Roda da inovação mostrando um detalhamento das tecnologias e aplicações relacionadas a palavra central da busca "*polymer*". Gráfico gerado pela plataforma PatSnap [5].

Apesar da sua indiscutível utilidade e aplicabilidade, têm-se discutido recentemente os efeitos deletérios do uso demasiado dos polímeros, em especial do plástico. Plásticos ou fragmentos de plásticos gerados pela degradação causada pelo tempo e intempéries com menos de 5 mm são denominados como microplásticos e são classificados como poluentes por não serem biodegradáveis, apresentarem elevada toxicidade e se acumularem no ambiente [7–9]. Os microplásticos têm sido encontrado em ambientes aquáticos e marinhos [10, 11], que alimentam todo o ecossistema do planeta, foram recentemente identificados em placenta humana [12], e por estas razões têm chamado a atenção devido ao potencial efeito danoso que pode apresentar, levantando a preocupação da comunidade científica, sociedade civil e agências regulatórias [13]. Desta forma, faz-se mais que necessário o entendimento ainda mais aprofundado dos polímeros, suas propriedades e aperfeiçoamento da sua manipulação para obter o máximo de benefício da sua aplicação sem comprometer o ambiente e a segurança dos organismos vivos.

Polímeros constituídos por dois ou mais tipos de monômeros são denominados copolímeros e, de acordo com a sua arquitetura molecular, os copolímeros podem ser classificados em aleatório, gradiente, em bloco ou enxertado, conforme ilustrado na Figura 5. Conforme as propriedades dos monômeros, tamanho e distribuição das cadeias e a arquitetura do polímero, as suas propriedades físico-químicas são afetadas. Copolímeros constituídos por grupos polares e apolares podem apresentar caráter anfifílico e se auto-organizar em solução aquosa como os surfactantes. Este comportamento é mais pronunciado em copolímeros em bloco e os mais estudados são os copolímeros em bloco de poli(óxido de etileno-*co*-óxido de propileno) (EO/PO), comumente conhecidos como Poloxamer ou Pluronic®.

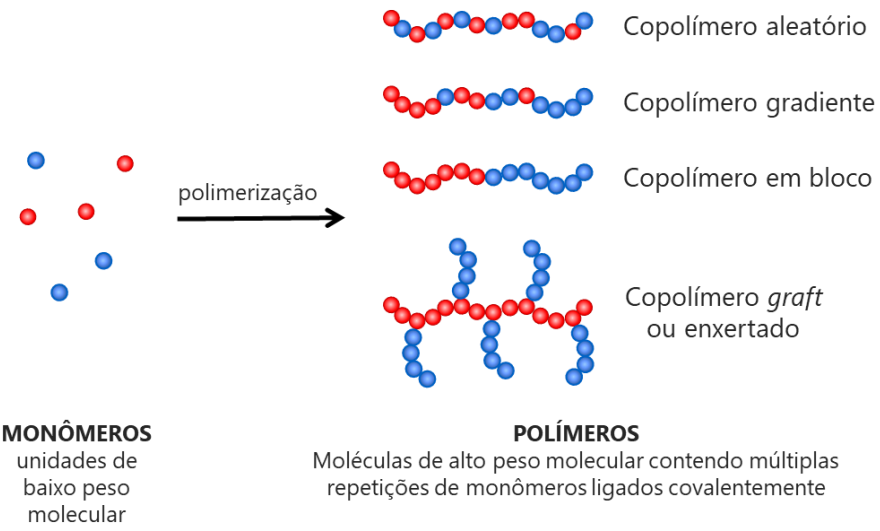

Figura 5: Representação da definição de monômeros e polímeros, e arquiteturas poliméricas mais relevantes para este estudo.

Recentemente, diversas metodologias de polimerização radicalar por desativação reversível (RDRP, do inglês *reversible-deactivation radical polymerization*)[2] [14] foram desenvolvidas possibilitando um maior controle na arquitetura do polímero, tais como as técnicas de polimerização radicalar por transferência de átomo (ATRP, do inglês *atom-transfer radical polymerization*), polimerização mediada por nitróxidos (NMP, do inglês *nitroxide-mediated polymerization*), e transferência reversível de cadeia por adição-fragmentação (RAFT, do inglês *reversible addition-fragmentation chain-transfer*). Estes polímeros com arquitetura controlada, sintetizados pelos mecanismos de reação representados na Figura 6, possuem funcionalidades especiais e são utilizados, inclusive em escala industrial [15, 16],

[2] Estas metodologias também são conhecidas como "polimerização radicalar controlada" ou "polimerização radicalar viva", termos desaconselhados pela IUPAC [14].

desde a aplicação em encapsulamento e liberação controlada [17, 18], dispersantes poliméricos de alta performance [19–21], como até aplicações ainda mais nobres como polímeros capazes de transferir uma informação específica como um "DNA sintético" [22].

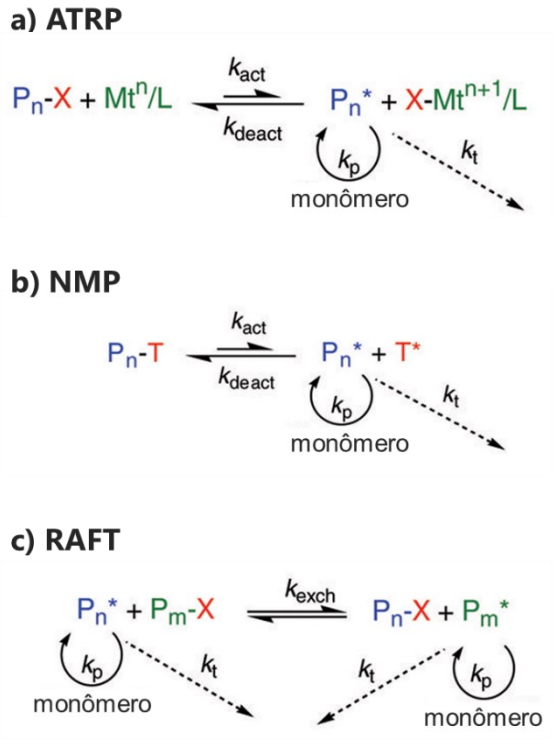

Figura 6: Esquema demonstrando o mecanismo das três principais técnicas de polimerização radicalar por desativação reversível (RDRP). Adaptado da referência [23]. © 2005 Elsevier.

Recentemente, muitos trabalhos têm sido publicados na literatura sobre polímeros que apresentam funcionalidade adicional respondendo a um estímulo do meio, como temperatura, força iônica, pH, radiação eletromagnética (luz), entre outros fatores. A resposta a estes estímulos é consequência da alteração das microestruturas da cadeia polimérica, modificando as suas propriedades físico-químicas. Polímeros termossensíveis ou termorresponsivos contêm grupos, tais como o óxido de etileno (EO) entre outros, que alteram a sua conformação e podem passar por separação de fase a uma temperatura crítica, como por exemplo a LCST[3] [24]. O grupo EO é também utilizado para aumentar a solubilidade de polímeros em água, possibilitando sua aplicação como dispersantes [25], por exemplo.

[3] Do inglês, *lower critical solution temperature* (LCST): é a menor temperatura de solubilidade de um polímero em um solvente. Abaixo desta temperatura o polímero é solúvel e o sistema monofásico. Acima desta temperatura o polímero altera o seu enovelamento e, portanto, a sua conformação e estruturação, tornando-se imiscível com o solvente e separando de fase, resultando um sistema bifásico.

Hidrogéis

Hidrogéis são definidos como "uma rede polimérica[4] não-fluida que é expandida ao longo de todo o seu volume por água" [26], absorvendo para isso uma elevada quantidade de água, dependendo da sua composição. Como a definição utiliza o termo volume, são consideradas para os hidrogéis as redes poliméricas tridimensionais. A reticulação do hidrogel pode ser química ou física. No hidrogel químico, os pontos de reticulação são formados por ligações químicas covalentes. Quando os pontos de reticulação são formados por outras interações, tais como, por exemplo, interações hidrofóbicas, emaranhamentos de cadeias poliméricas e ligações de hidrogênio, o material é denominado hidrogel físico. Em geral, os hidrogéis físicos apresentam como vantagens quando comparado ao químico: menor toxicidade, maior simplicidade, reversibilidade da reticulação e, portanto, um maior número de aplicações em geral. Hidrogéis encontram inúmeras aplicações na engenharia, na agricultura, na biotecnologia, nas indústrias farmacêutica, de alimentos, de cosméticos, dentre outras [27–34]. Hidrogéis termorresponsivos apresentam alterações de volume quando expostos a variações de temperatura em consequência de mudanças abruptas no coeficiente de intumescimento ou de transições sol-gel [35]. Este tipo de hidrogel pode ser aplicado, por exemplo, na liberação sustentada de fármacos [36, 37].

Celulose nanocristalina (CNC)

A celulose nanocristalina (CNC) é uma nanopartícula sustentável e biocompatível, derivada de plantas ou bactérias [38–41] (Figura 7) que pode ser utilizada em hidrogéis como agente de reforço, modificar suas propriedades, além de diminuir o teor de polímero necessário para formar o gel [42–44]. Em formato de bastão, a CNC apresenta-se com diâmetro em torno de 5–20 nm e comprimento de 100–200 nm, com uma grande área superficial [45]. O método de obtenção da CNC mais estudado e utilizado é através da extração por ácido sulfúrico, hidrolisando e esterificando a celulose (Figura 8), após o processo mecânico [46], resultando em nanopartículas de celulose cristalina contendo em superfície muitos grupos hidroxila e sulfato que são suscetíveis a modificações químicas, incluindo enxerto de polímeros específicos, o que melhora as suas propriedades e define diversas aplicações [47, 48]. A CNC pode ser aplicada a uma ampla gama de tecnologias, por exemplo, como liberação de ativos

[4] A IUPAC faz distinção e recomenda a utilização do termo "aquagel" para um hidrogel que é formado por uma rede coloidal ao invés de uma rede polimérica) [26].

[49], engenharia de tecidos [50–52], modificadores reológicos [53] e materiais funcionais [54–60].

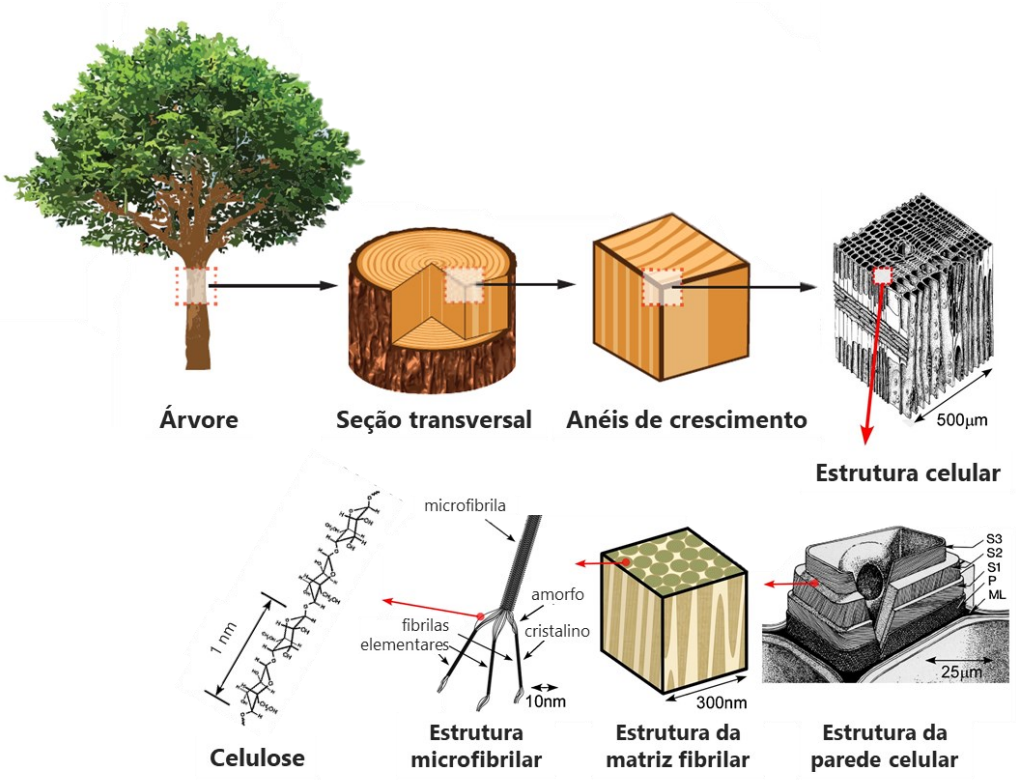

Figura 7: Esquema ilustrando a origem da celulose na célula vegetal. Adaptado das referências [40, 41]. © 2013 Elsevier. © 2021 American Chemical Society.

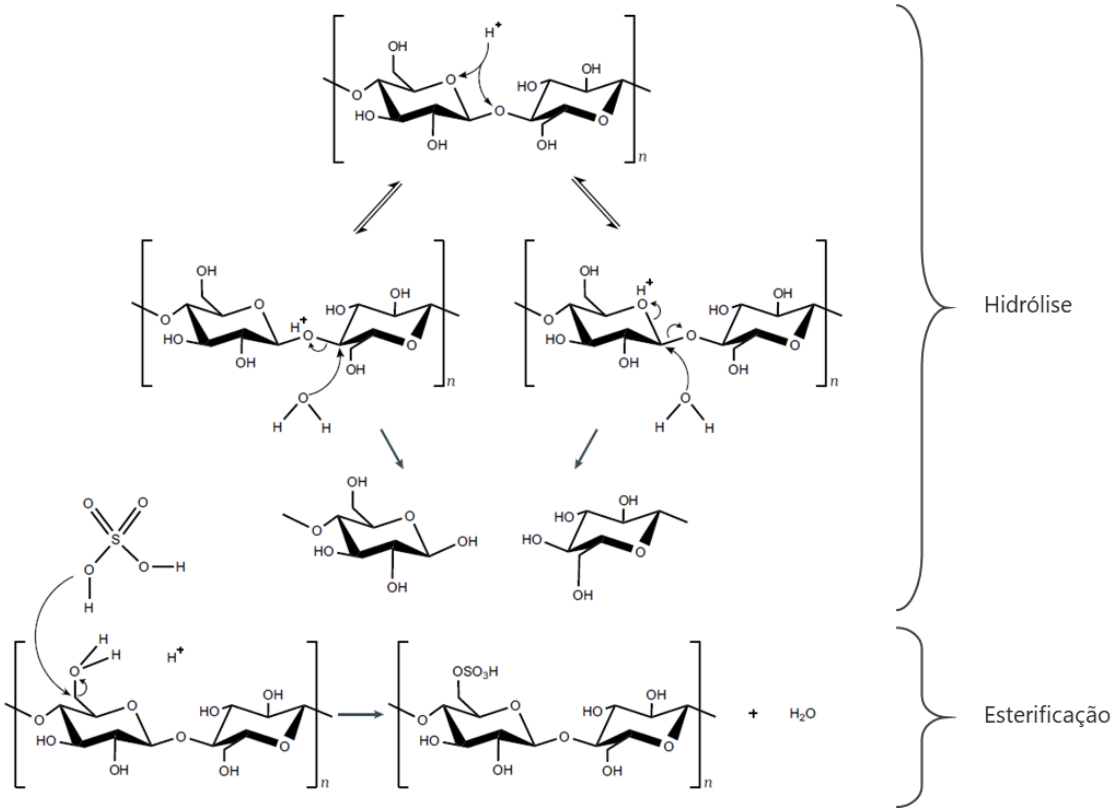

Figura 8: Mecanismo de hidrólise da celulose para obtenção da CNC. Adaptado da referência [46]. © 2020 Springer Nature.

Reticulação supramolecular

Hidrogéis com capacidade "*self-healing*"[5] são aqueles que conseguem reestruturar a sua rede após o seu rompimento através da regeneração das ligações de reticulação das cadeias poliméricas. As reticulações formadas por interações supramoleculares são reversíveis e assim apresentam esta propriedade. A grande vantagem desta abordagem se dá em aplicações em que o material pode sofrer rompimento sem que seja possível a sua substituição, como é o caso da engenharia biomédica de tecidos (cartilagem e pele artificiais), biomateriais para terapias médicas com liberação controlada de fármacos, cicatrização de feridas, entre outras [61–64]. A química supramolecular envolve o arranjo de sistemas complexos de moléculas unidos por múltiplas forças intermoleculares mais fracas que as ligações covalentes e que são, desta forma, reversíveis; por exemplo, as interações eletrostáticas, ligação de hidrogênio, coordenação de íon metálico, forças hidrofóbicas, forças de van der Waals, interações π-π, interações hospedeiro-hóspede, entre outras. Esta abordagem possibilita o desenvolvimento de sistemas formando complexos de inclusão (Figura 9) simples, como exemplo por ciclodextrina

[5] *Self-healing*, do inglês: auto-curável.

(hospedeiro) e cadeias de poli(etileno glicol) (PEG) (hóspede) [65], até complexos de inclusão mais avançados, como os rotaxanos (e pseudorotaxanos), que levaram ao desenvolvimento de maquinas moleculares e que foram, inclusive, objeto do Prêmio Nobel de Química de 2016 aos cientistas Jean-Pierre Sauvage, Sir J. Fraser Stoddart e Bernard L. Feringa [66].

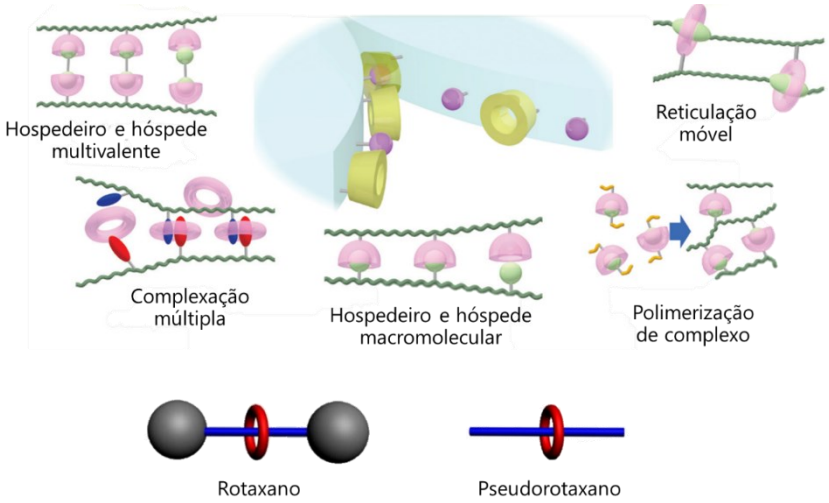

Figura 9: Representação de complexos de inclusão hospedeiro-hóspede. Adaptado das referências [67, 68] © 2015 American Chemical Society, © 2020 Royal Society of Chemistry.

2. Objetivos

O objetivo geral desta Tese é investigar o efeito da arquitetura molecular nos agregados formados em água por copolímeros da família POEGMA acima da temperatura crítica e sintetizar copolímeros desta família na superfície da celulose nanocristalina (POEGMA-*g*-CNC) para produzir hidrogéis físicos responsivos.

Para atingir este objetivo, foram usadas as seguintes estratégias:

- Síntese dos copolímeros da família POEGMA por metodologias de polimerização radicalar por desativação reversível (RDRP).
- Caracterização dos agregados formados acima da temperatura crítica, correlacionando as suas propriedades com a estrutura molecular.
- Síntese e caracterização de copolímeros POEGMA enxertados na superfície da CNC (POEGMA-*g*-CNC).
- Obter hidrogéis físicos a partir do material POEGMA-*g*-CNC sintetizado.

3. Comportamento dos copolímeros de POEGMA em solução aquosa

Estudos anteriores com polímeros responsivos a temperatura demonstraram os benefícios dos copolímeros da família poli[metacrilato de (oligoetileno glicol) metil éter] (POEGMA) frente ao amplamente conhecido e estudado poli(*N*-isopropil acrilamida) (PNIPAM). A família de copolímeros POEGMA, biocompatível e mais seguros que o PNIPAM, apresenta temperatura de transição de fase variável de acordo com a composição de grupos de óxido de etileno (EO) em sua cadeia, conforme ilustrado na Figura 10. O POEGMA é solúvel em água abaixo da sua LCST e exibe uma transição da estrutura *random coil* para globular na LCST com separação de fases. Esta transição é devida à desidratação dos grupos EO, que colapsa para o *backbone* hidrofóbico de metacrilato de metila [69], conforme ilustrado na Figura 11.

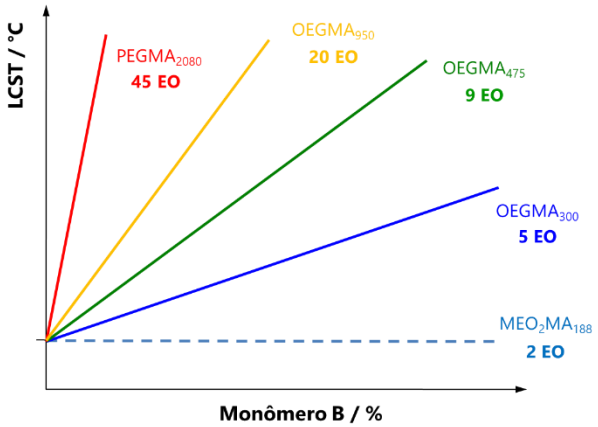

Figura 10: Variação da temperatura de transição de fase (LCST) em função da composição monomérica dos copolímeros POEGMA (P(EO_2MA-*co*-EO_xMA)), onde o monômero B corresponde ao composto indicado com massa molecular e número de grupos EO descritos. Os valores do eixo Y variam entre a temperatura crítica (LCST) do homopolímero P(MEO_2MA) até a ebulição da água.

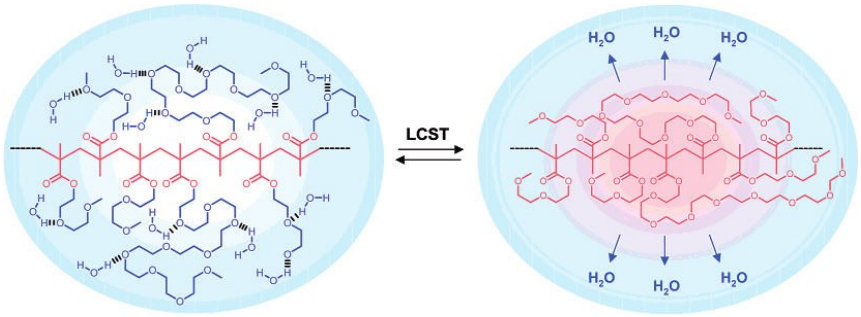

Figura 11: Abaixo da LCST, o POEGMA exibe uma conformação *random coil* do *backbone* hidrofóbico (em vermelho) com moléculas de água ligadas a hidrogênio a grupos EO de cadeias laterais (em azul), que é responsável pela solubilidade do polímero. Acima da LCST, o copolímero tem alterada a conformação da sua cadeia lateral de EO tornando-as insolúveis e causando o seu colapso junto com o *backbone* de metacrilato de metila. Adaptado da referência [69]. © 2007 American Chemical Society.

Os estudos da literatura, no entanto, focam majoritariamente na variação da temperatura de transição, medidas por técnicas de calorimetria e espalhamento de luz; sem observar alterações nos objetos formados com a separação de fase devido à temperatura.

Neste estudo, foram sintetizados por polimerização radicalar por desativação reversível (RDRP) e caracterizados por cromatografia de permeação em gel (GPC) e ressonância magnética nuclear (RMN) copolímeros do tipo *graft* da família POEGMA e foram estudados o comportamento térmico destes em água por espalhamento de luz dinâmico (DLS), turbidimetria, microcalorimetria (HSDSC), espalhamento de raios-X de baixo ângulo (SAXS) e espectrofotometria no UV-vis, detalhando a estrutura dos objetos formados acima da temperatura de transição de fase. De acordo com a arquitetura do copolímero, pode-se controlar não apenas a temperatura da transição de fase, mas também o objeto formado: micelas ou agregados que separam de fase macroscopicamente. Em alguns casos especiais, é possível obter ambos os objetos, em faixas de temperatura distintas. A quantidade de grupos EO se relacionam com a temperatura da transição de fase, enquanto que o comprimento das cadeias laterais de oligoetileno glicol afeta a estrutura formada, conforme representado na Figura 12.

A principal aplicação deste estudo é o desenvolvimento de sistemas inteligentes de entrega de moléculas funcionais através da temperatura. Estas moléculas podem atuar como ingredientes ativos em diversos segmentos, beneficiando principalmente as áreas farmacêuticas e biomédicas, cosmética e cuidados para a casa, de químicos para agricultura, entre outras. Este trabalho foi publicado na revista *Langmuir* [70] e encontra-se na íntegra na seção 3.1.

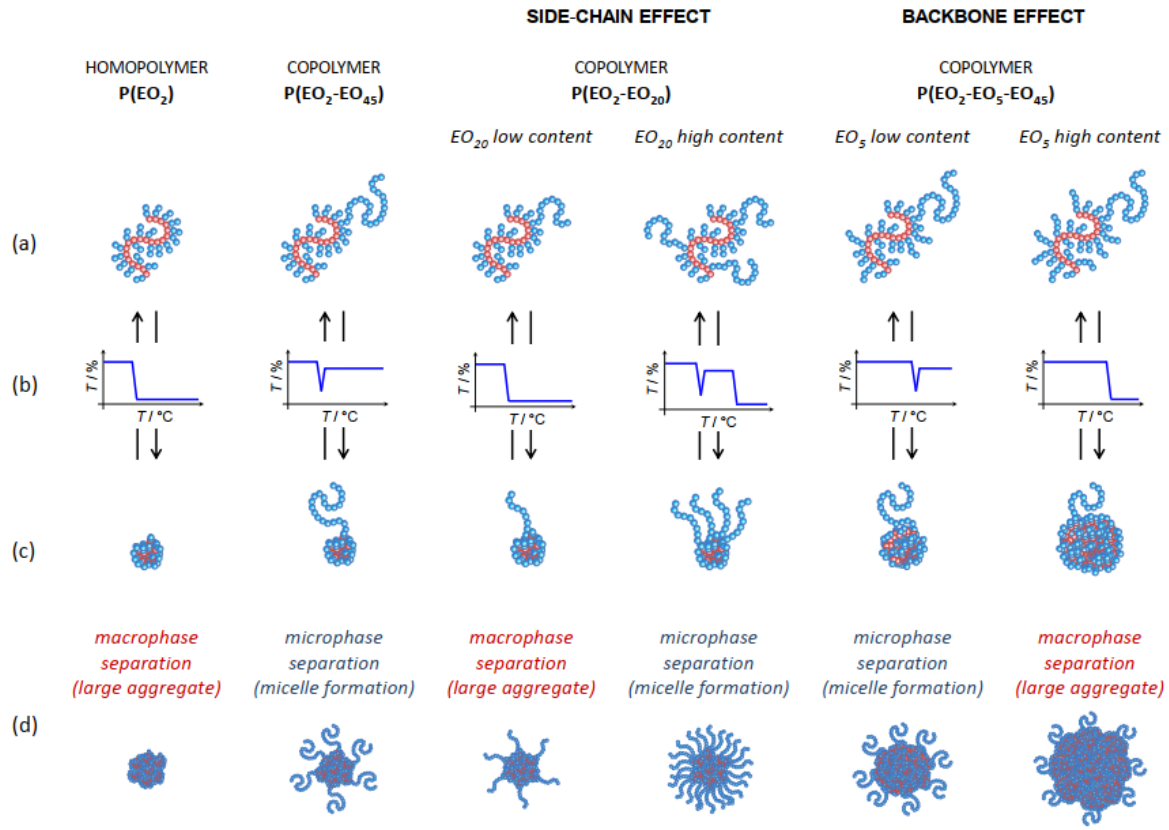

Figura 12: Representação do efeito do tamanho da cadeia colapsada e do comprimento e quantidade relativa da cadeia lateral na formação do agregado de POEGMA em micela ou separação de fase de um agregado maior. (a) Cadeias de polímeros solúveis existindo como unímeros em solução abaixo da temperatura crítica; (b) Perfil da curva de transmitância ao longo da transição de fase; (c) Cadeia de polímero individual colapsada acima de uma temperatura crítica; e (d) Tipo de transição de fase e uma representação fora da escala da partícula resultante (agregado macroscopicamente separado ou micela).

Efeito da variação da arquitetura molecular do POEGMA em solução aquosa

Os copolímeros de POEGMA foram sintetizados pela técnica de polimerização controlada ATRP, nos métodos normais e ARGET. Esta técnica de polimerização controlada garante uma baixa dispersidade de massa molar. O método ARGET, mais elaborado, utilizada uma concentração de Cu^{+} cerca de 40 vezes mais baixa que o método normal, gerando um produto com uma menor quantidade de contaminante após a purificação. Além disso, a utilização do agente redutor de estanho torna a reação menos sensível à presença de baixas concentrações de oxigênio.

O poli(metacrilato de metila) (PMMA) é um polímero insolúvel em água. No caso do POEGMA, o PMMA é o esqueleto principal (*backbone*) com enxertos de poli(óxido de etileno) (PEO), que garantem a sua solubilidade abaixo da sua LCST. Dependendo da sua

arquitetura, os copolímeros POEGMA formam diferentes estruturas de agregado acima da LCST: agregado micelar ou agregado não micelar. A fim de proporcionar uma melhor compreensão sobre a estrutura do agregado micelar, realizamos medições de espalhamento de luz utilizando o copolímero P(EO_2MA-*co*-EO_{45}MA) como modelo para o sistema de copolímeros POEGMA.

Abaixo da LCST o copolímero é solúvel e, com aquecimento da solução, a sua conformação é alterada, tornando-a menos polar e reduzindo a interação dos grupos EO das cadeias laterais com a água [24], com consequente desidratação parcial da cadeia polimérica colapsando-as junto ao *backbone* de metacrilato. Caso haja cadeias laterais de EO longas o suficiente para não se colapsarem com o *backbone*, a cadeia polimérica apresentará uma região hidrofóbica colapsada e outra região hidrofílica formada pela(s) cadeia(s) lateral(is) de EO que continuam solvatadas pela água. Esta estrutura anfifílica se auto-organiza em micelas. Este comportamento é bem conhecido para copolímeros de EO/PO em bloco (usualmente chamados pelo nome comercial "Pluronic®").

Com a adição de cadeias laterais com 5 unidades de grupos EO ao P(EO_2MA-*co*-EO_{45}MA), formando os copolímeros P(EO_2MA-*co*-EO_5MA-*co*-EO_{45}MA), o tamanho do esqueleto colapsado aumenta assim como a temperatura de transição de fase. Quanto mais cadeias laterais de EO_5MA forem adicionadas, maior o volume da região de caráter hidrofóbico. Com isso, a geometria do objeto anfifílico se altera e a cauda hidratada não é mais suficiente para mantê-lo estável em solução, induzindo o copolímero à separação macroscópica de fase. Por outro lado, uma cauda mais curta, como no caso do P(EO_2MA-*co*-EO_{20}MA), na mesma proporção monomérica que o P(EO_2MA-*co*-EO_{45}MA) (99:1), não é suficiente para manter a estrutura colapsada estável em solução; é necessária uma quantidade maior desta cauda hidratada para isso. No entanto, estas cadeias laterais suportam estabilizar o agregado até uma determinada temperatura, acima da qual também irá se desidratar e colapsar junto com o esqueleto já desidratado, levando também o copolímero à separação macroscópica de fase.

A Tabela 1 sumariza os resultados sobre o comportamento térmico dos copolímeros POEGMA. Os valores de entalpia da transição de fase se correlacionam com a razão EO/MA dos copolímeros. Isto indica que esta energia está relacionada à desidratação dos grupos metacrilatos, uma vez que esta energia diminui com a sua quantidade relativa no copolímero.

Tabela 1: Comportamento térmico dos copolímeros POEGMA sintetizados por ATRP.

POEGMA	$EO_2MA/EO_{20}MA/EO_5MA/EO_{45}MA$	razão EO/MA	*T** / °C	Δ*H* J g^{-1}	estrutura†
P(EO_2MA)	100/–/–/–	2,0	20,0	25,1	agg
P(EO_2MA-*co*-$EO_{45}MA$)	99/–/–/1	2,4	26,5	19,8	micela
P(EO_2MA-*co*-EO_5MA-*co*-$EO_{45}MA$)	94/–/5/1	2,6	31,0	15.1	micela
	89/–/10/1	2,7	34,5	16,2	micela
	79/–/20/1	2,9	40,5	16,5	agg
	69/–/30/1	3,2	46,0	16,0	agg
P(EO_2MA-*co*-$EO_{20}MA$)	99/1/–/–	2,2	21,5	23,5	agg
	95/5/–/–	2,9	32,0 47,5	14,0	ambas
	90/10/–/–	3,8	39,0 53,5	4,9	ambas

*Temperatura das transições de fases. †Estrutura identificada acima da temperatura de transição de fases (agg = agregado com separação de fase macroscópica).

Os resultados demonstraram que o volume do *backbone* colapsado, o comprimento da cadeia lateral de EO e seu teor na composição do copolímero determinaram as transições induzidas pela temperatura, levando à formação de micelas ou separação macroscópica de fase enquanto, em alguns casos, os dois eventos foram observados consecutivamente (Figura 12). Estes objetos apresentam a potencial aplicação dos copolímeros da família POEGMA como agentes de encapsulamento e liberação controlada de ativos.

3.1. Artigo publicado na *Langmuir* (Referência [70])

LANGMUIR

pubs.acs.org/Langmuir Article

Effect of Molecular Architecture and Composition on the Aggregation Pathways of POEGMA Random Copolymers in Water

Rafael Pires-Oliveira, Juntao Tang, Ana Maria Percebom, Cesar L. Petzhold, Kam C. Tam, and Watson Loh*

Cite This: *Langmuir* 2020, 36, 15018−15029 Read Online

ACCESS | Metrics & More | Article Recommendations | Supporting Information

ABSTRACT: Understanding of the temperature-induced phase transition of poly(oligo(ethylene glycol) methyl ether methacrylate) (POEGMA) random copolymers with varied composition remains largely incomplete. Upon heating they can form either macroscopically phase-separated aggregates or micelles. We examined the effect of polymer architecture by rationally designing and synthesizing various POEGMA copolymer structures via atom transfer radical polymerization using OEGMA monomers of different EO lengths. Micelle formation occurred for copolymers with a small fraction of long side chains counterbalanced by an appropriate number of short side chains, while macroscopic phase separation occurred for other copolymer compositions. In some copolymer compositions and architectures, micelle formation followed by macroscopic phase separation occurred, and the temperature of these phase transitions could be tailored accordingly. This new strategy allows the control over the microstructure and specific transition temperatures enabling, for instance, the preparation of nanocarriers for encapsulating hydrophobic compounds.

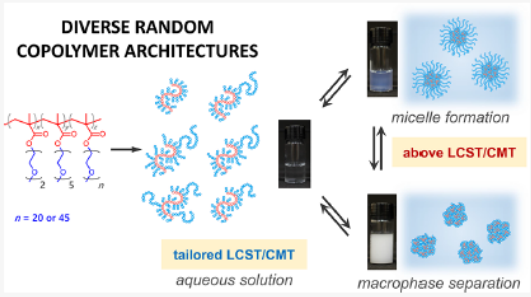

INTRODUCTION

Random copolymers with self-assembly behavior have attracted considerable attention due to their potential applications. This is a typical behavior of block copolymers which are capable of forming stable polymeric micelles in selective solvents, consisting of a hydrophobic core surrounded by a hydrophilic corona. Several nanostructures with different morphologies can be prepared using this strategy for a wide range of applications.[1] The most studied systems are a family of poly(ethylene oxide)−poly(propylene oxide)−poly(ethylene oxide) (PEO−PPO−PEO) copolymers (also known as Poloxamers or Pluronics) in aqueous solutions, whose aggregation behavior is well understood and that have similarity to low molecular weight surfactants.[2] More recently, other block copolymers with tunable amphiphilic characteristics have been developed as supramolecular nanocarriers for controlled release as well as other applications in biomedicine.[3−9] The possibility of forming polymeric micelles using stimuli-responsive random copolymers with block copolymer-like properties offers an important alternate route to prepare micellar structures in water, and, although there are some interesting works emerging on this theme,[10−12] it is still underexplored in the literature.

Poly(oligo(ethylene glycol) methyl ether methacrylate) (POEGMA) is a family of copolymers consisting of a hydrophobic methacrylate backbone and hydrophilic ethylene oxide (EO) side groups, where the EO segments enhance the solubility of the polymer in water, yielding many interesting properties. These copolymers are sufficiently hydrophilic with high water solubility, and they possess lower critical solution temperatures (LCST) depending on their chemical composition. Their water solubility is enhanced by the EO units yielding tailorable phase separation temperatures.[13−17] Upon heating, these EO groups alter their conformation, becoming less polar[18] and disrupting the hydrogen bonds between the ether group on EO segments and water. Consequently, the polymer−polymer interaction is favored over polymer−solvent interaction, which induces a reversible phase transition.

These polymer systems were initially prepared and reported by Lutz and co-workers[19] as alternative temperature responsive polymers to replace the well-known poly(*N*-isopropylacrylamide) (PNIPAM). POEGMA copolymers are biocompatible[20] and possess antifouling behavior,[21] and the monomers are not toxic compared to that of PNIPAM,[22] making them safer for use in biomedicine.[23] As previously reported,[24,25] a POEGMA

Received: August 27, 2020
Revised: November 25, 2020
Published: December 4, 2020

https://dx.doi.org/10.1021/acs.langmuir.0c02538
Langmuir 2020, 36, 15018−15029

Scheme 1. Synthesis of P(EO_2MA-*co*-EO_5MA-*co*-EO_{45}MA) and P(EO_2MA-*co*-EO_nMA) (n = 20 or 45), by Normal ATRP (Top) and ARGET ATRP (Bottom), Respectively

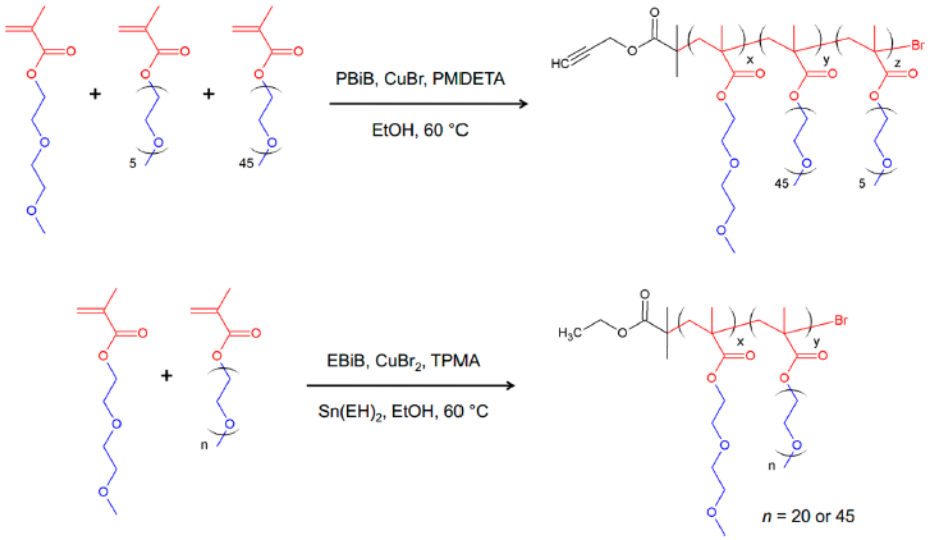

copolymer containing a specific ratio of long and short EO side chains, P(EO_2MA-*co*-EO_{45}MA) at a molar ratio of 99:1, displayed a temperature-induced phase behavior forming macromolecular aggregates or micelles beyond the critical phase transition temperature, as opposed to macroscopic phase separation observed for copolymers with other compositions. This observation prompted us to perform a more systematic investigation on the solution and association behavior of a series of copolymers from the POEGMA family, whose compositions were varied with respect to the length of their EO side groups and their EO composition (molar fraction of EO per chain).

We rationally designed and synthesized a series of POEGMA random copolymers with EO side chains bearing 2, 5, 20, and 45 EO units by atom transfer radical polymerization (ATRP), a reversible-deactivation radical polymerization (RDRP) method. We investigated aqueous solutions of these copolymers using techniques such as turbidimetry, high-sensitivity differential scanning microcalorimetry (HSDSC), and light scattering and small-angle X-ray scattering (SAXS) measurements in order to elucidate the impact of molecular architecture on their aggregation. Moreover, using a model hydrophobic compound we examined whether they could be used to encapsulate hydrophobic compounds as a potential nanocarrier for the controlled delivery of drugs. In this study, we report a straightforward approach to tailor a random copolymer with self-assembly behavior, producing either a micelle or a cluster structure at well-defined temperatures and at low concentration (5.0 mg mL^{-1}).

■ EXPERIMENTAL SECTION

Materials. Di(ethylene glycol) methyl ether methacrylate (EO_2MA) (M_n = 188 g mol^{-1}) and oligo(ethylene glycol) methyl ether methacrylate (EO_nMA, n = 5, 20, and 45 EO units, M_n = 300, 950, and 2080 g mol^{-1}, respectively) (from Sigma-Aldrich) were passed through an alumina column to remove inhibitors. Copper(I) bromide (CuBr, Aldrich, 99.999%), copper(II) bromide ($CuBr_2$, Aldrich, 99.999%), *N*,*N*,*N*′,*N*″,*N*″-pentamethyldiethylenetriamine (PMDETA, Aldrich, 99%), tris(2-pyridylmethyl)amine (TPMA, Aldrich, 98%), tin(II) 2-ethylhexanoate ($Sn(EH)_2$, Aldrich, ≥92.5%), ethyl α-bromoisobutyrate (EBiB, Aldrich, 98%), ethanol (Aldrich, reagent grade), and Reichardt's dye (Sigma, 90%) were used without further purification. Propargyl 2-bromoisobutyrate (PBiB) synthesized following the method described elsewhere[26] was kindly supplied by Dr. Hairong Wang (Soochow University, China), and it was characterized by NMR spectroscopy (Figure S1 in the Supporting Information). Milli-Q system water (resistivity greater than 18.2 MΩ·cm) was used to prepare all the solutions.

Copolymers Synthesis. We synthesized all copolymers via the atom transfer radical polymerization (ATRP) with some modifications according to previous reports.[13,24,27] The synthesis routes are shown in Scheme 1. Typical procedures for the synthesis conducted by normal ATRP and by activators regenerated by electron transfer (ARGET) ATRP are described in detail in the Supporting Information.

Gel Permeation Chromatography. We performed gel permeation chromatography (GPC) in a Viscotek GPCmax VE 2001 chromatograph equipped with a Viscotek VE 3580 RI Detector and Viscotek UV Detector 2500. A Viscotek TGuard 10 × 4.6 mm guard column and three Shodex KF-806 M or T6000 M columns were used and maintained at 40 °C. Anhydrous tetrahydrofuran (THF) (Sigma-Aldrich, HPLC grade) was used to prepare polymer solutions of 8.0 mg mL^{-1}, and it was also used as an eluent at a flow rate of 1.0 mL min^{-1}. A calibration curve was constructed using polystyrene (PS) standards (Malvern).

^{1}H NMR Spectroscopy. ^{1}H NMR nuclear magnetic resonance (NMR) spectra were recorded in $CDCl_3$ in Bruker Avance NMR spectrometers operating at 400 or 500 MHz. The experimental conditions are described as follows: pulse program: zg30; spectral width: from −4.00 to 16.00 ppm; spectral size: 32 768 points; 90° pulse: 11.75 μs; delay: 5 s; number of scans: 16. Tetramethylsilane (TMS) was used as an internal standard for calibrating chemical shifts.

Turbidimetry. We determined the cloud points of 5.0 mg mL^{-1} aqueous copolymer solution in a Varian Cary 100 UV−vis spectrophotometer equipped with a temperature controller. The cloud point was determined when the temperature started to deviate from 100% transmission. The measurements were performed at a

https://dx.doi.org/10.1021/acs.langmuir.0c02538
Langmuir 2020, 36, 15018−15029

Table 1. Composition and Characterization of the Synthesized POEGMA Copolymers[a]

entry	POEGMA type	reaction system	$EO_2MA/EO_{20}MA/EO_5MA/EO_{45}MA$	conv.[b]	$M_{n,theo}$[c] (g mol^{-1})	$M_{n,GPC}$ (g mol^{-1})	$Đ$	$H_{d,theo}$	$H_{d,NMR}$[e]
1	$P(EO_2MA)$	ARGET ATRP	100/−/−/−	0.88	16600	21500	1.99	600	587
2	$P(EO_2MA\text{-}co\text{-}EO_{45}MA)$	normal ATRP	99/−/−/1	n.d.	20700[d]	18500	2.05	772	782
3	$P(EO_2MA\text{-}co\text{-}EO_5MA\text{-}co\text{-}EO_{45}MA)$	normal ATRP	94/−/5/1	n.d.	21300[d]	24000	2.08	822	844
4		normal ATRP	89/−/10/1	n.d.	21800[d]	13000	2.03	872	890
5		normal ATRP	79/−/20/1	n.d.	22900[d]	15100	1.98	972	980
6		normal ATRP	69/−/30/1	n.d.	24000[d]	16300	2.10	1072	1008
7	$P(EO_2MA\text{-}co\text{-}EO_{20}MA)$	ARGET ATRP	99/1/−/−	0.97	19000	16900	1.54	672	661
8		ARGET ATRP	95/5/−/−	0.97	22100	16800	1.35	960	977
9		ARGET ATRP	90/10/−/−	0.92	24700	14200	1.35	1320	1296

[a]Experimental conditions: normal ATRP: $[PBiB]_0/[CuBr]_0/[PMDETA]_0$ = 1/2/4. ARGET ATRP: $[EBiB]_0/[CuBr_2]_0/[TPMA]_0/[Sn(EH)_2]_0$ = 1/0.05/0.2/0.1. All polymerization reactions were conducted in EtOH/monomers = 1.25:1 (v/v) at 60 °C. [b]Conversion calculated by ^{1}H NMR; more detail can be found in the Supporting Information. [c]$M_{n,theo} = ([M]_0/[I]_0) \times$ conversion $\times M_{monomer}$. [d]Considering target M_n. [e]EO content in the POEGMA polymer chain quantified from ^{1}H NMR spectra (H_d is assigned the methylenic protons CH_2CH_2O of the EO group). n.d. = not determined.

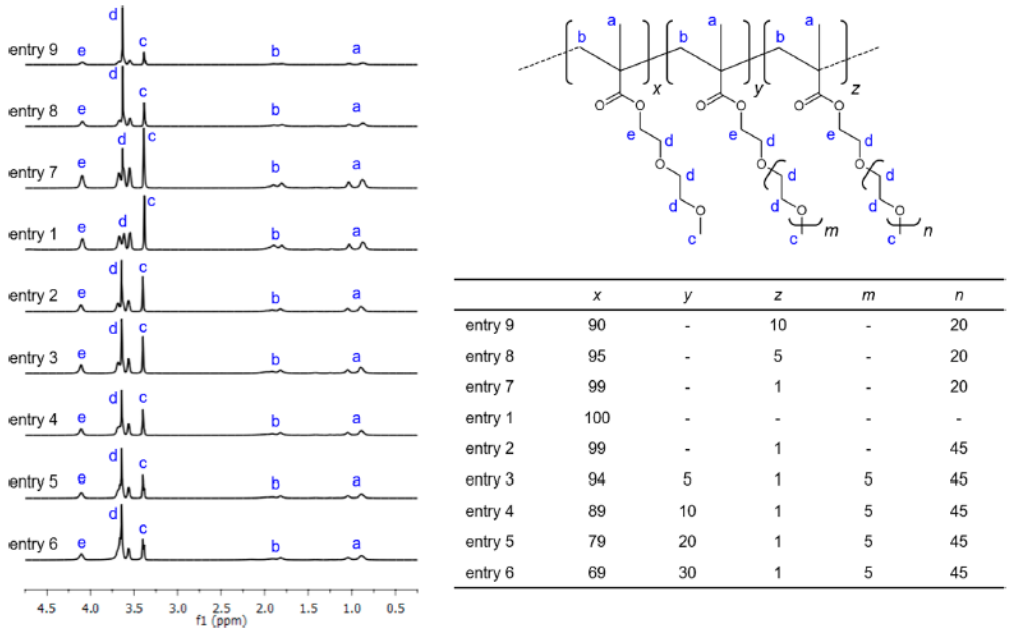

	x	y	z	m	n
entry 9	90	-	10	-	20
entry 8	95	-	5	-	20
entry 7	99	-	1	-	20
entry 1	100	-	-	-	-
entry 2	99	-	1	-	45
entry 3	94	5	1	5	45
entry 4	89	10	1	5	45
entry 5	79	20	1	5	45
entry 6	69	30	1	5	45

Figure 1. ^{1}H NMR spectra of all synthesized POEGMA copolymers (see Table 1) recorded in $CDCl_3$ with all protons identified.

wavelength of 500 nm with three cycles of heating and cooling at 0.5 °C min^{-1}, after an equilibration time of 120 s at each step.

Microcalorimetry. The thermal behavior of 5.0 mg mL^{-1} aqueous copolymer solution was monitored by high-sensitivity differential scanning microcalorimetry (HSDSC) in a MicroCal VP-DSC (Northampton, USA), equipped with 0.54 mL cells. Three consecutive cycles of heating and cooling were performed from 5 to 90 °C at a scanning rate of 60 °C h^{-1}; the first run was considered to have erased the polymer thermal history, and all curves were identical. The reference cell was filled with Milli-Q water. All samples were kept at the starting temperature for 20 min prior to the measurements. The blank reference, obtained by conducting an experiment with both cells filled with water, was subtracted from the sample thermograms. The enthalpy change (ΔH, expressed as J g^{-1} of polymer) was calculated by integrating the area below the curve after subtracting the baseline.

Dynamic Light Scattering. Dynamic light scattering (DLS) analyses of 1.0 mg mL^{-1} aqueous $P(EO_2MA\text{-}co\text{-}EO_{45}MA)$ solutions were performed on a Zetasizer Nano ZS (Malvern Instruments, Worcestershire, U.K.), equipped with a He−Ne laser red (λ = 632.8 nm). The scattering intensities were detected at an angle of 173°. Prior to the experiments, all the solutions were filtered through a 0.45 μm disposable filter. More experimental details are provided in the Supporting Information.

Small-Angle X-ray Scattering. We performed small-angle X-ray scattering (SAXS) measurements at the SAXS1 beamline of the Brazilian Synchrotron Laboratory (LNLS) at the Brazilian Center for Research in Energy and Materials (CNPEM), in Campinas, Brazil. The 5.0 mg mL^{-1} aqueous copolymer solution was added to a cell with two flat mica windows under water-bath temperature control. Experiments were performed at 25 and 37 °C, and the samples were

https://dx.doi.org/10.1021/acs.langmuir.0c02538
Langmuir 2020, 36, 15018−15029

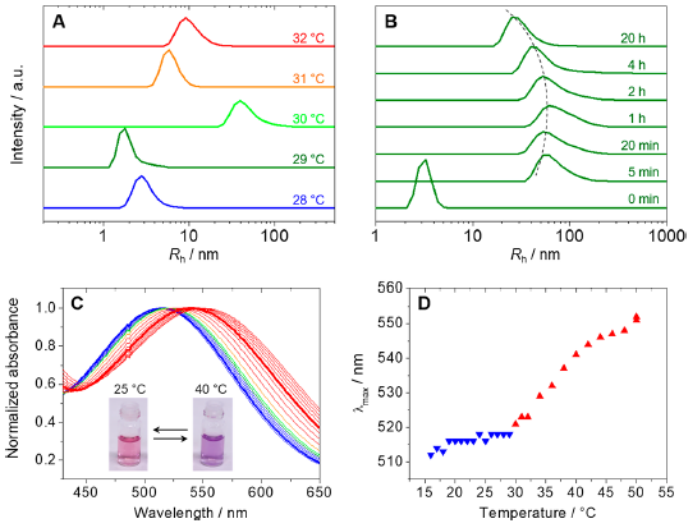

Figure 2. DLS measurements of 1.0 mg mL^{-1} aqueous solution of the P(EO_2MA-*co*-EO_{45}MA) 99:1 copolymer: (A) number-weighted intensity as a function of temperature (indicated in each curve) and (B) number-weighted intensity as a function of time at T = 29 °C. All measurements were performed at θ = 173°. (C) UV−vis spectra from 18 to 50 °C (thicker lines in blue and red for 25 and 40 °C, respectively) and (D) λ_{max} of Reichardt's dye as a function of temperature in 5.0 mg mL^{-1} aqueous P(EO_2MA-*co*-EO_{45}MA) solution.

maintained at this temperature for at least 1 h prior to the measurements. The distance between the sample holder and detector was 912 mm, and the X-ray wavelength was λ = 1.550 Å. The detailed data fitting procedure is described in the Supporting Information.

Solvatochromic Dye Incorporation. Reichardt's dye was incorporated into the POEGMA copolymer by employing the coprecipitation technique. A 1.0 mM Reichardt's dye solution in acetone was prepared, and 400 μL was added to 2.0 mL of a 0.01 wt % P(EO_2MA-*co*-EO_{45}MA) solution in acetone and well mixed. The solvent was evaporated under N_2 flow. Subsequently, 3.0 mL of a cold 10.0 mg mL^{-1} aqueous P(EO_2MA-*co*-EO_{45}MA) solution was added and vortexed for 60 s to dissolve all the precipitate. The aqueous Reichardt's dye POEGMA solution was then further diluted to 5.0 mg mL^{-1}, and the UV−vis spectra were recorded as a function of temperature in a HP8453 spectrophotometer equipped with Peltier temperature control after an equilibration time of 120 s at each step of 1.0 °C.

RESULTS AND DISCUSSION

Polymer Characterization. The purified POEGMA copolymers appeared transparent with a well-defined structure and a monomeric composition close to the feed ratio (Table 1). This was confirmed by the integration of the ^{1}H NMR signal at 3.75−3.48 ppm (spectra shown in Figure 1) that corresponds to the methylenic protons from the EO groups.[28] The conversion was calculated by ^{1}H NMR (more detail can be found in the Supporting Information). Pietsch et al.[29] found that the EO_{20}MA is more reactive than EO_2MA under reversible addition−fragmentation chain transfer (RAFT) polymerization conditions, and then the POEGMA copolymers should exhibit a monomer gradient along the polymer chain that gradually changes from a high EO_{20}MA content to a high EO_2MA content during the polymerization. The number-average molecular weight (M_n) and dispersity ($Đ = M_w/M_n$) of each polymer were determined by GPC in THF using a polystyrene standard calibration curve, shown in Table 1 and in the Supporting Information Figure S2. Since polystyrene has a different hydrodynamic volume in THF than POEGMA copolymers, a deviation between theoretical and experimental number-average molecular weight was observed. Moreover, copolymers with longer EO side chain monomer behave as comb-shaped polymers and have significantly smaller hydrodynamic radii when compared to the PS calibration standards.

All polymers were synthesized by either normal ATRP or ARGET methods. ATRP is a reversible-deactivation radical polymerization that enables the control over molar mass with a dispersity ($Đ = M_w/M_n$) typically below 1.5.[30] ARGET, a more elaborate technique, uses a copper concentration around 40 times lower than the normal ATRP, yielding less copper contamination after purification. Moreover, the reducing agent ($Sn(EH)_2$) makes the reaction less sensitive to the presence of oxygen at lower concentrations. All these features enable the development of tailored "smart" functional copolymers with controlled architecture and microstructure, with control over the molar mass and dispersity on an industrial scale achieving superior performance.[31]

Higher dispersity values have also been observed for other POEGMA polymerizations,[13,24,27,32] and in our case it might also be due to the complex polymerization of three monomers by normal ATRP. It is worth mentioning that the somewhat broader dispersity did not affect the thermal-induced self-assembly properties of POEGMA,[33] as indicated by the copolymers prepared via the free radical polymerization. The main advantage of using the ATRP technique in this study is to produce controlled polymer architecture that enables a systematic study on the effects of the EO side chain.

POEGMA Particle Size As a Function of Temperature and Time. The number-weighted DLS curves for the P(EO_2MA-*co*-EO_{45}MA) copolymer as a function of temperature are shown in Figure 2A. In this experiment, the sample was heated from 18 to 50 °C, with measurements in steps of 1.0 °C (Figure S3B). At each step, the sample equilibrated at the temperature for at least 5 min, and after an equilibration time of 120 s, three measurements were performed, and the

https://dx.doi.org/10.1021/acs.langmuir.0c02538
Langmuir 2020, 36, 15018−15029

average results were plotted. At temperatures below the critical temperature, the copolymer displayed a random coil conformation with a particle apparent hydrodynamic radius (R_h) of approximately 3 nm. The thermally induced phase transition of P(EO_2MA-*co*-EO_{45}MA) copolymer in water occurs in a multistep aggregation process.[25] First, upon heating, the hydrophilic EO side chains become less hydrated and collapse onto the hydrophobic backbone, achieving a R_h of around 2 nm at the cloud point (29 °C, determined by the size distribution curves from DLS measurements, please see Figure S3A), as also reported by Lutz and co-workers.[28] As the temperature was further increased, the dehydrated copolymer chains began to aggregate and concomitantly underwent a reorganization of the collapsed EO side chains exposing the polar ether oxygen groups to the outside of the aggregate, forming a loose dense structure with an R_h of 40 nm. Upon further increase beyond 31−32 °C, the longer EO side chains rearranged allowing the EO groups to interact with water forming the outer layer of the aggregate while the short EO side chains remain closer to the backbone, forming the denser hydrophobic core of the micelle structure with an R_h of around 9 nm. The coil−globule phase transition was reversible. The cooling process (Figure S3A) followed a different pathway from the heating process, similar to the behavior reported for the PNIPAM-*g*-PEO copolymer.[34] The aggregate structure is uniform and becomes swollen via the rehydration of EO moieties during the cooling process, in contrast to the heat-induced shrinking process.

This behavior resembles that of other associating alkoxylate block copolymers, such as the PEO−PPO−PEO, which aggregate upon heating, forming well-defined micelles due to PO chain dehydration. For these triblock copolymers, the phase transition is associated with the critical micelle temperature (CMT), which is similar to the critical micelle concentration. For the P(EO_2MA-*co*-EO_{45}MA) copolymer a similar behavior was observed, and the CMT for this copolymer at 5 mg mL^{-1} was approximately 29 °C (from DLS measurements).

In another experiment, the sample was conditioned at room temperature and placed in the sample holder when the equipment was equilibrated at the CMT of 29 °C. The measurements were performed over 20 h, and the aggregate size was determined after an equilibration time of 120 s. Figure 2B shows the evolution of aggregate size as a function of time, and the DLS results revealed that the thermal-induced aggregation process is associated with a slow and complex kinetics. At the CMT, the P(EO_2MA-*co*-EO_{45}MA) copolymer first formed a large structure that rearranged into smaller aggregates consisting of several dehydrated copolymer chains in a collapsed globule state. It should be noted that even up to 20 h at 29 °C, the system did not reach an equilibrium, with a particle radius of around 10 nm, as observed in the experiment raising the temperature (please see Figure 2A). The long equilibration time is a commonly observed behavior for thermoresponsive polymers,[35] and it might be due to two factors: the complex dehydration process of the polymer moieties[25] and the presence of slightly more hydrophobic copolymer chains[36] present in the heterogeneity of the polydisperse POEGMA copolymer.

Additional DLS measurements were conducted for all nine POEGMA copolymers prepared in this study, below and above their CMT, and all results are shown in Table S2. For selected entries we also measured the particle size after 24 and 48 h maintained above their CMT to validate the same trend observed for the P(EO_2MA-*co*-EO_{45}MA) copolymer (entry 2), shown in Figure 2B. These data show unimer size with a range of R_h from approximately 5 to 20 nm when the POEGMA copolymer is fully solubilized below the phase transition temperature, and upon heating above the CMT a large aggregate with a R_h around 50−180 nm, which rearranges with time into smaller aggregates, is found, similar to the behavior noticed for the P(EO_2MA-*co*-EO_{45}MA) copolymer (entry 2). It is worth mentioning that the most appropriate micelle particle size is the R_h value measured after a prolonged equilibration time. In addition, the R_h value of the micelle formed by each macromolecule agrees with their EO group content.

Above the LCST, when displayed by the POEGMA copolymer, macroscopic phase separation occurred with eventual settling of a concentrated white gel phase rich in copolymer when the solution was maintained above this temperature, as seen in Figure S4. Overall, these results confirm the behavior discussed above: the copolymers appear as nonaggregated molecules at low temperature, and upon increase in the temperature, some form well-defined micelles at a certain CMT, while at higher temperatures macroscopic phase separation is observed, associated with a LCST.

One of the characteristics of the micelles formed by thermal-induced aggregation of POEGMA is the formation of a hydrophobic core. In order to assess this feature, we used the solvatochromic Reichardt's dye that changes color according to the polarity of the solvent.[37] The shift to higher λ_{max} values indicates a decrease in the local polarity. The formation of micelles was confirmed by the reversible shift of λ_{max} of Reichardt's dye with temperature in aqueous POEGMA solution. Figures 2C and D show the shift from ca. 516 nm (below the CMT) to 551 nm at 50 °C (above the CMT), where the color changed from pink to purple due to changes in the polarity around the dye. A very similar color (represented by its λ_{max})[38] was reported for the micellization of a series of PEO−PPO−PEO block copolymers, suggesting a similarity between the micelles of POEGMA and of block copolymers.

Characterization of the Copolymer Micellar Aggregate by SAXS Measurements. The SAXS data provide information on the size and shape of the scattering objects, and the measurements were performed to elucidate the copolymer structure below and above the CMT. Figure 3 shows the experimental SAXS curves of P(EO_2MA-*co*-EO_{45}MA) copolymer below and above the CMT. The SAXS data at 25 °C (i.e., below the CMT) could be fitted with the Gaussian model with an average gyration radius (R_g) of 5.2 nm (blue curve in Figure 3) indicating that the copolymer chains assume a Gaussian chain conformation. However, a different curve was obtained for the sample above the CMT (red curve in Figure 3). Two R_g were determined by fitting the SAXS data using the Beaucage method[39] and assuming the aggregate is a fractal object (i.e., macromolecular globules in a hierarchical arrangement) with two levels of aggregation. The thermal-induced aggregation process yielded particles with a fractal nanostructure with R_{g2} around 30 ± 3 nm (corresponding to the second association level) comprised of several smaller collapsed objects with R_{g1} of 2.9 ± 0.1 nm (related to the first association level). For P(EO_2MA-*co*-EO_5MA-*co*-EO_{45}MA) containing a molar ratio of 94:5:1 of EO_2:EO_5:EO_{45} side chains (entry 3), the SAXS data (shown in Figure S5) suggested a similar behavior: R_g of approximately 6.9 nm for the completely soluble copolymer

https://dx.doi.org/10.1021/acs.langmuir.0c02538
Langmuir 2020, 36, 15018−15029

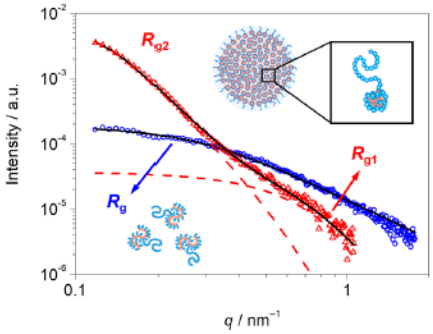

Figure 3. SAXS data obtained from the 5.0 mg mL^{-1} aqueous solutions of the P(EO_2MA-*co*-EO_{45}MA) 99:1 copolymer (blue ○) below (T = 25 °C) and (red △) above (T = 37 °C) the CMT. Blue data fitted as a spherical model (R_g = 5.2 nm) and red data fitted with the Beaucage method (R_{g2} = 30 nm, R_{g1} = 2.9 nm).

(below CMT) and two gyration radii of 2.8 ± 0.1 and 26 ± 4 nm for the fractal copolymer aggregate (above the CMT).

Thermosensitivity of P(EO_2MA-*co*-EO_5MA-*co*-EO_{45}MA) Copolymers Aqueous Solutions Assessed by Turbidimetry and Calorimetry. Turbidimetry measurements allow a direct determination of the solutions' cloud point, i.e., the temperature when the solutions become cloudy (indicated by a reduction in the transmittance). On the other hand, HSDSC measurements allow the determination of the temperature at which polymer chain dehydration occurs and the associated energetics of this process. It has been shown in the literature that for thermosensitive polymers such as PNIPAM, phase separation and dehydration occurred simultaneously, supported by data from both techniques.[40] For block copolymers that micellize, such as PEO−PPO−PEO, the changes in turbidity agreed with the endothermic peak ascribed to polymer dehydration determined with HSDSC,[41,42] allowing the determination of CMT values and elucidating the driving forces for micellization. In addition to the endothermic dehydration process of the copolymer, there is a larger entropy increase due to the release of water molecules that were solvating the hydrophobic moieties of the polymer (in our case mostly methacrylate and less polar EO groups above their LCST), and thus this should be also an entropy-driven process.[2,18]

We prepared aqueous POEGMA copolymer solutions using cold water and keeping it overnight at 8 °C prior to measurements to ensure that an equilibrium condition was reached. The thermal behavior of the copolymers was determined by turbidimetry and calorimetry, revealing that the cloud point increased with increasing EO content on the side chains of POEGMA copolymers (Figure 4). In all cases, the phase transitions were reversible, as indicated by superimposable curves for successive heating measurements (please see Figure S6). Similar behavior was observed previously by Percebom et al.[43] when using the same techniques to investigate another POEGMA solution.

The transition temperature for the P(EO_2MA) homopolymer (entry 1) and the P(EO_2MA-*co*-EO_{45}MA) copolymer (entry 2) were 20.0 and 26.5 °C, respectively, which agreed with previously reported results.[24,44] The P(EO_2MA-*co*-EO_5MA-*co*-EO_{45}MA) copolymers with different content of EO_5MA and 1 mol % EO_{45}MA content displayed a transition temperature of 31.0, 34.5, 40.5, and 46.0 °C, respectively, for 5 (entry 3), 10 (entry 4), 20 (entry 5), and 30 mol % (entry 6) of EO_5MA. As expected, the higher the EO content, the greater the copolymer cloud point.

Interestingly, different transmittance curve profiles were obtained for each set of POEGMA compositions. On the one hand, an abrupt reduction of transmission from 100 to 0% was observed for solutions of P(EO_2MA) homopolymer and P(EO_2MA-*co*-EO_5MA-*co*-EO_{45}MA) copolymers with EO_5MA side chain content above 20 mol %. On the other hand, the transmittance decreased to less than 50% and then increased to

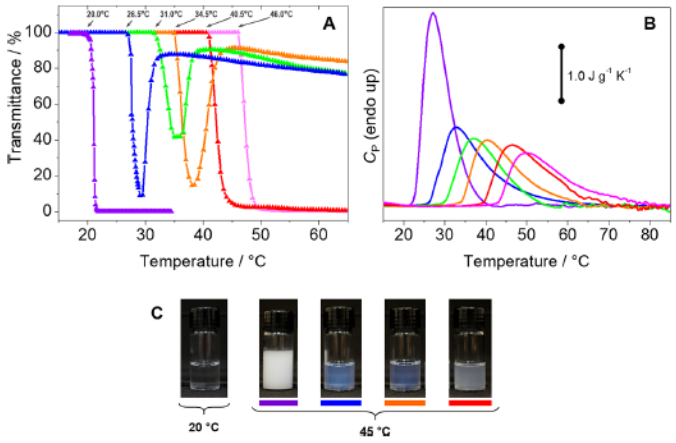

Figure 4. (A) Turbidimetry and (B) HSDSC curves of 5.0 mg mL^{-1} aqueous solutions of the (purple ▲) P(EO_2MA) homopolymer (entry 1) and P(EO_2MA-*co*-EO_5MA-*co*-EO_{45}MA) copolymers with [EO_2MA]:[EO_5MA]:[EO_{45}MA] molar ratios of (blue ▲) 99:0:1 (entry 2), (green ▲) 94:5:1 (entry 3), (orange ▲) 89:10:1 (entry 4), (red ▲) 79:20:1 (entry 5), and (pink ▲) 69:30:1 (entry 6). Turbidimetry heating rate = 0.5 °C min^{-1}, λ = 500 nm. HSDSC heating rate = 1.0 °C min^{-1}. (C) Photographs of aqueous POEGMA solutions: the first flask is a representative picture of all samples at 20 °C (all aqueous polymer solutions were equally clear transparent at this temperature) and flasks of aqueous POEGMA solutions (indicated by the colored bottom line) at 45 °C.

https://dx.doi.org/10.1021/acs.langmuir.0c02538
Langmuir 2020, 36, 15018−15029

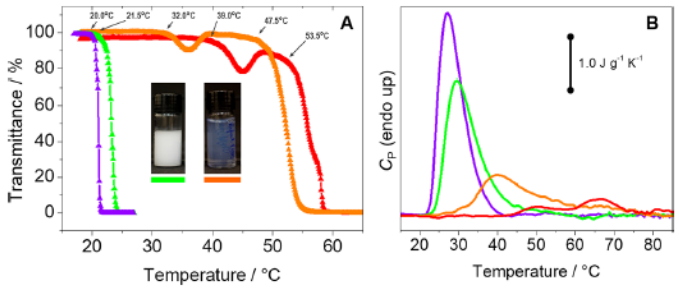

Figure 5. (A) Turbidimetry and (B) HSDSC curves of 5.0 mg mL^{-1} aqueous solutions of the (purple ▲) P(EO_2MA) homopolymer (entry 1) and P(EO_2MA-*co*-EO_{20}MA) copolymers with EO_2MA:EO_{20}MA molar ratios of (green ▲) 99:1 (entry 7), (orange ▲) 95:5 (entry 8), and (red ▲) 90:10 (entry 9). Turbidimetry heating rate = 0.5 °C min^{-1}, λ = 500 nm. HSDSC heating rate = 1.0 °C min^{-1}. Inset photographs: aqueous POEGMA solutions (indicated by the colored bottom line) at 45 °C.

about 80% for the P(EO_2MA-*co*-EO_5MA-*co*-EO_{45}MA) copolymers with EO_5MA side chains up to 10 mol %.

HSDSC curves (Figure 4B) show that the critical temperature followed the same trend as the cloud point, although the endothermic transition peak (T_{onset}) commenced at a slightly lower temperature compared to the cloud point measurements. This difference is due to the fact that a larger amount of collapsed polymer chains is required to produce a solution turbidity that could be detected by the UV−vis compared to the more sensitive HSDSC and was also reported for other thermosensitive polymers.[45,46] The calorimetric data contained asymmetric endothermic peaks with a long tail indicating consecutive processes of dehydration of polymer chains and aggregation, as shown by the deconvoluted HSDSC curve in Figure S7. The enthalpy changes (ΔH) of the phase transition processes are 26.3, 19.9, and (15.9 ± 0.6) J g^{-1} for P(EO_2MA), P(EO_2MA-*co*-EO_{45}MA), and P(EO_2MA-*co*-EO_5MA-*co*-EO_{45}MA) (the last one with different monomer ratios), respectively. Furthermore, the HSDSC curves possessed similar profiles for all the copolymers studied, which were different from those observed in turbidimetry, indicating that the energetics of the processes are identical, other than a monotonic change of cloud point and enthalpies of transition as a function of the polymer structure.

The aggregation behavior displayed by the copolymer solutions depicted by the increase in the transmittance after the initial decrease upon heating (as shown in Figure 4A) resembled the aggregation of the P(EO_2MA-*co*-EO_{45}MA) 99:1 copolymer discussed earlier. Based on the same arguments, we propose that they form micelles at the CMT, after which they remain essentially unchanged. The copolymer solutions that possessed an abrupt reduction in transmittance displayed a macroscopic phase separation that is associated with the copolymer dehydration. The fact that the energetics of the phase transition did not differ significantly for the two groups of copolymers suggests that the most intense enthalpic contribution is associated with the dehydration of groups that form the core of the copolymer aggregates, similar to that reported for PEO−PPO−PEO copolymers.[47]

Thermosensitivity of P(EO_2MA-*co*-EO_{20}MA) Copolymers by Turbidimetry and Calorimetry. A peculiar behavior was observed for the POEGMA system comprised of the comonomer EO_{20}MA. Figure 5A shows the turbidimetry results of the P(EO_2MA-*co*-EO_{20}MA) copolymers with 1, 5, and 10 mol % EO_{20}MA. As expected, the higher the EO content, the greater is the copolymer transition temperature. Again, the difference lies in the profiles of the transmittance curves. The P(EO_2MA-*co*-EO_{20}MA) copolymers with EO_2MA:EO_{20}MA molar ratio of 99:1 (entry 7) displayed a transition temperature of 21.5 °C with a curve profile similar at a temperature slightly higher than the P(EO_2MA) homopolymer (20.0 °C) (no alteration on the transmittance 0% was observed up to 50 °C, and the data were omitted in the graphic to facilitate reading). In a different manner, the P(EO_2MA-*co*-EO_{20}MA) copolymers with EO_2MA:EO_{20}MA molar ratios of 95:5 (entry 8) and 90:10 (entry 9) displayed a different transmittance curve profile, with two transitions. In these cases, for the EO_2MA:EO_{20}MA molar ratios of 95:5 and 90:10, a first transition occurred at 32.0 and 39.0 °C followed by a second transition at 47.5 and 53.5 °C, respectively, with an abrupt decrease to 0% transmission.

The HSDSC results (Figure 5B) show that the ΔH values of the phase transition processes were 23.5, 14.0, and 4.9 J g^{-1} for the P(EO_2MA-*co*-EO_{20}MA) copolymers with 1, 5, and 10 mol % of EO_{20}MA content, respectively—a difference of around 9.3 J g^{-1} in the ΔH for each increase of EO moieties in the copolymer chain. Moreover, very interestingly, the HSDSC peak of the P(EO_2MA-*co*-EO_{20}MA) copolymer with 10 mol % of EO_{20}MA displayed an apparent separation into two peaks that began at temperatures close to the temperature of each transitions observed by turbidimetry measurements. Following the previous discussion for the other copolymers, the first peak should be related to the formation of copolymer micelles, followed by macroscopic phase separation.

The Phase Transition Temperature and Energy. In the literature, the term "lower critical solution temperature" (LCST) is commonly used indiscriminately for both macroscopic and microscopic phase separation. However, the former is the lowest temperature where a macroscopic phase transition occurs at a specific lower critical solution concentration (LCSC) of the binodal curve in the phase diagram, while the transition temperature value (regardless of the LCSC) is the cloud point temperature. For further details, please see refs 35 and 45. On the other hand, microscopic phase separation is in fact the reaching of the critical micelle temperature (CMT). Depending on the architecture and composition of the POEGMA copolymers, only one phase transition (micro- or macroscopic phase separation) occurs, and in some other cases, both are present and micellization precedes macroscopic phase separation upon heating. Therefore, it is important to delineate the different processes, where the cloud point and

https://dx.doi.org/10.1021/acs.langmuir.0c02538
Langmuir 2020, 36, 15018−15029

CMT refer to the macroscopic phase separation and micelle formation, respectively.

Although there is no great difference among the energetics of phase transition for the different aggregates formed, the phase transition ΔH values decreased with the EO content, as shown in Figure 6. A linear decrease of ΔH values was

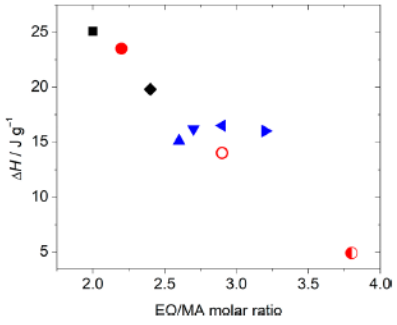

Figure 6. Enthalpy change versus EO/MA ratio for each polymer: (■) $P(EO_2MA)$ homopolymer (entry 1), (◆) $P(EO_2MA$-*co*-$EO_{45}MA)$ 99:1 copolymer (entry 2), $P(EO_2MA$-*co*-EO_5MA-*co*-$EO_{45}MA)$ copolymers with $[EO_2MA]$:$[EO_5MA]$:$[EO_{45}MA]$ molar ratios of (blue ▲) 94:5:1 (entry 3), (blue ▼) 89:10:1 (entry 4), (blue ◀) 79:20:1 (entry 5), and (blue ▶) 69:30:1 (entry 6), and $P(EO_2MA$-*co*-$EO_{20}MA)$ copolymers with $[EO_2MA]$:$[EO_{20}MA]$ molar ratios of (red ●) 99:1 (entry 7), (red ○) 95:5 (entry 8), and (red ◐) 90:10 (entry 9).

observed with the EO to MA molar ratio of the $P(EO_2MA)$ homopolymer and copolymers comprised of EO_{20} or EO_{45} with EO_2 monomer (black and red data points in Figure 6). Surprisingly, a roughly constant ΔH value around 15.9 ± 0.6 J g^{-1} was displayed for more complex copolymers with three monomers bearing EO_2, EO_5, and EO_{45} side chains (blue data points in Figure 6). This unexpected effect is not fully understood at this moment but might be due to the increased local EO crowding caused by the EO_5, decreasing the hydration of the EO moieties and consequently decreasing their individual dehydration energy.[48] It is worth mentioning that the contribution of the entropic effect for the phase transition processes might be smaller as the copolymer solubility increases with higher EO groups content, and the chain conformation in solution of these larger copolymers becomes constricted.

Aggregate Structures Formed above the Critical Temperature. In order to provide a better understanding of the aggregate structure and phase transition processes, we performed light scattering and SAXS measurements using the copolymer $P(EO_2MA$-*co*-$EO_{45}MA)$ (entry 2) as a model (and the DLS results trend was confirmed for other POEGMA copolymers, please see Table S2). The thermal behavior in aqueous solution of all other POEGMA copolymers with different architectures and compositions was characterized by turbidimetry and calorimetry (HSDSC).

Depending on its architecture and composition, POEGMA copolymers formed different aggregate structures, such as micelles or large phase-separated aggregates. In all cases, the copolymer was hydrated and soluble below its critical temperature. Upon heating, it underwent a phase transition forming aggregates comprised of dehydrated copolymer chains which eventually precipitated out of the solution (macrophase separation) or self-assembled into a hierarchical nanostructure forming a micelle (microphase separation), as shown in Figure S4.

When macroscopic phase separation occurred, SAXS analyses revealed the polymer-rich phase was not structured, in contrast to what was observed for PEO−PPO−PEO copolymers that phase separated into liquid crystalline mesophases. A similar observation was reported for a different POEGMA copolymer indicating no structuring was observed in the concentrated solution.[43] In detail, the dehydrated EO groups from the shorter side chains collapsed with the hydrophobic methacrylate backbone while the EO groups from the longer side chains remained hydrated, imparting the amphiphilic behavior to the block copolymer (see inset of Figure 3). Several copolymer chains self-assembled into a micelle-like structure consisting of a hydrophobic core and a hydrophilic PEG corona.

Micelle Formation and Its Structure. The ρ-ratio, $\rho = R_g/R_h$, provides additional information on the morphology of the scattering objects, with predicted values varying from 0.778 for spheres[49] to 1.16 for random coils.[50] The ρ-ratio values for $P(EO_2MA$-*co*-$EO_{45}MA)$ were 1.12 and 0.92 at 25 and 37 °C, respectively. The decrease in the value of the ρ-ratio above the CMT suggests a shift from a random coil configuration to a collapsed fractal structure that was denser, signifying that there was less trapped water than below the CMT when the polymer chains were fully hydrated.

Using the particle size data from SAXS measurements (Figure 3) and the relationship of radius with volume ($V = 4/3\pi r^3$), it is possible to estimate the volume of the individual collapsed copolymer chain and of the micelle. Considering that the volume of the micelle was comprised of the sum of all the collapsed copolymer chains above the CMT, and assuming the complete dehydration with no trapped water, we could estimate that the micellar aggregate was composed of approximately 1100 individual copolymer chains.

In terms of a microstructure based on the observed similarities with the micellization of PEO−PPO−PEO block copolymers, we propose that the POEGMA copolymer micelles were composed of a core of mostly dehydrated methacrylate backbone surrounded by a corona consisting of hydrophilic EO chains. This picture was confirmed by the results obtained with the solvatochromic dye that indicated a less polar solubilization environment, very similar to the ones reported for the PEO−PPO−PEO micelles. One remarkable finding of this study is, under isothermal conditions and close to their CMT, the macromolecular association forming copolymer micelles could take more than 20 h to reach completion when maintained at this temperature, although this phase transition process was accelerated by increasing the temperature. In order to ensure that this object is in thermodynamic equilibrium, different pathways were used (e.g., different heating rates, heating vs cooling processes, etc.) (please see Figure S6), and identical and superposable curves were always obtained, reinforcing the proposal of formation of an equilibrium micelle. The hysteresis between the heating and cooling processes (Figure S6B) may be assigned to the additional energy required to disrupt intrachain hydrogen bonding in the collapsed copolymer chains.

The CMT measurements suggested the formation of micelles at the same temperature as determined by other techniques, such as DLS, turbidimetry, and microcalorimetry. The maximum absorption wavelengths (λ_{max}) of Reichardt's

https://dx.doi.org/10.1021/acs.langmuir.0c02538
Langmuir 2020, 36, 15018−15029

Scheme 2. Effect of Collapsed Backbone Size and Length of the Longer Side Chain and Its Content on the Formation of POEGMA Aggregate in a Micelle or a Phase Separation[a]

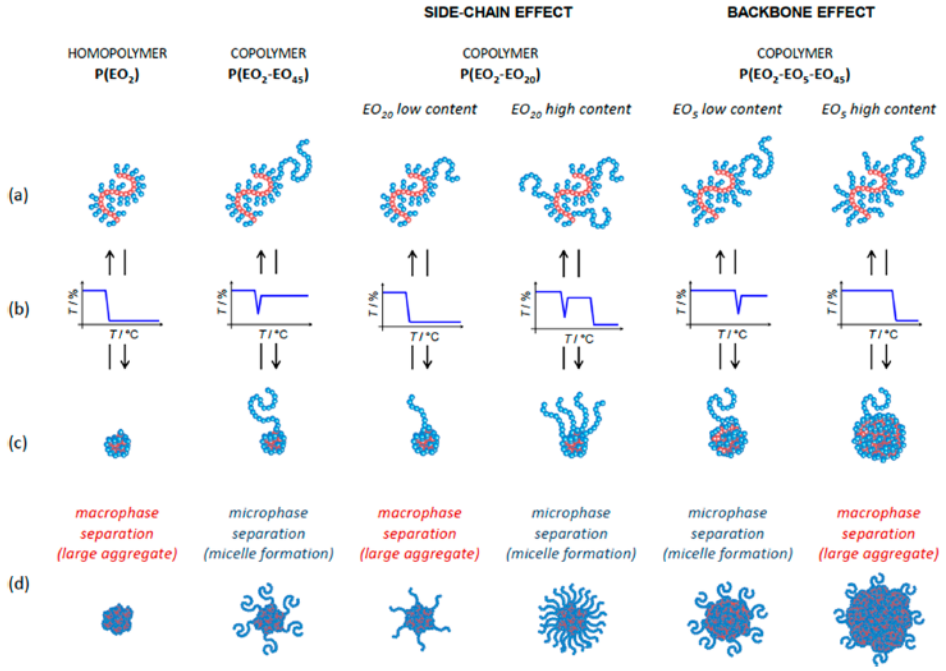

[a](a) Soluble polymer chains existing as unimers in solution below critical temperature; (b) transmittance curve profile through the phase transition; (c) individual polymer chain above a critical temperature; and (d) type of phase transition and a not-to-scale representation of the resulting particle (macroscopically phase-separated aggregate or micelle).

dye in aqueous P(EO_2MA-*co*-EO_{45}MA) solution above the CMT were close to values obtained for block copolymers and normal surfactant micelles,[38] indicating the same polarity for the POEGMA micelle. Moreover, the size of spherical micelles formed by P(EO_2MA-*co*-EO_{45}MA) (this work) was similar to that reported for different block copolymers[51,52] including the PEO−PPO−PEO block copolymers.[2] These similarities suggest potential applications for POEGMA aggregates that were similar to those reported for other block copolymers, such as controlled release systems, as reported by Magnusson et al.[53] using saline and kosmotrope solutions to trigger the release of trapped molecules.

POEGMA Micellization vs Phase Separation. In the present study, different profiles were determined for changes in turbidity upon heating, which are ascribed to different aggregation pathways. An abrupt decrease from 100% to 0% transmission indicated a macrophase separation, as displayed by the P(EO_2MA) homopolymer and P(EO_2MA-*co*-EO_5MA-*co*-EO_{45}MA) copolymers with EO_5MA side chains more than 20 mol %. In addition to the increasing cloud points, the incorporation of the longer EO_{45}MA side chain in the P(EO_2MA-*co*-EO_{45}MA) altered the phase behavior from macro- to microphase separation, the latter resulting in micelle formation. In this case, there is a transmittance reduction associated with the formation of a transient large aggregate structure that reorganized into a micellar structure, as reported previously.[24] Further copolymerization of P(EO_2MA-*co*-EO_5MA-*co*-EO_{45}MA) with EO_5MA side chains up to 10 mol % increased the micelle formation temperature but did not alter the type of aggregation. Above this content, the copolymer underwent a macroscopic phase separation when the critical temperature was exceeded. Micelle formation upon heating was observed in the majority of block copolymers,[54] and the present results highlight a convenient approach to prepare micelles using a random copolymer.

For the P(EO_2MA-*co*-EO_{20}MA) copolymers, a different behavior was observed for the compositions consisting of 5 and 10 mol % of EO_{20}MA, which displayed an unusual transmittance curve profile of double phase transitions at two critical temperatures. The first transition is associated with the micelle formation at a CMT, and the second transition (cloud point) corresponds to the macroscopic phase separation and at a higher temperature. In this case, the micelles are stable only within a narrow and tunable temperature range. Similar behavior has been previously reported for highly concentrated (100 mg mL^{-1}) POEGMA aqueous solution[25] but not at as low of a concentration as 5.0 mg mL^{-1} (this study). This rich behavior opens up a series of possible applications for these copolymers, where by heating or cooling, one could reversibly interchange dissolved polymer chains, their micelles, and macroscopic phase separation, associated with the incorporation/release of hydrophobic cargo or easy removal upon separation of immiscible phases.

It is interesting that calorimetry (in this case HSDSC), which is regarded as a very sensitive technique, is not conclusive in discriminating which different phase transitions

https://dx.doi.org/10.1021/acs.langmuir.0c02538
Langmuir 2020, 36, 15018−15029

take place, as evident from the results shown in Figures 4 and 5. Large enthalpy changes (endothermic process) were associated with the macroscopic phase separation when it occurred prior to micellization. Smaller, but still positive, values are associated with micellization, which relates to the partial dehydration of the backbone and EO units. However, the macroscopic phase separation observed after micellization involved smaller enthalpy changes, an indication that this event is associated with fewer, but crucial, dehydration processes (as the majority of the dehydration process occurs during the micellization) in addition to entropic effects mentioned earlier.

Structure Formed above the Critical Temperature. The particular behavior of POEGMA random copolymers is an effect related to both volume of collapsed backbone and EO side chain length. The present results show that it is possible to control the type of aggregate structure (micelle or phase separation) at a certain temperature by adjusting the content and length of EO side chains. In Scheme 2 we depict a pictorial representation of the different processes observed upon heating and the effect of collapsed backbone volume and of EO side chain length.

The different copolymer configurations in solution may be related to POEGMA hydration. At low temperature, although the MA backbone is less polar, copolymer solubility is promoted by the very favorable hydration of EO blocks. Therefore, the ratio between these components is important for the solution behavior of POEGMA in water. As temperature is increased, the EO blocks tend to become less hydrated, and as a consequence, polymer−polymer interaction begins to dominate over the polymer−water interactions.[18] The P(EO_2MA) homopolymer, the compound with the lowest EO content, phase separates at around 20 °C. The addition of 1 mol % EO_{45} increased the hydrophilicity of the copolymer, thereby increasing the phase separation temperature. The dehydration of EO groups reaches a condition where the micelles are formed upon heating, an indication of the partial dehydration of EO groups; however, there is still a significant copolymer−water interaction of the EO segments at the corona that ensures the aggregate solubility and stability.

By the addition of EO_5 to the copolymer structure, the phase transition temperature was increased. However, as more EO_5 was incorporated, the dehydration of EO groups did not lead to the formation of aggregates; instead, it led to macroscopic phase separation. From this observation, one could conclude that an increased ratio of EO to MA groups did not favor the balance of interactions necessary to form POEGMA micelles but, instead, the solubility of the copolymer yielding individual chains that phase separated at a higher temperature.

A more complex behavior was observed when comparing copolymers with increasing amounts of EO_{20} side chains. In this case, at lower EO_{20} contents, macroscopic phase separation occurred, with no micelle formation. At higher EO_{20} contents, micelles were formed upon heating and macroscopic phase separation occurred at higher temperatures, confirming that they were consecutive phase transitions.

Overall, whether micelles or macroscopic phase separation is observed will depend not only on the temperature but more importantly on the EO groups remaining hydrated to form the micelle corona; otherwise, phase separation will occur. A similar result was reported by Sezonenko and co-workers,[46] for an arm star block copolymer with a hydrophobic dehydrated core and hydrophilic outer surface capable of forming micelle, whereas the opposite arm block, with a hydrophilic core and dehydrated hydrophobic at the periphery, formed a precipitated aggregate in water upon heating.

This sequence of events (micelle formation and macroscopic phase separation) and the dependency on the ratio of polar and apolar groups are also observed for PEO−PPO−PEO copolymers, for the latter represented by the EO/PO ratio. The only major difference is that macroscopic phase separation for PEO−PPO−PEO copolymers is mostly associated with the formation of mesophases, a typical surfactant-like behavior due to their amphiphilic structure.[2,43] For these POEGMA random copolymers, however, no liquid crystalline structure was detected in the phase-separated phases.

CONCLUSIONS

This study describes a detailed energetic and structural characterization of the phase transitions displayed by different compositions of aqueous POEGMA copolymers solutions. The results demonstrated that the collapsed backbone volume, EO side chain length, and its content in the copolymer composition determined the temperature-induced transitions, leading to micelle formation or macroscopic phase separation while, in some cases, the two events were observed consecutively. These POEGMA micelles resembled those formed by other copolymers, most notably PEO−PPO−PEO copolymers; however, our study indicated that micelles could be formed by random copolymers, which are typically easier to synthesize. Therefore, for this family of copolymers, reversible-deactivation radical polymerization could be used to tailor copolymer architecture envisaging specific aggregation states at certain temperatures and a specific sequence of phase transitions. In addition, the reversible transformation of the state of the polymer solution upon heating and cooling could allow for the control over properties, such as incorporation/release of hydrophobic molecules (e.g., drugs, fragrances, pesticides, catalyst) or dissolution/recovery by phase separation of potential relevance for a variety of processes.

ASSOCIATED CONTENT

Supporting Information

The Supporting Information is available free of charge at https://pubs.acs.org/doi/10.1021/acs.langmuir.0c02538.

Detailed procedure for copolymers syntheses, additional data and procedure information for DLS and SAXS, and extra figures (PDF)

AUTHOR INFORMATION

Corresponding Author

Watson Loh − *Institute of Chemistry, University of Campinas, Campinas, São Paulo 13084-970, Brazil;* orcid.org/0000-0002-8049-3321; Email: wloh@iqm.unicamp.br

Authors

Rafael Pires-Oliveira − *Institute of Chemistry, University of Campinas, Campinas, São Paulo 13084-970, Brazil; Department of Chemical Engineering and Waterloo Institute of Nanotechnology, University of Waterloo, Waterloo, Ontario, Canada N2L 3G1;* orcid.org/0000-0003-1855-5322

Juntao Tang − *Department of Chemical Engineering and Waterloo Institute of Nanotechnology, University of Waterloo, Waterloo, Ontario, Canada N2L 3G1; College of Chemistry and Chemical Engineering, Central South University,*

https://dx.doi.org/10.1021/acs.langmuir.0c02538
Langmuir 2020, 36, 15018−15029

Changsha, Hunan, China; orcid.org/0000-0002-7398-3605

Ana Maria Percebom − *Department of Chemistry, Pontifical Catholic University of Rio de Janeiro, Gávea, Rio de Janeiro 22541-041, Brazil;* orcid.org/0000-0002-1511-8656

Cesar L. Petzhold − *Institute of Chemistry, Federal University of Rio Grande do Sul, Porto Alegre, Rio Grande do Sul 90040-060, Brazil*

Kam C. Tam − *Department of Chemical Engineering and Waterloo Institute of Nanotechnology, University of Waterloo, Waterloo, Ontario, Canada N2L 3G1;* orcid.org/0000-0002-7603-5635

Complete contact information is available at: https://pubs.acs.org/10.1021/acs.langmuir.0c02538

Notes

The authors declare no competing financial interest.

■ ACKNOWLEDGMENTS

We thank Julia B. Sabadini for DLS measurements in the ALV equipment. R.P.-O. thanks the Brazilian Agencies CAPES and CNPq for the Science Without Borders Program scholarship (project A128/2013) and a Ph.D. fellowship (159080/2013-4), respectively. Financial support from FAPESP through project 2015/254060-5 and CNPq in the form of a productivity grant to W.L. is also acknowledged. We gratefully acknowledge the Brazilian Synchrotron Light Laboratory (LNLS) for the allocation of SAXS beamtime.

■ REFERENCES

(1) Li, L.; Raghupathi, K.; Song, C.; Prasad, P.; Thayumanavan, S. Self-assembly of random copolymers. *Chem. Commun.* **2014**, *50*, 13417−13432.

(2) Loh, W. Block Copolymer Micelles. In *Encyclopedia of Colloid and Surface Science*; Hubbard, A., Ed.; Marcel Dekker: New York, 2002; pp 802−813.

(3) Cayre, O. J.; Chagneux, N.; Biggs, S. Stimulus responsive core-shell nanoparticles: Synthesis and applications of polymer based aqueous systems. *Soft Matter* **2011**, *7*, 2211−2234.

(4) Weber, C.; Hoogenboom, R.; Schubert, U. S. Temperature responsive bio-compatible polymers based on poly(ethylene oxide) and poly(2-oxazoline)s. *Prog. Polym. Sci.* **2012**, *37*, 686−714.

(5) Warren, N. J.; Armes, S. P. Polymerization-induced self-assembly of block copolymer nano-objects via RAFT aqueous dispersion polymerization. *J. Am. Chem. Soc.* **2014**, *136*, 10174−10185.

(6) Xu, J.; Li, J.; Yang, Y.; Wang, K.; Xu, N.; Li, J.; Liang, R.; Shen, L.; Xie, X.; Tao, J.; Zhu, J. Block copolymer capsules with structure-dependent release behavior. *Angew. Chem., Int. Ed.* **2016**, *55*, 14633−14637.

(7) Yang, H.; Zhao, X.; Zhang, X.; Ma, L.; Wang, B.; Wei, H. Optimization of bioreducible micelles self-assembled from amphiphilic hyperbranched block copolymers for drug delivery. *J. Polym. Sci., Part A: Polym. Chem.* **2018**, *56*, 1383−1394.

(8) Zhang, Y.; Wang, Z.; Matyjaszewski, K.; Pietrasik, J. Evolution of Morphology of POEGMA-*b*-PBzMA Nano-Objects Formed by PISA. *Macromol. Rapid Commun.* **2019**, *40*, 1800331.

(9) De France, K. J.; Babi, M.; Vapaavuori, J.; Hoare, T.; Moran-Mirabal, J.; Cranston, E. D. 2.5D Hierarchical Structuring of Nanocomposite Hydrogel Films Containing Cellulose Nanocrystals. *ACS Appl. Mater. Interfaces* **2019**, *11*, 6325−6335.

(10) Li, L.; Raghupathi, K.; Song, C.; Prasad, P.; Thayumanavan, S. Self-assembly of random copolymers. *Chem. Commun.* **2014**, *50*, 13417−13432.

(11) Galli, G.; Martinelli, E. Amphiphilic Polymer Platforms: Surface Engineering of Films for Marine Antibiofouling. *Macromol. Rapid Commun.* **2017**, *38*, 1600704.

(12) Jiang, Z.; Liu, H.; He, H.; Ribbe, A. E.; Thayumanavan, S. Blended Assemblies of Amphiphilic Random and Block Copolymers for Tunable Encapsulation and Release of Hydrophobic Guest Molecules. *Macromolecules* **2020**, *53*, 2713−2723.

(13) Han, S.; Hagiwara, M.; Ishizone, T. Synthesis of thermally sensitive water-soluble polymethacrylates by living anionic polymerizations of oligo(ethylene glycol) methyl ether methacrylates. *Macromolecules* **2003**, *36*, 8312−8319.

(14) Zhao, B.; Li, D.; Hua, F.; Green, D. R. Synthesis of thermosensitive water-soluble polystyrenics with pendant methoxyoligo(ethylene glycol) groups by nitroxide-mediated radical polymerization. *Macromolecules* **2005**, *38*, 9509−9517.

(15) Lutz, J. F.; Hoth, A. Preparation of ideal PEG analogues with a tunable thermosensitivity by controlled radical copolymerization of 2-(2-methoxyethoxy)ethyl methacrylate and oligo(ethylene glycol) methacrylate. *Macromolecules* **2006**, *39*, 893−896.

(16) Yamamoto, S. I.; Pietrasik, J.; Matyjaszewski, K. The effect of structure on the thermoresponsive nature of well-defined poly(oligo-(ethylene oxide) methacrylates) synthesized by ATRP. *J. Polym. Sci., Part A: Polym. Chem.* **2008**, *46*, 194−202.

(17) Lutz, J. F. Polymerization of oligo(ethylene glycol) (meth)-acrylates: Toward new generations of smart biocompatible materials. *J. Polym. Sci., Part A: Polym. Chem.* **2008**, *46*, 3459−3470.

(18) Kronberg, B.; Holmberg, K.; Lindman, B. Surfactants and Polymers Containing Oxyethylene Groups Show a Complex Behavior. *Surface Chemistry of Surfactants and Polymers*, 1st ed.; John Wiley & Sons: Chichester, U.K., 2014; pp 137−152.

(19) Lutz, J. F.; Akdemir, Ö.; Hoth, A. Point by point comparison of two thermosensitive polymers exhibiting a similar LCST: Is the age of poly(NIPAM) over? *J. Am. Chem. Soc.* **2006**, *128*, 13046−13047.

(20) Alejo, T.; Prieto, M.; García-Juan, H.; Andreu, V.; Mendoza, G.; Sebastián, V.; Arruebo, M. A facile method for the controlled polymerization of biocompatible and thermoresponsive oligo-(ethylene glycol) methyl ether methacrylate copolymers. *Polym. J.* **2018**, *50*, 203−211.

(21) Ma, H.; Hyun, J.; Stiller, P.; Chilkoti, A. Non-fouling" oligo(ethylene glycol)- functionalized polymer brushes synthesized by surface-initiated atom transfer radical polymerization. *Adv. Mater.* **2004**, *16*, 338−341.

(22) Cooperstein, M. A.; Canavan, H. E. Assessment of cytotoxicity of (*N*-isopropyl acrylamide) and poly(*N*-isopropyl acrylamide)-coated surfaces. *Biointerphases* **2013**, *8*, 19.

(23) De France, K. J.; Badv, M.; Dorogin, J.; Siebers, E.; Panchal, V.; Babi, M.; Moran-Mirabal, J.; Lawlor, M.; Cranston, E. D.; Hoare, T. Tissue response and biodistribution of injectable cellulose nanocrystal composite hydrogels. *ACS Biomater. Sci. Eng.* **2019**, *5*, 2235−2246.

(24) Peng, B.; Grishkewich, N.; Yao, Z.; Han, X.; Liu, H.; Tam, K. C. Self-assembly behavior of thermoresponsive oligo(ethylene glycol) methacrylates random copolymer. *ACS Macro Lett.* **2012**, *1*, 632−635.

(25) Zhang, B.; Tang, H.; Wu, P. In depth analysis on the unusual multistep aggregation process of oligo(ethylene glycol) methacrylate-based polymers in water. *Macromolecules* **2014**, *47*, 4728−4737.

(26) Ge, Z.; Wang, D.; Zhou, Y.; Liu, H.; Liu, S. Synthesis of organic/inorganic hybrid quatrefoil-shaped star-cyclic polymer containing a polyhedral oligomeric silsesquioxane core. *Macromolecules* **2009**, *42*, 2903−2910.

(27) Oh, J. K.; Min, K.; Matyjaszewski, K. Preparation of poly(oligo(ethylene glycol) monomethyl ether methacrylate) by homogeneous aqueous AGET ATRP. *Macromolecules* **2006**, *39*, 3161−3167.

(28) Lutz, J. F.; Weichenhan, K.; Akdemir, Ö.; Hoth, A. About the phase transitions in aqueous solutions of thermoresponsive copolymers and hydrogels based on 2-(2-methoxyethoxy)ethyl methacrylate and oligo(ethylene glycol) methacrylate. *Macromolecules* **2007**, *40*, 2503−2508.

(29) Pietsch, C.; Fijten, M. W. M.; Lambermont-Thijs, H. M. L.; Hoogenboom, R.; Schubert, U. S. Unexpected reactivity for the RAFT copolymerization of oligo(ethylene glycol) methacrylates. *J. Polym. Sci., Part A: Polym. Chem.* **2009**, *47*, 2811−2820.
(30) Wang, J. S.; Matyjaszewski, K. Controlled/"living" radical polymerization. Atom transfer radical polymerization in the presence of transition-metal complexes. *J. Am. Chem. Soc.* **1995**, *117*, 5614−5615.
(31) Destarac, M. Industrial development of reversible-deactivation radical polymerization: is the induction period over? *Polym. Chem.* **2018**, *9*, 4947−4967.
(32) Simakova, A.; Averick, S. E.; Konkolewicz, D.; Matyjaszewski, K. Aqueous ARGET ATRP. *Macromolecules* **2012**, *45*, 6371−6379.
(33) Liu, M.; Leroux, J. C.; Gauthier, M. A. Conformation−function relationships for the comb-shaped polymer pOEGMA. *Prog. Polym. Sci.* **2015**, *48*, 111−121.
(34) Chen, H.; Li, J.; Ding, Y.; Zhang, G.; Zhang, Q.; Wu, C. Folding and unfolding of individual PNIPAM-*g*-PEO copolymer chains in dilute aqueous solutions. *Macromolecules* **2005**, *38*, 4403−4408.
(35) Halperin, A.; Kröger, M.; Winnik, F. M. Poly(*N*-isopropylacrylamide) Phase Diagrams: Fifty Years of Research. *Angew. Chem., Int. Ed.* **2015**, *54*, 15342−15367.
(36) Zhou, Z.; Chu, B. Anomalous micellization behavior and composition heterogeneity of a triblock ABA copolymer of (A) ethylene oxide and (B) propylene oxide in aqueous solution. *Macromolecules* **1988**, *21*, 2548−2554.
(37) Reichardt, C. Solvatochromic dyes as solvent polarity indicators. *Chem. Rev.* **1994**, *94*, 2319−2358.
(38) Lopes, J. R.; Loh, W. Investigation of self-assembly and micelle polarity for a wide range of ethylene oxide−propylene oxide−ethylene oxide block copolymers in water. *Langmuir* **1998**, *14*, 750−756.
(39) Beaucage, G. Small-angle scattering from polymeric mass fractals of arbitrary mass-fractal dimension. *J. Appl. Crystallogr.* **1996**, *29*, 134−146.
(40) Loh, W.; Teixeira, L. A. C.; Lee, L. T. Isothermal Calorimetric Investigation of the Interaction of Poly(*N*-isopropylacrylamide) and Ionic Surfactants. *J. Phys. Chem. B* **2004**, *108*, 3196−3201.
(41) Beezer, A. E.; Loh, W.; Mitchell, J. C.; Royall, P. G.; Smith, D. O.; Tute, M. S.; Armstrong, J. K.; Chowdhry, B. Z.; Leharne, S. A.; Eagland, D.; Crowtherg, N. J. An Investigation of Dilute Aqueous Solution Behavior of Poly(oxyethylene) + Poly(oxypropylene) + Poly(oxyethylene) Block Copolymers. *Langmuir* **1994**, *10*, 4001−4005.
(42) Gaisford, S.; Beezer, A. E.; Mitchell, J. C.; Loh, W.; Finnie, J. K.; Williams, S. J. Diode-array UV spectrometric evidence for a concentration dependent phase transition in dilute aqueous solutions of pluronic F87 (poloxamer 237). *J. Chem. Soc., Chem. Commun.* **1995**, *18*, 1843−1844.
(43) Percebom, A. M.; Barbosa, L. R. S.; Itri, R.; Loh, W. How Does the Ethoxylated Grafting of Polyelectrolytes Affect the Self-Assembly of Polyanion−Cationic Surfactant Complex Salts? *Langmuir* **2014**, *30*, 11493−11503.
(44) Becer, C. R.; Hahn, S.; Fijten, M. W. M.; Thijs, H. M. L.; Hoogenboom, R.; Schubert, U. S. Libraries of methacrylic acid and oligo(ethylene glycol) methacrylate copolymers with LCST behavior. *J. Polym. Sci., Part A: Polym. Chem.* **2008**, *46*, 7138−7147.
(45) Zhang, Q.; Weber, C.; Schubert, U. S.; Hoogenboom, R. Thermoresponsive polymers with lower critical solution temperature: From fundamental aspects and measuring techniques to recommended turbidimetry conditions. *Mater. Horiz.* **2017**, *4*, 109−116.
(46) Sezonenko, T.; Qiu, X. P.; Winnik, F. M.; Sato, T. Dehydration, micellization, and phase separation of thermosensitive polyoxazoline star block copolymers in aqueous solution. *Macromolecules* **2019**, *52*, 935−944.
(47) Löf, D.; Schillén, K.; Loh, W.; Olofsson, G. A Calorimetry and Light Scattering Study of the Formation and Shape Transition of Mixed Micelles of $EO_{20}PO_{68}EO_{20}$ Triblock Copolymer (P123) and Nonionic Surfactant ($C_{12}EO_6$). *J. Phys. Chem. B* **2007**, *111*, 5911−5920.
(48) Stanzione, F.; Jayaraman, A. Hybrid atomistic and coarse-grained molecular dynamics simulations of polyethylene glycol (PEG) in explicit water. *J. Phys. Chem. B* **2016**, *120*, 4160−4173.
(49) Brewer, A. K.; Striegel, A. M. Characterizing the size, shape, and compactness of a polydisperse prolate ellipsoidal particle via quadruple-detector hydrodynamic chromatography. *Analyst* **2011**, *136*, 515−519.
(50) ter Meer, H. U.; Burchard, W.; Wunderlich, W. Quasi-elastic light scattering from polymethylmethacrylate in a good and a theta solvent. *Colloid Polym. Sci.* **1980**, *258*, 675−684.
(51) Holder, S. J.; Sommerdijk, N. A. J. M. New micellar morphologies from amphiphilic block copolymers: Disks, toroids and bicontinuous micelles. *Polym. Chem.* **2011**, *2*, 1018−1028.
(52) Gaucher, G.; Dufresne, M. H.; Sant, V. P.; Kang, N.; Maysinger, D.; Leroux, J. C. Block copolymer micelles: Preparation, characterization and application in drug delivery. *J. Controlled Release* **2005**, *109*, 169−188.
(53) Magnusson, J. P.; Khan, A.; Pasparakis, G.; Saeed, A. O.; Wang, W.; Alexander, C. Ion-sensitive "isothermal" responsive polymers prepared in water. *J. Am. Chem. Soc.* **2008**, *130*, 10852−10853.
(54) Hua, F.; Jiang, X.; Zhao, B. Temperature-induced self-association of doubly thermosensitive diblock copolymers with pendant methoxytris(oxyethylene) groups in dilute aqueous solutions. *Macromolecules* **2006**, *39*, 3476−3479.

https://dx.doi.org/10.1021/acs.langmuir.0c02538
Langmuir 2020, 36, 15018−15029

Supporting Information

Effect of molecular architecture and composition on the aggregation pathways of POEGMA random copolymers in water

*Rafael Pires-Oliveira[1,2], Juntao Tang[2,3], Ana Maria Percebom[4], Cesar L. Petzhold[5], Kam C. Tam[2], and Watson Loh[1]**

1. Institute of Chemistry, University of Campinas, Campinas, Brazil

2. Department of Chemical Engineering and Waterloo Institute of Nanotechnology, University of Waterloo, Waterloo, Canada

3. College of Chemistry and Chemical Engineering, Central South University, Changsha, China

4. Department of Chemistry, Pontifical Catholic University of Rio de Janeiro, Rio de Janeiro, Brazil

5. Institute of Chemistry, Federal University of Rio Grande do Sul, Porto Alegre, Brazil

Corresponding Author

*wloh@iqm.unicamp.br

Experimental details

Materials

Di(ethylene glycol) methyl ether methacrylate (EO_2MA) (M_n = 188 g mol^{-1}) and oligo(ethylene glycol) methyl ether methacrylate (EO_nMA, n = 5, 20 and 45 EO units, M_n = 300, 950 and 2,080 g mol^{-1}, respectively) (from Sigma-Aldrich) were passed through an alumina column prior to use, to remove inhibitors. Copper(I) bromide (CuBr, Aldrich, 99.999%), copper(II) bromide ($CuBr_2$, Aldrich, 99.999%), N,N,N′,N″,N″-pentamethyldiethylenetriamine (PMDETA, Aldrich, 99%), tris(2-pyridylmethyl)amine (TPMA, Aldrich, 98%), tin(II) 2-ethylhexanoate ($Sn(EH)_2$, Aldrich, ≥92.5%), ethyl α-bromoisobutyrate (EBiB, Aldrich, 98%), and ethanol (Aldrich, reagent grade), were used without further purification. Propargyl 2-bromoisobutyrate (PBiB) was kindly supplied by Dr. Hairong Wang (Soochow University, China) synthesized following the method described elsewhere[1], and characterized by NMR spectroscopy (Figure S1).

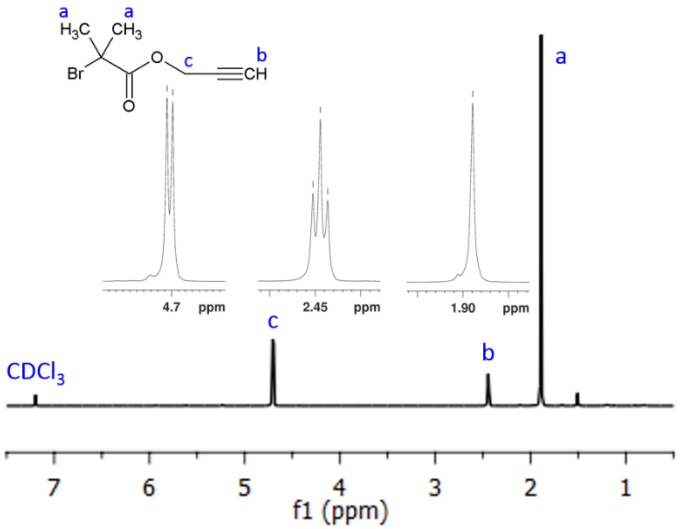

Figure S1. ^{1}H NMR spectrum of the synthesized propargyl 2-bromoisobutyrate (PBiB) ($CDCl_3$, δ, ppm, TMS, 300 MHz): 4.7 (2H, –CH_2O), 2.4 (1H, –C≡CH), and 1.9 (6H, –C(CH_3)$_2$Br).

Copolymers synthesis

All copolymers were synthesized using the atom transfer radical polymerization (ATRP) method according to previous reports[2–4] with modifications. Typical procedures for the synthesis conducted by normal ATRP and by activators regenerated by electron transfer (ARGET) ATRP are described in the sequence.

Normal ATRP. A Schlenk flask was charged with CuBr (2 equiv) and PMDETA (4 equiv), sealed with a septum and purged with argon for 30 minutes. A degassed mixture of the monomers as described in Table 1 (please refer to the full article) (100 equiv total), and ethanol (monomers/ethanol ~1:1.25 v/v) was added through the septum with a double-tipped needle into the flask and purged once more with argon for 30 min. The reaction system was heated to 60 °C and polymerization was started by adding PBiB (1 equiv).

ARGET ATRP. A Schlenk flask was charged with monomers as described in Table 1 (please refer to the full article) (100 equiv total), $CuBr_2$ (0.05 equiv), TPMA (0.2 equiv), $Sn(EH)_2$ (0.1 equiv) and ethanol (monomers/ethanol ~1:1.25 v/v). *N*,*N*-dimethylformamide (DMF) (Synth) (200 μL) was added to the mixture as a reference for posterior ^{1}H NMR analysis. The solution was purged with argon for 30 minutes and the reaction system was heated to 60 °C. Polymerization was started by adding EBiB (1 equiv).

The reactions were stopped by removing the stopper from the flask, thereby exposing the catalyst to air and turning off the heater. The reacted mixtures were purified by dialysis against cold water for seven days (dialysis membrane molecular weight cutoff 12,000 Da, VWR Canada). Following, the final product was collected after freeze-drying.

Monomer conversion determination

The monomer conversion was calculated by the ^{1}H NMR spectra of duplicate reaction samples. These spectra were integrated using TMS (δ = 0.0 ppm) and DMF (δ = 8.02 ppm, assigned to one H from $(CH_3)_2NC\mathbf{H}O$) as reference to normalize signals. Monomer conversion was then calculated by the Equation S1, using the integrated signal at 6.14–5.59 ppm, assigned to the vinylic H of the monomers ($C\mathbf{H}_2$=$C(CH_3)COOR$), as shown in Table S1.

$$conversion = \left(1 - \frac{\int VH_{final}}{\int VH_{t=0}}\right) \qquad \text{Equation S1}$$

where *VH* is the integrated signal of vinylic H of the monomers at the end (VH_{final}) and at the start ($VH_{t=0}$) of the polymerization.

Dynamic light scattering measurements

We carried out dynamic light scattering (DLS) measurements of POEGMA aqueous solutions at different temperatures in two different DLS instruments. The copolymer P(EO_2MA-*co*-EO_{45}MA) was analyzed in a Zetasizer Nano ZS (Malvern Instruments, Worcestershire, UK), equipped with a He-Ne laser red (λ = 632.8 nm). Samples of

1.0 mg mL^{-1} aqueous P(EO_2MA-*co*-$EO_{45}MA$) solutions were heated or cooled automatically by the integrated temperature controller and an equilibration time of 6 min was set for each temperature. The scattering intensities were detected at an angle of 173° after an equilibration time of 120 s. Prior to the experiments, all the solutions were filtered through a 0.45 μm disposable filter.

Table S1. Monomer conversion calculated by the integrated signal of the vinylic H assigned to the monomers at the end and start of the polymerization.

		vinylic H integrated signal		
Entry	Polymer	$VH_{t=0}$	VH_{final}	Conversion
1	P(MEO_2MA)	10.28155	1.24290	0.88
7	P(EO_2MA-*co*-$EO_{20}MA$) 99:01	8.95210	0.27245	0.97
8	P(EO_2MA-*co*-$EO_{20}MA$) 95:05	9.12605	0.26570	0.97
9	P(EO_2MA-*co*-$EO_{20}MA$) 90:10	8.90555	0.67065	0.92

Size distributions were analyzed by the equipment's software (Zetasizer Software 7.11) using inverse Laplace transformation method and Non-Negative Least Squares (NNLS) algorithms. The apparent hydrodynamic radius (R_h) values were number-weighted using the d*n*/d*c* for P(EO_2MA-*co*-$EO_{45}MA$) in water at 25 °C (7.445×10^{-2} mL g^{-1}) determined using a Brookhaven BI-DNDC differential refractometer. Additional DLS measurements were performed on a CGS-3-based compact goniometer system (ALV-GmbH, Langen, Germany) equipped with a detection system in a pseudo−cross-geometry, with a 22 mW He−Ne laser (λ = 632.8 nm) and an ALV 7004 multi-tau correlator. Samples of 1.0 mg mL^{-1} aqueous POEGMA solutions (please see Table S2) were prepared, filtered through a 0.22 μm disposable syringe filter, and placed in capped test tubes previously washed with Hellmanex 3%. The scattering intensities were detected at an angle of 90° and cis-Decalin was used as the refractive index-matching liquid. The temperature was controlled at 20.00, 25.00, 37.00 or 45.00 ± 0.01 °C. In both cases, the R_h was calculated according to the Stokes–Einstein equation:

$$R_h = \frac{k_B T}{6\pi\eta D_{app}} \qquad \text{Equation S2}$$

where k_B is the Boltzmann constant, T is the absolute temperature, η is the viscosity of the solvent (water) and D_{app} is the apparent diffusion coefficient.

The DLS data of aqueous POEGMA solutions obtained on the ALV instrument (Table S2) show unimer size with a range of R_h from approximately 5 nm to 20 nm when the

POEGMA copolymer is fully solubilized below the phase transition temperature, then upon heating above the critical micelle temperature (CMT) an large aggregate with a R_h around 50 nm to 180 nm, that rearranges with time into smaller aggregates, likewise noticed for the P(EO_2MA-*co*-EO_{45}MA) (entry 2) as shown in Figure 2B (please refer to the full article). Above the lower critical solution temperatures (LCST), when displayed by the POEGMA copolymer, macroscopic phase separation occurred with eventual settling of a concentrated white gel phase rich in copolymer when the solution was maintained above this temperature, as seen in the Figure S4. Overall, these results confirm the behavior already discussed in the manuscript: the copolymers appear as non-aggregated molecules at low temperature and, upon increasing temperature, some form well defined micelles at a certain CMT, while at higher temperatures macroscopic phase separation is observed, associated to a LCST. Please note that, due to the kinetics of the micelle formation, the most appropriate value for the micelle particle size is the R_h value measured after a longer equilibration time, i.e. after 48 hours in these cases.

Small Angle X-ray scattering measurements

Small angle X-ray scattering (SAXS) measurements were performed at the SAXS1 beamline of the Brazilian Synchrotron Laboratory (LNLS) at the Brazilian Center for Research in Energy and Materials (CNPEM), in Campinas, Brazil. The 5.0 mg mL^{-1} aqueous copolymer solution was added to a cell with two flat mica windows under water-bath temperature control. Experiments were performed at 25 and 37 °C and the samples were kept at this temperature for 1 h prior to measurements. The distance between the sample holder and detector was 912 mm, and the X-ray wavelength was λ = 1.550 Å. Fit2D software[5] was used to integrate CCD images and to subtract parasitic background and solvent scattering (blank) whenever necessary. The resulting scattering data are presented as plots of intensity as a function of the scattering vector (q), where $q = 4\pi \sin(\theta/2)/\lambda$, θ being the scattering angle and λ being the wavelength.

The software SASfit 0.92.3 was used to apply the Gaussian model (Equation S3) (incorporated to its library) to the SAXS data obtained at 25 °C.[6,7] The Beaucage method[8] was employed to fit the SAXS data obtained at 37 °C. This data was fitted using a multi-level unified model (Equation S4) implemented in the Irena package 2.57[9–11] running on Igor Pro 6.36 software[12]. The best fittings for all curves are presented in Figure 3 (please see full article).

$$I(q) = I_0 2 \frac{\exp\left(-q^2 R_g^2\right) + q^2 R_g^2 - 1}{(q^2 R_g^2)^2} \qquad \text{Equation S3}$$

where $I(q)$ is the scattering intensity, I_0 is the forward scattering for $q = 0$, and R_g is the gyration radius.

$$I(q) = \sum_{i=1}^{n} \left[G_i \exp\left(\frac{-q^2 R_{g_i}^2}{3}\right) + B_i \exp\left(\frac{-q^2 R_{g_{(i+1)}}^2}{3}\right) \times \left\{ \frac{\left[\operatorname{erf}\left(\frac{q\, R_{g_i}}{\sqrt{6}}\right)\right]^3}{q} \right\}^{P_i} \right] \quad \text{Equation S4}$$

where n is the number of structural levels observed in the scattering data, G is the Guinier prefactor, and B is a prefactor specific to the power-law scattering, which is specified by the exponent P.

Table S2. Critical micelle temperature (CMT), lower critical solution temperatures (LCST), particle size and polydispersity index (PDI) of aqueous POEGMA solutions measured on an ALV instrument after 1, 24 and 48 h of equilibration at the specified temperature.

		$EO_2MA/EO_{20}MA/$ $EO_5MA/EO_{45}MA$	CMT / °C	LCST / °C	T* / °C	R_h (PDI) / nm		
						1 h	24 h	48 h
Entry 1	P(EO_2MA)	100/–/–/–	–	20.0	20	**10.4** (0.6)		
Entry 2	P(EO_2MA-*co*-$EO_{45}MA$)	99/–/–/1	26.5	–	25	**20.8** (0.5)		
					37	**45.9** (0.3)	n.d.	n.d.
Entry 3	P(EO_2MA-*co*-EO_5MA-*co*-$EO_{45}MA$)	94/–/5/1	31.0	–	25	**9.7** (0.4)		
					45	**75.0** (0.1)	**73.6** (0.1)	**54.6** (0.2)
Entry 4	P(EO_2MA-*co*-EO_5MA-*co*-$EO_{45}MA$)	89/–/10/1	34.5	–	25	**7.8** (0.6)		
					45	**47.6** (0.08)	**143.9** (0.04)	**92.2** (0.2)
Entry 5	P(EO_2MA-*co*-EO_5MA-*co*-$EO_{45}MA$)	79/–/20/1	–	40.5	25	**7.3** (0.5)		
Entry 6	P(EO_2MA-*co*-EO_5MA-*co*-$EO_{45}MA$)	69/–/30/1	–	46.0	25	**8.5** (0.5)		
Entry 7	P(EO_2MA-*co*-$EO_{20}MA$)	99/1/–/–	–	21.5	20	**5.0** (0.4)		
Entry 8	P(EO_2MA-*co*-$EO_{20}MA$)	95/5/–/–	32.0	47.5	25	**9.3** (0.5)		
					45	**13.7** (0.3)	**115.5** (0.2)	**111.6** (0.4)
Entry 9	P(EO_2MA-*co*-$EO_{20}MA$)	90/10/–/–	39.0	53.5	25	**7.9** (0.6)		

*Temperature of DLS measurement. n.d. = not determined.

Extra figures

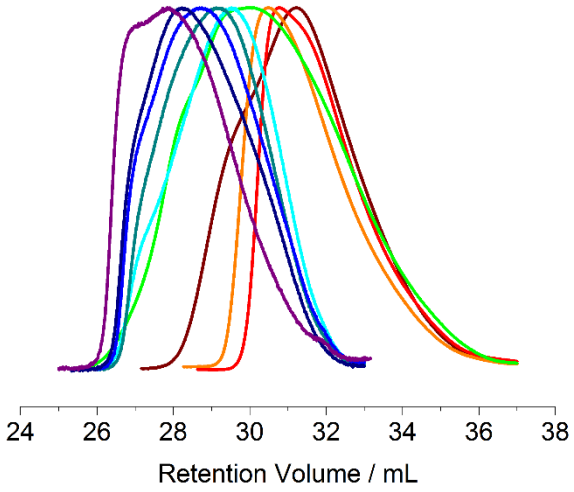

Figure S2. Normalized GPC traces of the (■) P(EO_2MA) homopolymer, P(EO_2MA-*co*-EO_5MA-*co*-EO_{45}MA) copolymers with [EO_2MA]:[EO_5MA]:[EO_{45}MA] molar ratios of (■) 99:0:1, (■) 94:5:1, (■) 89:10:1, (■) 79:20:1, and (■) 69:30:1, and P(EO_2MA-*co*-EO_{20}MA) copolymers with [EO_2MA]:[EO_{20}MA] molar ratios of (■) 99:1, (■) 95:5, and (■) 90:10.

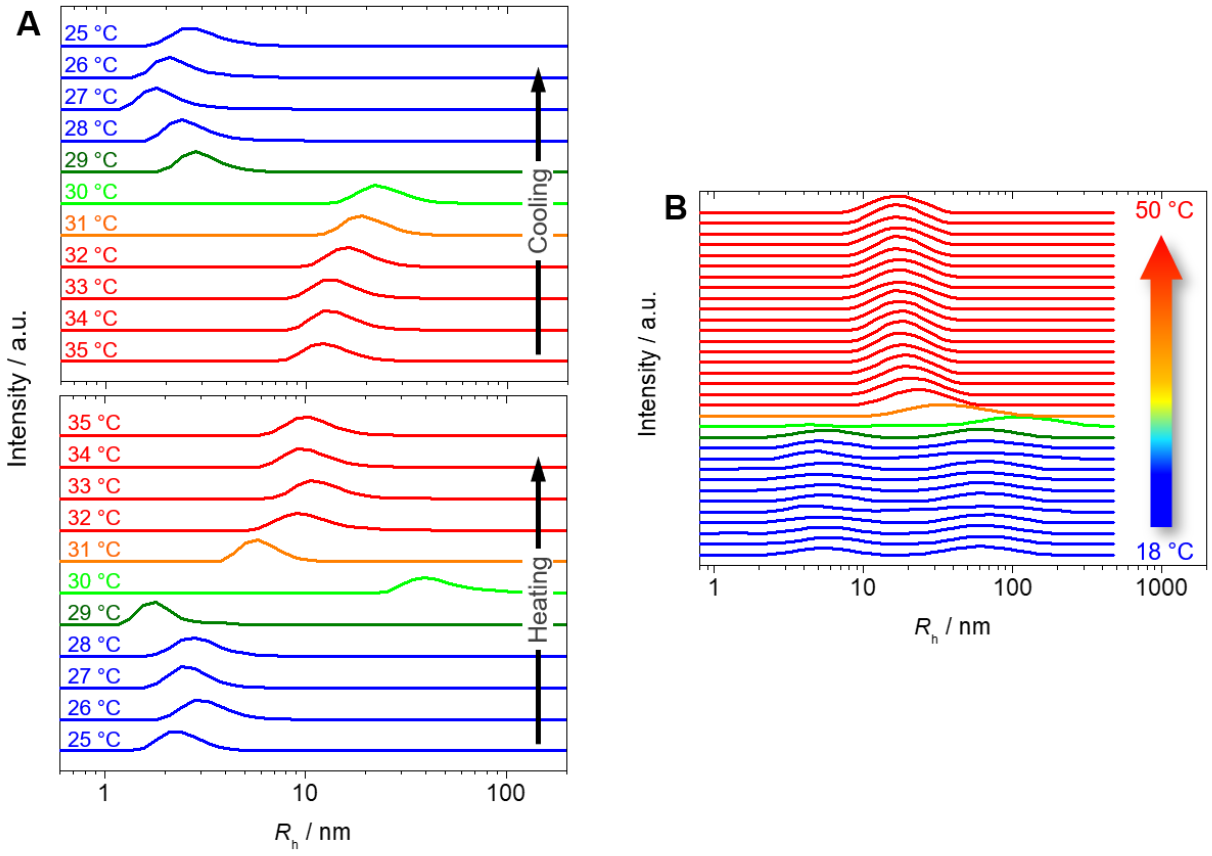

Figure S3. (A) Number-weighted and (B) intensity distributions of R_h as a function of temperature from DLS measurements of the P(EO_2MA-*co*-EO_{45}MA) 99:1 copolymer during heating and cooling processes. Measurements were performed at θ = 173°, from 18 to 50 °C. Data points are colored in blue (below CMT), green (at CMT) and red (above CMT).

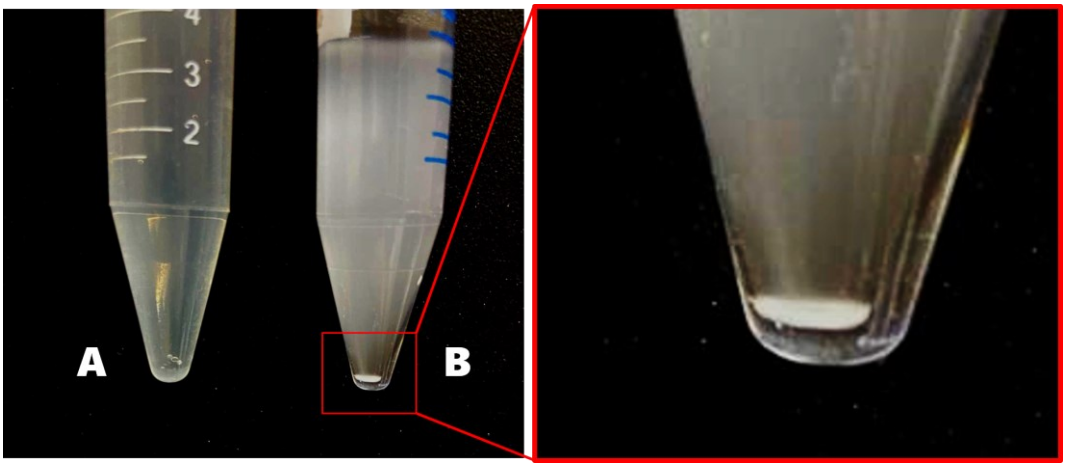

Figure S4. Photographs of 1.0 mg mL^{-1} aqueous POEGMA solutions at 45 °C for 48 h. (A) P(EO_2MA-*co*-EO_{45}MA) 99:1 and (B) P(MEO_2MA). In the right-side image a zoom showing the settling of the P(MEO_2MA) above its LCST, which is not observed in copolymers solutions above their CMT.

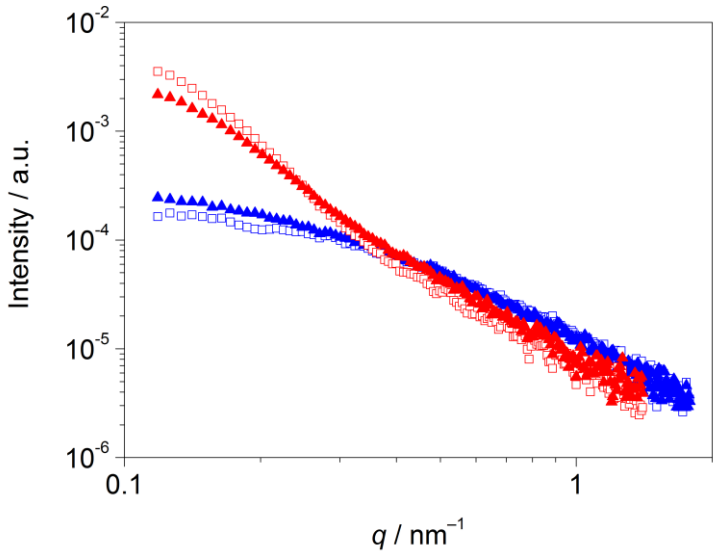

Figure S5. SAXS data obtained from the 5.0 mg mL^{-1} aqueous solutions of the (□) P(EO_2MA-*co*-EO_{45}MA) 99:1 and (▲) P(EO_2MA-*co*-EO_5MA-*co*-EO_{45}MA) 94:5:1 copolymers (□▲) below (T = 25 °C) and (□▲) above (T = 37 °C) the CMT.

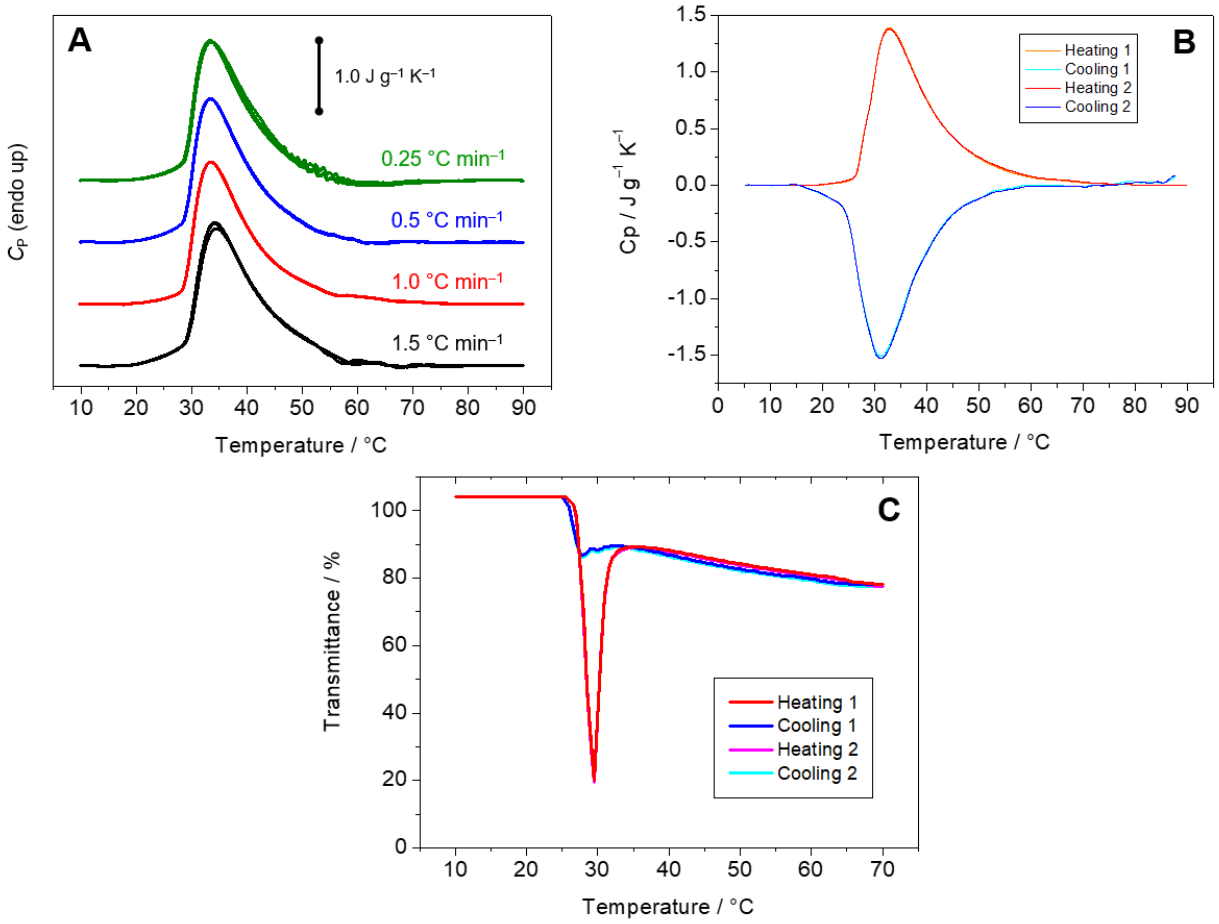

Figure S6. Confirmation of the thermodynamic equilibrium of the nanostructure formed above LCST using different pathways. (A) Different heating rates and (B) sequential heating–cooling processes during HSDSC measurements; and (C) sequential heating–cooling processes during UV–vis measurements: identical and superposed curves.

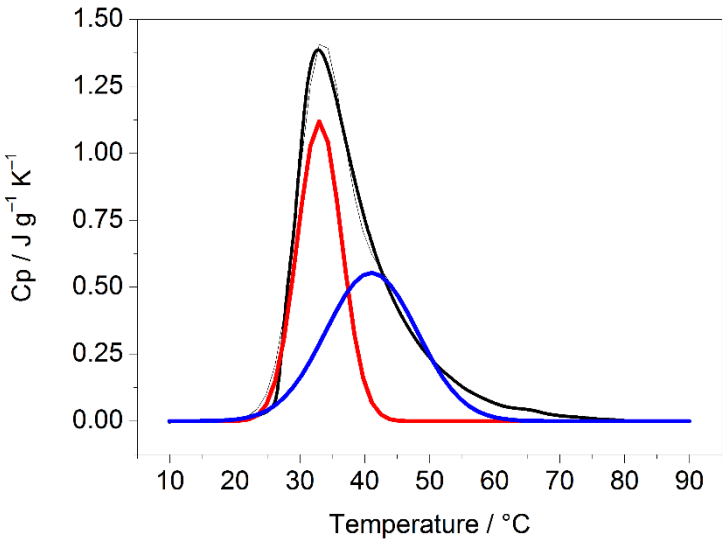

Figure S7. Deconvoluted peak from HSDSC measurement of 5.0 mg mL^{-1} aqueous P(EO_2MA-*co*-EO_{45}MA) copolymer solution with [EO_2MA]:[EO_{45}MA] molar ratio of 99:1. The red line is assigned to the dehydration of polymer chains and the blue one to aggregation process. Scan heating rate = 1.0 °C min^{-1}.

References

1. Ge, Z.; Wang, D.; Zhou, Y.; Liu, H.; Liu, S. Synthesis of organic/inorganic hybrid quatrefoil-shaped star-cyclic polymer containing a polyhedral oligomeric silsesquioxane core. *Macromolecules* **2009**, *42*, 2903–2910.

2. Han, S.; Hagiwara, M.; Ishizone, T. Synthesis of thermally sensitive water-soluble polymethacrylates by living anionic polymerizations of oligo(ethylene glycol) methyl ether methacrylates. *Macromolecules* **2003**, *36*, 8312–8319.

3. Peng, B.; Grishkewich, N.; Yao, Z.; Han, X.; Liu, H.; Tam, K. C. Self-assembly behavior of thermoresponsive oligo(ethylene glycol) methacrylates random copolymer. *ACS Macro Lett.* **2012**, *1*, 632–635.

4. Oh, J. K.; Min, K.; Matyjaszewski, K. Preparation of poly(oligo(ethylene glycol) monomethyl ether methacrylate) by homogeneous aqueous AGET ATRP. *Macromolecules* **2006**, *39*, 3161–3167.

5. Hammersley, A. P. *FIT2D: An Introduction and Overview*, ESRF Internal Report, ESRF97HA02T, 1997.

6. Breßler, I.; Kohlbrecher, J.; Thünemann, A. F. SASfit: A tool for small-angle scattering data analysis using a library of analytical expressions. *J. Appl. Crystallogr.* **2015**, *48*, 1587–1598.

7. Debye, P. Molecular-weight determination by light scattering. *J. Phys. Chem.* **1947**, *51*, 18–32.

8. Beaucage, G. Small-angle scattering from polymeric mass fractals of arbitrary mass-fractal dimension. *J. Appl. Crystallogr.* **1996**, *29*, 134–146.

9. Ilavsky, J.; Jemian, P. R. Irena: Tool suite for modeling and analysis of small-angle scattering. *J. Appl. Crystallogr.* **2009**, *42*, 347−353.

10. Nelson, A. Co-refinement of multiple-contrast neutron/X-ray reflectivity data using MOTOFIT. *J. Appl. Crystallogr.* **2006**, *39*, 273−276.

11. Beaucage, G. Approximations leading to a unified exponential/power-law approach to small-angle scattering. *J. Appl. Crystallogr.* **1995**, *28*, 717−728.

12. Kline, S. R. Reduction and analysis of SANS and USANS data using IGOR Pro. *J. Appl. Crystallogr.* **2006**, *39*, 895–900.

4. Enxertia de POEGMA na superfície da CNC

O objetivo neste capítulo foi estudar a formação de hidrogéis a partir de celulose nanocristalina com copolímeros da família POEGMA enxertados na superfície, POEGMA-*g*-CNC, produzindo materiais funcionais responsivos. Este trabalho ainda não foi publicado na literatura e continua sendo estudado pelo grupo de pesquisa. Em um estudo similar a este, trabalhei também em colaboração com o César Brinatti, e publicamos em 2019 na revista *Journal of Colloid and Interface Science* o artigo intitulado *Controlled coagulation and redispersion of thermoresponsive poly di(ethylene oxide) methyl ether methacrylate grafted cellulose nanocrystals* [71]. Minha colaboração naquele trabalho foi a síntese de algumas amostras, medida de HSDSC e discussão dos dados. Este artigo na íntegra está como anexo.

4.1. Introdução

A fim de reduzir a quantidade de derivados de petróleo, têm-se buscado a utilização de polímeros naturais, de origem renovável e sustentável, onde a celulose nanocristalina (CNC) se enquadra. Com modificações em sua superfície, adaptando e adequando as suas propriedades físico-químicas, a CNC tem sido extensivamente empregada na formação de hidrogéis e aerogéis para as mais diversas aplicações [64].

Por exemplo, Lin e Dufresne [72] enxertaram ciclodextrina na superfície da CNC e formaram um hidrogel supramolecular na presença de um copolímero tribloco. A síntese de um hidrogel em presença de uma fase quiral de CNC resultou em um hidrogel fotorresponsivo, que manteve o ordenamento nemático quiral [73] O grupo de pesquisa da Profa. Emily Cranston vem preparando hidrogéis e aerogéis de CNC para aplicações em sistemas purificadores de água [74], materiais supercapacitores [58, 75], além de aplicações biomédicas. Yang e colaboradores [76] funcionalizaram a superfície da CNC com aldeídos preparando um hidrogel injetável para aplicações biomédicas. Mais recentemente, De France e colaboradores [43] demonstrou que a CNC promove um significativo reforço mecânico necessário aos hidrogéis para aplicações biomédicas, em especial hidrogéis injetáveis anisotrópicos, com potencial aplicação para engenharia de tecidos ou músculos cardíacos, por exemplo.

Outros materiais "*smart*" foram preparados pela enxertia de PNIPAM em CNC, resultando em aumento da estabilidade coloidal e em nanocompósitos termorresponsivos [77–79]. PNIPAM enxertado na superfície da CNC, PNIPAM-*g*-CNC, foi estudado pelos grupos de pesquisa de Rojas e de Boluk [77, 79]. Verificou-se que as propriedades de agregação variam

com a densidade do enxerto e com o grau de polimerização bem como com a força iônica da solução. Além disso, a estabilidade coloidal de PNIPAM-*g*-CNC se dá principalmente pelos fatores estéricos do polímero enxertado do que pelas forças repulsivas das cargas negativas de superfície modificada da CNC. PNIPAM, no entanto, não é um polímero biocompatível.

Poli(oxazolina) e POEGMA, por outro lado, apresentam biocompatibilidade além das propriedades termorresponsiva e têm sido empregados tal qual no desenvolvimento de hidrogéis [80–82], assim como combinado com a CNC ou enxertado sobre a sua superfície [51, 83, 84], mantendo suas propriedades térmicas [85, 86]. Os copolímeros derivados de oxazolina, no entanto, são comumente sintetizados por polimerização catiônica por abertura de anel, o que dificulta a sua copolimerização com outros monômeros derivados de (met)acrilato, sendo necessário, para isso, passos adicionais prévios à copolimerização [87, 88]. Os copolímeros da família POEGMA apresentam, portanto, a vantagem adicional de processo possibilitando a reação direta com uma vasta gama de monômeros vinílicos. Apesar do aumento recente do número de trabalhos publicados utilizando-se o copolímero POEGMA em combinação com a CNC, variações na composição monomérica do POEGMA enxertado sobre a CNC, afetando as propriedades para formação de hidrogéis, e a caracterização do sistema POEGMA-*g*-CNC a partir de novas metodologias são ainda necessárias neste campo de estudo e desenvolvimento.

4.2. Experimental

Reagentes

Metacrilato de dietileno glicol metil éter (EO_2MA) (M_n = 188 g mol^{-1}) e metacrilato de oligoetileno glicol metil éter (EO_xMA, x = 5, 9, 20 e 45 unidades de EO, M_n = 300, 475, 950 e 2.080 g mol^{-1}, respectivamente) (Sigma-Aldrich) foram purificados passando por uma coluna de alumina básica para remover os inibidores. Celulose nanocristalina (CelluForce), nitrato de amônio e cério(IV) (CAN, Sigma-Aldrich, ≥98,5%) e cloreto de sódio (NaCl, Synth, P.A. ACS) foram utilizados sem purificação adicional. Água do sistema Milli-Q® (resistividade de 18,2 MΩ·cm) foi utilizada no preparo de todas as soluções e reações.

Enxertia do POEGMA sobre a superfície da CNC

Utilizando a técnica de "*grafting-from*", fez-se a copolimerização de forma aleatória de POEGMA a partir da superfície CNC (POEGMA-*g*-CNC), utilizando CAN como iniciador iônico em água em temperatura ambiente por 24 h. Os produtos foram lavados

extensivamente com água sob centrifugação. Por esta técnica, foram enxertados na superfície da CNC os copolímeros da família POEGMA-*g*-CNC compreendendo diferentes monômeros e razões monoméricas, indicados como subíndices, representados por *Y* e *Z* no exemplo: $P(EO_2MA\text{-}co\text{-}EO_xMA)_{Y:Z}$. Em um procedimento típico, foram utilizados 10 mmol dos monômeros para 1,0 g de CNC e 200 mg de CAN. Variações foram realizadas empregando-se quantidades 5 vezes maiores ou menores de iniciador CAN ou de total de monômeros.

Microscopia eletrônica de transmissão

As amostras foram preparadas pulverizando-se uma dispersão aquosa de 0,01% sobre grades de cobre (200 mesh revestida com cobre), deixada secar ao ar e observadas em um microscópio eletrônico de transmissão (MET) Philips CM10 com uma voltagem de aceleração de 60 kV. A fim de melhorar a observação da morfologia das nanopartículas, todas as amostras foram coradas com 3 gotas de solução de Fe^{+3} 1,0 M.

Infravermelho com transformada de Fourier

Os espectros de infravermelho com transformada de Fourier (FT-IR) foram obtidos na resolução de 4 cm^{-1} em um espectrômetro Bruker Tensor 27 em temperatura ambiente utilizando pastilha de KBr.

Análise termogravimétrica

A análise termogravimétrica (TGA) foi realizada em um analisador termogravimétrico TA Instruments Q500 sob um fluxo de N_2 seco a 50 mL min^{-1} e a uma taxa de aquecimento de 10,0 °C min^{-1}.

Espectroscopia de fotoelétrons excitados por raios-X

As análises químicas da superfície das amostras de POEGMA-*g*-CNC foram realizadas por espectroscopia de fotoelétrons excitados por raios-X (XPS), utilizando um espectrômetro fotoelétrico de raio-X K-Alpha (Thermo Fisher Scientific, Reino Unido) equipado com um analisador hemisférico de elétrons e radiação monocromática Al *K*α (1486,6 eV), no Laboratório Nacional de Nanotecnologia (LNNano) no Centro Nacional de Pesquisa em Energia e Materiais (CNPEM) em Campinas (SP). Os espectros de *survey* (gama completa) e de alta resolução para C foram adquiridos usando energia de passagem de 200 e 50

eV, respectivamente. Os dados foram analisados utilizando o software Thermo Avantage (versão 5.921) e os resultados de XPS apresentados neste trabalho correspondem a uma média de três medições realizadas em diferentes regiões ao longo das amostras. Os resultados foram atribuídos de acordo com as ligações do C: carbono ligado a carbono ou hidrogênio por ligações simples, C–**C**–C ou C–**C**–H (C1), carbono ligado a oxigênio por ligação simples, **C**–O (C2), carbono ligado a dois oxigênios através de ligações simples, O−**C**−O (C3), ou carbono de carbonila, O=**C**–O (C4).

Turbidimetria

O ponto de turvação das soluções aquosas de copolímero a 0,5 % (m/m) foi determinado em um espectrofotômetro Varian Cary 100 UV−vis equipado com um controlador de temperatura Cary ou em um UV−Vis HP8453 com um controlador de temperatura Peltier. O ponto de turvação foi determinado como o último ponto de transmitância 100%. As medições foram realizadas em λ = 500 nm com três ciclos de aquecimento a 0,5 °C min^{-1}. O primeiro ciclo foi usado para condicionar a amostra apagando o histórico térmico anterior e a curva foi negligenciada.

Calorimetria diferencial exploratória

O comportamento térmico de soluções aquosas de copolímero a 0,5% (m/m) foi determinado por calorimetria diferencial exploratória (DSC) em um MicroCal VP-DSC (Northampton, EUA), equipado com celas gêmeas de 0,54 mL. Três ciclos consecutivos de aquecimento e resfriamento foram realizados de 5 a 90 °C e a uma taxa de varredura de 60 °C h^{-1} e o primeiro foi usado para condicionar a amostra apagando o histórico térmico anterior. A célula de referência continha água Milli-Q®. Todas as amostras foram mantidas à respectiva temperatura de partida durante 20 min. A referência em branco, obtida pela condução do experimento com ambas as células contendo água, foi subtraída dos termogramas da amostra. A entalpia (ΔH) foi calculada integrando a área abaixo da curva após a subtração da linha de base.

4.3. Resultados e discussão

Enxerto de POEGMA na superfície da CNC

O P(EO_2MA-*co*-EO_{45}MA)$_{99:1}$ foi polimerizado na superfície da CNC pela reação com CAN utilizando a técnica "*grafting-from*". Nesta metodologia, o radical é desenvolvido na superfície da CNC, e a partir deste ponto ocorre a polimerização com o crescimento da cadeia e a reação pode ser denominada polimerização iniciada na superfície (ou, no inglês, "*Surface-Initiated Polymerization*").

O hidrogel deste trabalho (discutido no próximo capítulo) é formado pelo copolímero termorresponsivo POEGMA enxertado na superfície da CNC (POEGMA-*g*-CNC). A técnica de polimerização controlada ATRP é adequada para produzir o copolímero em solução [85], mas não é a maneira mais simples de produzir o copolímero enxertado na superfície da CNC. A polimerização por radicais livres iniciada por cério(IV) é a técnica mais apropriada para obter este produto. Nesta reação, o Ce^{+4} forma um complexo com os grupos hidroxila da superfície da CNC, abre o anel de glucose da celulose e forma um radical local, como ilustrado na Figura 13. Os monômeros reagiram a partir deste radical formado na superfície da CNC produzindo o polímero enxertado. Esta reação ocorre em meio aquoso, em temperatura ambiente, com apenas um reagente adicional aos monômeros e CNC, e ocorre em apenas uma etapa, conforme esquematizado na Figura 14. Perde-se, no entanto, o controle sobre o tamanho da cadeia polimérica e dificultando a caracterização do produto POEGMA-*g*-CNC obtido.

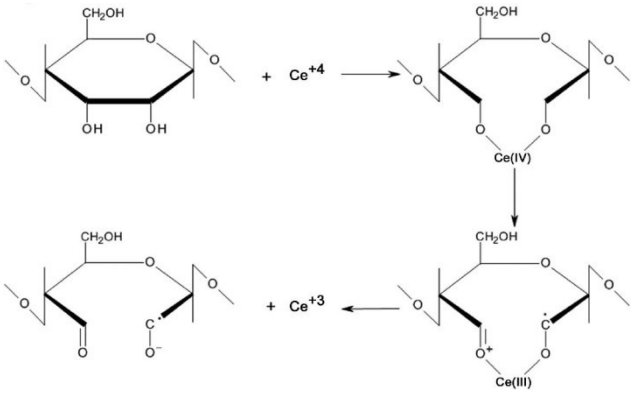

Figura 13: Mecanismo da polimerização radicalar pelo método "*grafting-from*" iniciada por cério (IV). Reproduzido da referência [89] © 2013 American Chemical Society.

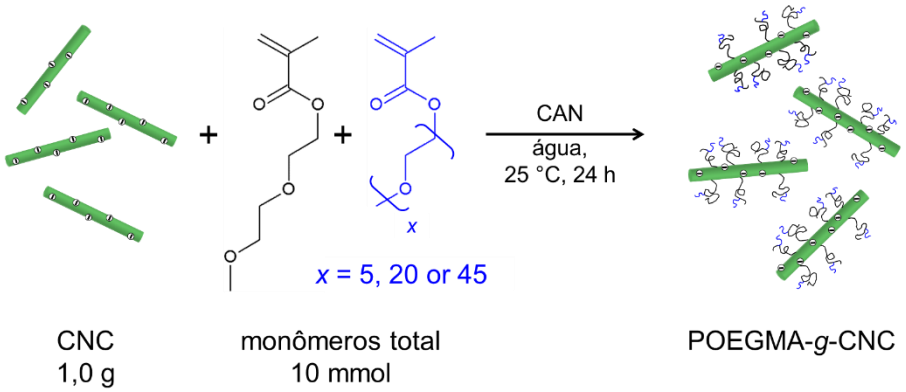

Figura 14: Esquema da copolimerização de POEGMA, P(EO_2MA-*co*-EO_xMA), enxertados sobre a superfície da CNC através da reação de síntese utilizando-se o iniciador CAN.

Caracterização da POEGMA-g-CNC

Os espectros de FT-IR (Figura 15-A) mostram que o copolímero P(EO_2MA-*co*-EO_{45}MA)$_{99:1}$ foi enxertado com sucesso na superfície da CNC por esta metodologia de polimerização. A banda em 1729 cm^{-1} é atribuída ao estiramento da carbonila do copolímero [87]. A Figura 15-B mostra que produto P(EO_2MA-*co*-EO_{45}MA)$_{99:1}$-*g*-CNC apresenta uma temperatura de degradação mais baixa (~150 °C) em comparação com a CNC não modificada e com o copolímero (~250 °C), que também é relatado na literatura [89]. Isto pode ser um efeito da degradação da CNC pela abertura do anel de glucose pelo mecanismo da reação com cério (IV) (Figura 13) [90]. A Figura 16 apresenta as imagens de caracterização da CNC não-modificada e da CNC com o polímero P(EO_2MA-*co*-EO_{45}MA)$_{99:1}$ enxertado em sua superfície.

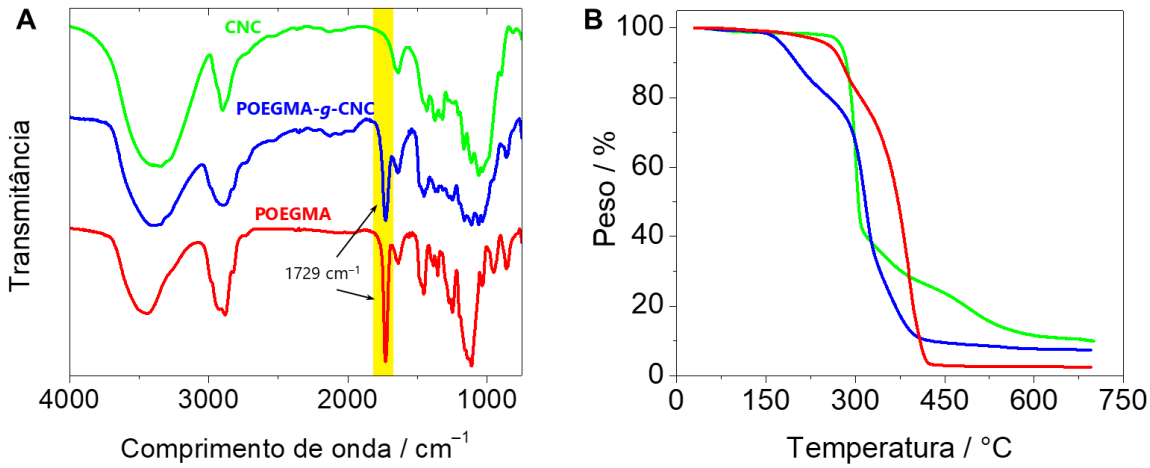

Figura 15: (A) Espectros de FT-IR e (B) curvas termogravimétricas das amostras de (■) CNC não-modificada, (■) P(EO_2MA-*co*-EO_{45}MA)$_{99:1}$-*g*-CNC e (■) P(EO_2MA-*co*-EO_{45}MA)$_{99:1}$.

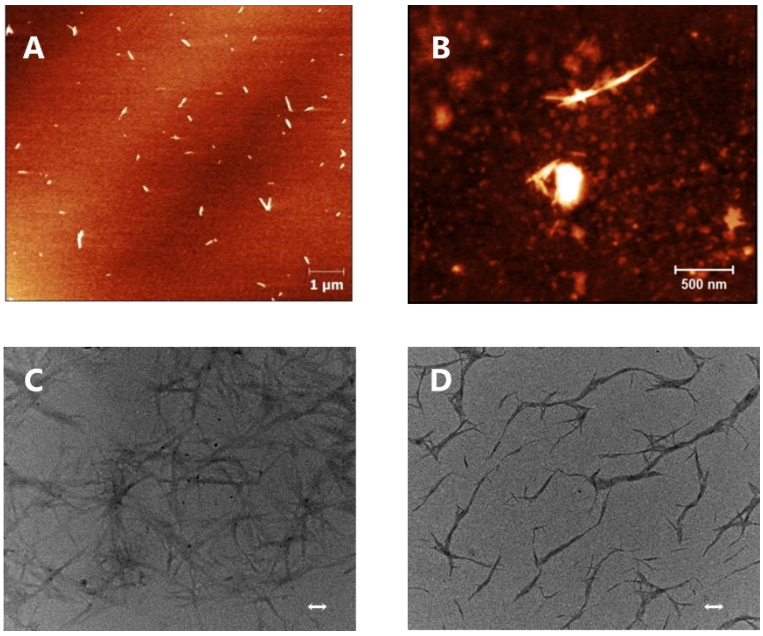

Figura 16: Imagens de microscopia AFM (acima, A e B) e MET (abaixo, C e D) das amostras de CNC não-modificada (à esquerda, A e C) e P(EO_2MA-*co*-EO_{45}MA)$_{99:1}$-*g*-CNC (à direita, B e D). Nas imagens de MET as barras de escala equivalem a 100 nm.

Foram também realizadas modificações na quantidade adicionada de CAN (5 vezes menor e 5 vezes maior) a fim de se obter diferentes graus de modificação da superfície da CNC. A Figura 17 mostra os espectros de alta resolução de XPS de C 1s para os produtos P(EO_2MA-*co*-EO_{45}MA)$_{99:1}$-*g*-CNC e a Tabela 2 sumariza estes resultados. Vê-se que o espectro da CNC está de acordo com a literatura [45, 90]. A CNC não-modificada apresenta uma baixa quantidade de C4, o que pode ser atribuído à oxidação da superfície, e a razão molar O/C de 0,74, como reportado na literatura [45]. Foram ainda identificados os átomos de enxofre (0,61%) e sódio (0,8%), atribuídos ao grupo sulfato de sódio presente na superfície da CNC, derivado do processo da CelluForce para obtenção da CNC através de hidrólise ácida utilizando-se ácido sulfúrico.

Após a polimerização de P(EO_2MA-*co*-EO_{45}MA)$_{99:1}$ sobre a superfície da CNC, o perfil dos espectros varia consideravelmente, comprovando a sua ocorrência. A razão de C1 e de C4 presentes nas amostras aumenta, enquanto a razão de C3 diminui. Não há diferença considerável entre as três amostras de POEGMA-*g*-CNC com diferentes graus de modificação.

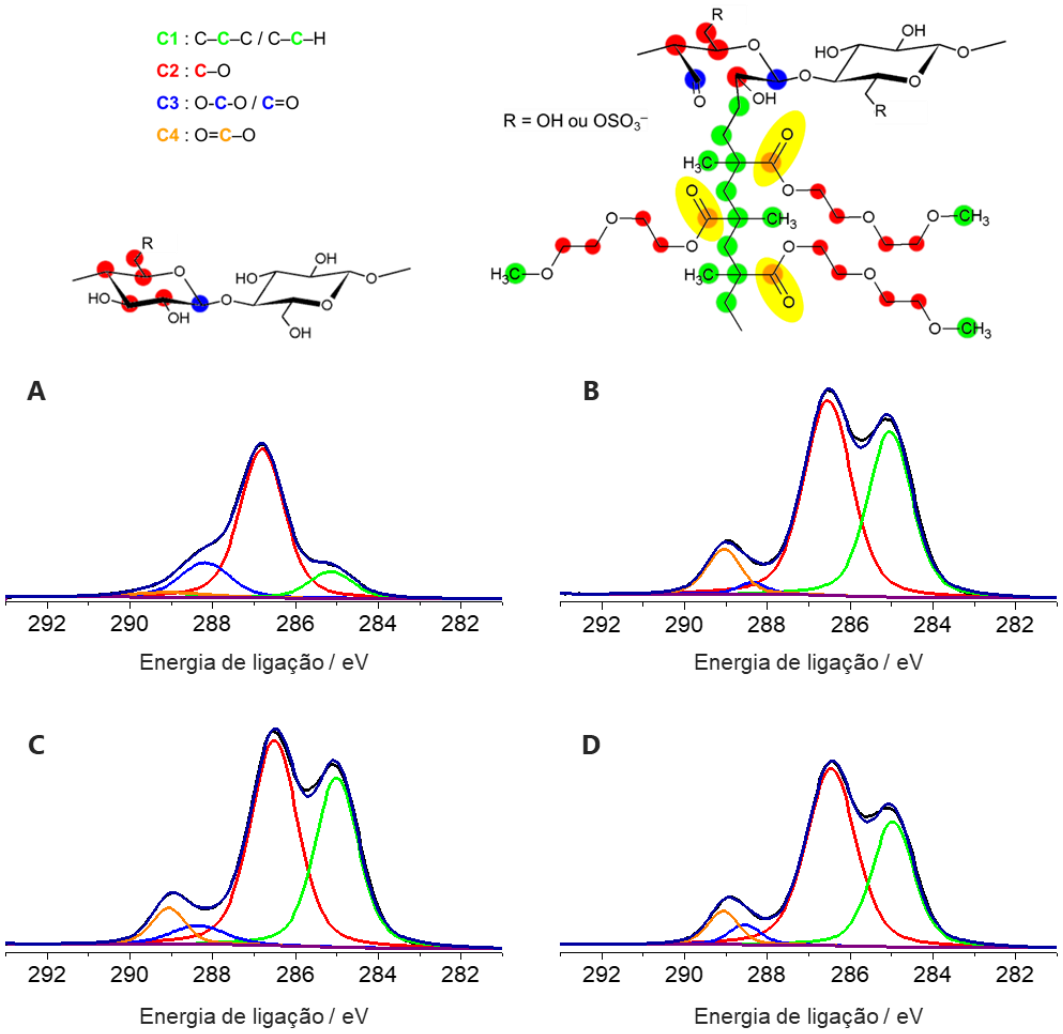

Figura 17: Espectros de alta resolução de XPS de C 1s. (A) CNC pura e P(EO_2MA-*co*-EO_{45}MA)$_{99:1}$-*g*-CNC com (B) a protocolo tradicional, (C) 5× menos CAN, e (D) 5× mais CAN. (■) C1, (■) C2, (■) C3, (■) C4, (■) contagem, (■) *background*, e (■) envelope.

Tabela 2 Composição de carbono determinada por XPS de P(EO_2MA-*co*-EO_{45}MA)$_{99:1}$-*g*-CNC com diferentes quantidades de iniciador (CAN) na reação e a razão oxigênio/carbono.

	Composição percentual				
Amostra	C1	C2	C3	C4	O/C
CNC não modificada	10,8	73,4	13,3	2,5	0,74
POEGMA-*g*-CNC 5× menos CAN	37,6	51,2	5,3	5,9	0,42
POEGMA-*g*-CNC tradicional	36,4	53,6	1,9	8,2	0,42
POEGMA-*g*-CNC 5× mais CAN	37,6	51,8	4,3	6,3	0,42

A propriedade termorresponsiva da amostra P(EO_2MA-*co*-EO_{45}MA)$_{99:1}$-*g*-CNC foi caracterizada por turbidimetria e por microcalorimetria, cujos resultados são apresentados na

Figura 18. A CNC com o P(EO_2MA-*co*-EO_{45}MA)$_{99:1}$ enxertado em sua superfície exibe, acima da LCST, um comportamento de agregação diferente do copolímero não-enxertado: o P(EO_2MA-*co*-EO_{45}MA)$_{99:1}$-*g*-CNC forma uma separação de fases macroscópica, diferentemente do P(EO_2MA-*co*-EO_{45}MA)$_{99:1}$, que forma uma estrutura micelar (como já discutido no capítulo anterior) mesmo na presença da CNC. Todas as transições de fase foram reversíveis observadas pelas técnicas de turbidimetria, microcalorimetria e visualmente em ciclos consecutivos. A temperatura de transição de fase do polímero é similar para os três casos estudados, ainda que a transição se inicie em uma temperatura mais baixa (cerca de 4 °C) quando o polímero está enxertado na superfície da nanopartícula.

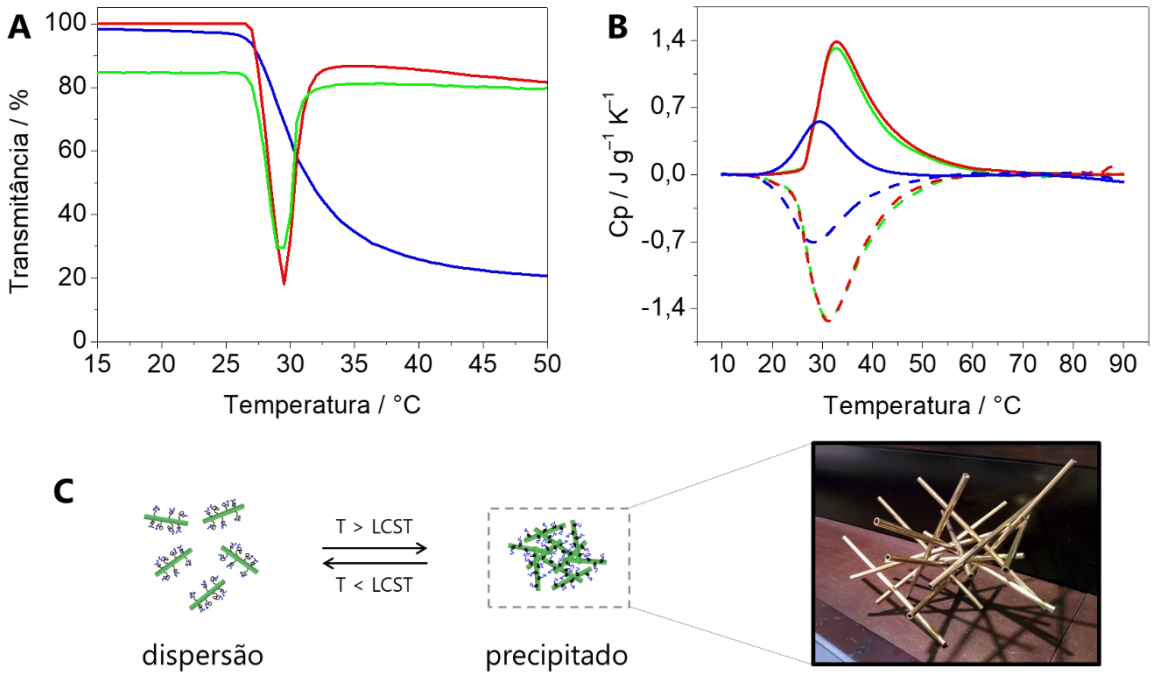

Figura 18: (A) Curvas de turbidimetria e (B) microcalorimetria de soluções aquosas de (■) P(EO_2MA-*co*-EO_{45}MA)$_{99:1}$ a 0,5%, (■) mistura física de P(EO_2MA-*co*-EO_{45}MA)$_{99:1}$ a 0,5% com CNC a 1,0% e (■) P(EO_2MA-*co*-EO_{45}MA)$_{99:1}$-*g*-CNC a 0,25% (turbidimetria) e a 0,5% (microcalorimetria). Medidas de turbidimetria com taxa de aquecimento = 0,5 °C min^{-1} em λ = 500 nm. Medidas de microcalorimetria com taxa de aquecimento = 1,0 °C min^{-1}, processo de aquecimento em linha sólida e processo de resfriamento em linha tracejada. (C) Representação do processo reversível de precipitação e visualização conceitual do precipitado formado.

Estimativa da densidade de POEGMA enxertado na superfície da CNC

A determinação da densidade de polímero gerado na superfície da CNC é um desafio analítico. Este parâmetro depende do tamanho das cadeias poliméricas e do número de pontos de iniciação da reação da polimerização, o que é difícil de controlar pela técnica de

polimerização radicalar iniciada por cério(IV). De forma geral, é necessário clivar a cadeia polimérica da superfície da nanopartícula e então realizar a análise por cromatografia de permeação em gel (GPC/SEC), espectrometria de massas (MS), ressonância magnética nuclear (RMN), entre outras técnicas que não são triviais e que consomem tempo e reagentes. Para contornar este problema, foram utilizados os dados obtidos por microcalorimetria, sendo possível estimar a densidade de polímero na CNC.

A energia de transição detectada pelo microcalorímetro é devido à desidratação e agregação do polímero, conforme descrito no capítulo anterior. Desta forma, é possível correlacionar a energia envolvida na transição de fase com a quantidade de polímero presente. Para esta metodologia, é importante que apenas o polímero seja termorresponsivo, além de se conhecer como a energia de transição varia de acordo com a quantidade de polímero utilizado e estimar uma curva de correlação a partir da integração das curvas calorimétricas.

Considerando o caso da solução aquosa de POEGMA-*g*-CNC, apenas o POEGMA apresenta resposta no microcalorímetro, e não a CNC. A quantidade total de amostra corresponde a uma fração de POEGMA mais uma fração de CNC, sendo que o microcalorímetro só "enxerga" o POEGMA. Assim, foram determinadas as curvas calorimétricas de soluções aquosas de POEGMA (sem e com a presença da CNC) em diferentes concentrações (0,25%, 0,50% e 1,0%) (Figura 19-A) e estimou-se a energia de transição absoluta (J) para cada uma delas, construindo a curva de correlação (Figura 19-B) de equação de reta $y = 9{,}9\,x$, com $R^2 = 0{,}9992$.

A integração da curva da amostra POEGMA-*g*-CNC resultou em 32,2 ± 0,5 J, o que, pela curva de correlação, corresponde a aproximadamente 3,2 g L^{-1} de polímero na amostra. Desta forma, a amostra analisada, na concentração de 10,0 g L^{-1}, possui aproximadamente 30% de polímero e 70% de CNC em sua composição. Para a síntese do POEGMA-*g*-CNC é adicionado aproximadamente o dobro da massa de monômeros em relação a massa de CNC, o que indica que uma quantidade expressiva de monômeros não foi reagida ou não foi polimerizada na superfície da CNC, mas livre em solução e acabou sendo extraído no processo de purificação por lavagem do produto reacional. Esta é a primeira vez que a técnica de microcalorimetria é utilizada para estimar a densidade de polímero enxertado sobre a superfície de uma nanopartícula e este trabalho continua sendo investigado pelo grupo, avaliando outras composições poliméricas e comparando com técnicas de RMN de ^{13}C no estado sólido. A microcalorimetria é uma técnica simples, rápida, robusta, de baixo custo e não-destrutiva que pode ser utilizada para se estimar a densidade de polímero termorresponsivo enxertado na superfície de uma nanopartícula.

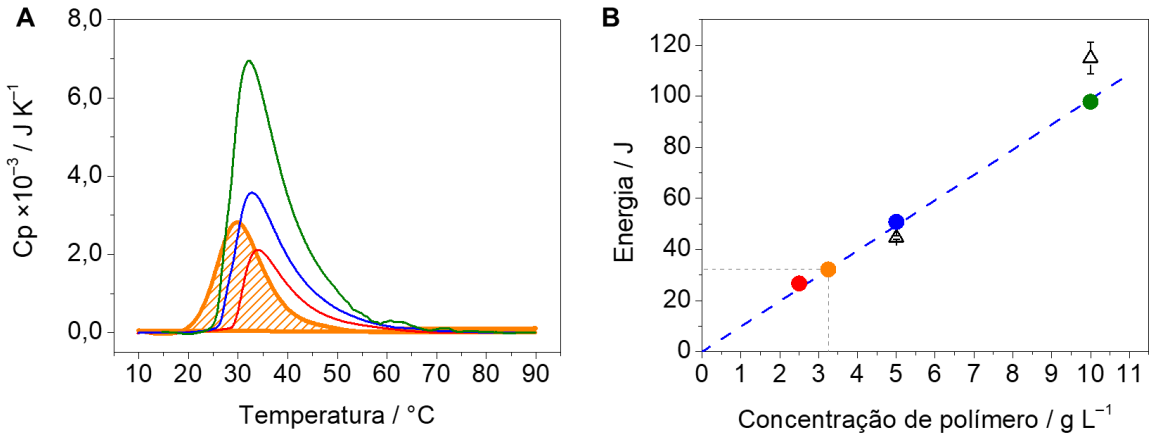

Figura 19: Estimativa da densidade de polímero enxertado na superfície da CNC, determinada por microcalorimetria. (A) Curvas calorimétricas e (B) curva de correlação da energia de transição com a quantidade de polímero presente nas amostras de P(EO_2MA-*co*-EO_{45}MA)$_{99:1}$ a (■) 0,25%, (■) 0,50% e (■) 1,0%, e (■) P(EO_2MA-*co*-EO_{45}MA)$_{99:1}$-*g*-CNC a 1,0%. Os pontos (Δ) representam misturas físicas de POEGMA (na concentração indicada) com CNC a 1,0% demostrando que não há interferência significativa desta na medida da energia de transição.

4.4. Conclusões

Pelas técnicas de FT-IR, TGA, XPS, e turbidimetria obtivemos evidências da presença do polímero sobre a CNC, ainda que sem sua quantificação. Os resultados obtidos por XPS não apresentam diferença entre os carbonos quantificados nas amostras de POEGMA-*g*-CNC sintetizados com diferentes graus de modificação da superfície da CNC. Este resultado leva a crer que esta técnica detectou apenas a camada de polímero na superfície da CNC, sem identificar os carbonos da CNC, apenas do polímero. Uma nova metodologia foi apresentada para a estimativa quantitativa do teor de polímero enxertado na superfície da CNC, necessitando ainda ser validada para identificação dos limites deste método e ampla utilização. Este trabalho ainda abre a oportunidade de realizar-se a síntese e a caracterização da temperatura de transição de fase de outros copolímeros da família POEGMA.

5. Formação de hidrogéis de POEGMA-*g*-CNC

O objetivo deste capítulo foi estudar a formação de hidrogéis físicos a partir de copolímeros da família POEGMA enxertados na superfície da celulose nanocristalina (POEGMA-*g*-CNC) descritos no capítulo anterior, produzindo materiais funcionais responsivos. Apesar das diversas frentes de avaliação e caracterização concluídas e demonstradas a seguir, este trabalho abriu novas portas e ainda demanda mais estudos sistemáticos, que estão atualmente em andamento por outros membros do grupo de pesquisa, para ser então publicado.

5.1. Experimental

Formação de hidrogéis

Hidrogéis de POEGMA-*g*-CNC sintetizados conforme descrito no capítulo 4, foram gerados com a adição de quantidades de solução aquosa salina ou com o aumento da temperatura. Tipicamente, foram realizadas misturas na proporção de 1:1 de dispersão aquosa de POEGMA-*g*-CNC e de solução aquosa de NaCl, agitadas levemente com a mão e mantidas em repouso em temperatura ambiente. Foram gerados também hidrogéis com o aumento da temperatura, mantendo a dispersão aquosa de POEGMA-*g*-CNC em estufa ou banho de água com controle de temperatura.

Medidas reológicas

As medidas reológicas foram realizadas em um reômetro HAAKE RheoStress 1 equipado com geometria *double-gap* (DG43) com diâmetro externo de 43 mm. A temperatura do experimento foi controlada com banho externo de água HAAKE F8. As amostras de POEGMA-*g*-CNC foram adicionadas lentamente, evitando a incorporação de bolhas de ar e o sistema foi previamente termostatizado por ao menos 10 min. No estudo realizado em função da temperatura, a amostra foi mantida sob cisalhamento, sem interrupção ou troca de geometria e realizou-se a rampa de aquecimento. As medidas foram realizadas em triplicatas equivalentes.

Microtomografia de raios-X

Amostra do aerogel formado por P(EO_2MA-*co*-EO_9MA)$_{90:10}$-*g*-CNC liofilizado, com dimensão aproximada de 5 mm × 5 mm × 5 mm, foi analisada em um microtomógrafo de

raios-X (microCT), modelo SkyScan 1272 (Bruker). O equipamento foi operado com energia da fonte de raios-X de 20 kV e corrente de 175 µA. As imagens foram analisadas pelo software CT Analyser (Special build) Version: 1.13.10.1, nativo do equipamento.

Análise termomecânica

As medidas termomecânicas foram realizadas em equipamento 2940 TMA V2.3A (TA Instruments) equipado com o módulo TMA Standard e sonda dilatômetro. Amostras do hidrogel formado por P(EO_2MA-*co*-EO_9MA)$_{90:10}$-*g*-CNC com dimensões aproximadas de 4–5 mm foram avaliadas por duas metodologias:

Método estático:

1: Equilibrar em 10,00 °C

2: Isotérmico por 15,0 min

3: Rampa 1,00 °C min^{-1} a 60,00 °C

Método cíclico:

1: Equilibrar em 20,00 °C ou 50,00 °C

2: Isotérmico por 3,0 min

3: Força de rampa 0,050 N min^{-1} a 0,100 N

4: Força de rampa 0,050 N min^{-1} a 0,000 N

5: Repetir os passos 3 e 4 mais quatro vezes.

5.2. Resultados e discussão

Soluções aquosas de P(EO_2MA-*co*-EO_9MA)$_{90:10}$-*g*-CNC em concentrações acima de cerca de 3% apresentam-se como um gel. A adição de uma pequena quantidade de cloreto de sódio à uma solução aquosa de P(EO_2MA-*co*-EO_9MA)$_{90:10}$-*g*-CNC resultou em um precipitado que, após meses, formou um hidrogel sólido (Figura 20). Este hidrogel apresenta uma significante capacidade de absorção de água (11 $g_{água}/g_{hidrogel}$), o que possibilita sua aplicação em diversas áreas. O vídeo do link (https://youtu.be/a2wq28Qse0U) demonstra esta propriedade.

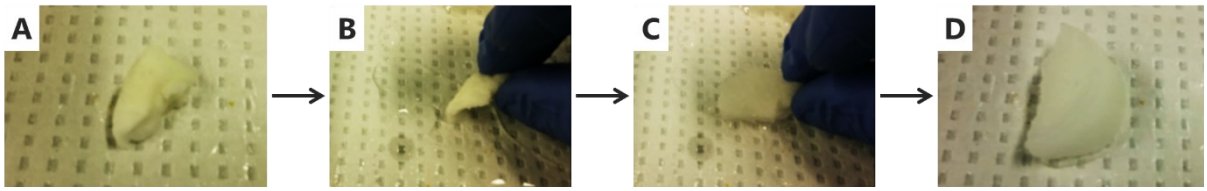

Figura 20: Sequência fotográfica mostrando o hidrogel de P(EO_2MA-*co*-EO_9MA)$_{90:10}$-*g*-CNC desidratado após ser pressionado e, em seguida reabsorvendo água e retomando sua forma natural.

As propriedades termomecânicas do hidrogel formado por P(EO_2MA-*co*-EO_9MA)$_{90:10}$-*g*-CNC após a precipitação com NaCl foram determinadas em um equipamento termomecânico em uma análise estática em função da temperatura e em outra análise com ciclos isotérmicos de compressão em duas temperaturas: 20 °C e 50 °C. No experimento estático, o hidrogel inicia uma redução de tamanho com o aquecimento a partir de cerca de 35 °C (Figura 21-A), valor próximo ao da transição de fase do polímero 39 °C [91]. Na análise com ciclos isotérmicos, vê-se que o hidrogel apresenta reversibilidade na compressão (Figura 21-B). Nas medidas realizadas a 20 °C (abaixo da LCST do polímero), o hidrogel apresenta uma amplitude maior de variação dimensional, enquanto acima da LCST o hidrogel já inicia as medidas com uma altura menor indicando que possivelmente já tenha perdido uma pequena quantidade de água, ou seja, houve uma pequena contração de volume.

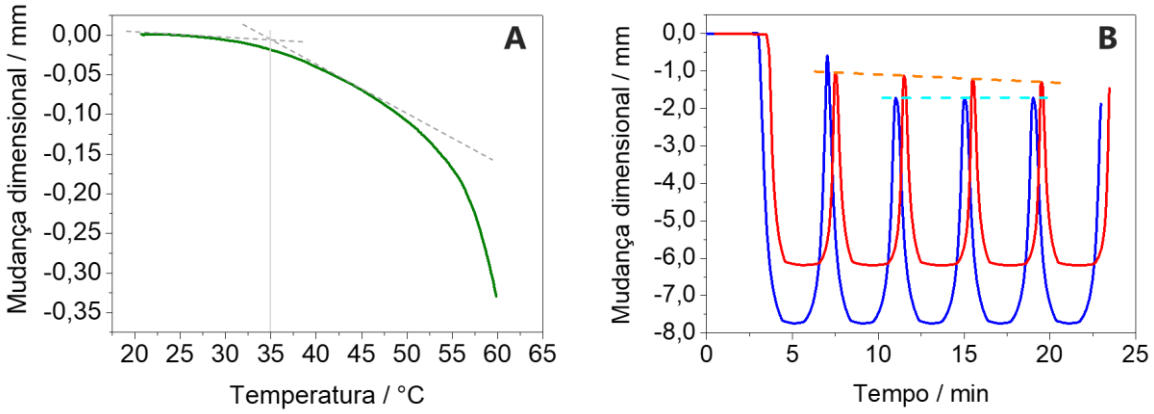

Figura 21: Propriedades termomecânicas do hidrogel formado por P(EO_2MA-*co*-EO_9MA)$_{90:10}$-*g*-CNC. (A) Análise estática (força = 0) em função da temperatura. (B) Ciclos isotérmicos a (■) 20 °C e a (■) 50 °C com pressão intermitente de 0,1 N; a curva vermelha foi deslocada 30 s para eliminar a sobreposição e facilitar a visualização das curvas; as equações de reta dos pontos máximos são: $y = 1{,}07\,x - 1730{,}4$ a 20 °C (azul claro) e $y = -20{,}9\,x - 881{,}7$ a 50 °C (vermelho claro).

A caracterização estrutural e morfológica do hidrogel de P(EO_2MA-*co*-EO_9MA)$_{90:10}$-*g*-CNC foi realizada por microtomografia de raios-X e por imagens de microscopia eletrônica de varredura, mostradas na Figura 22. Para a realização destas análises, o hidrogel foi liofilizado formando um aerogel com morfologia afetada pelo congelamento da água [44, 57].

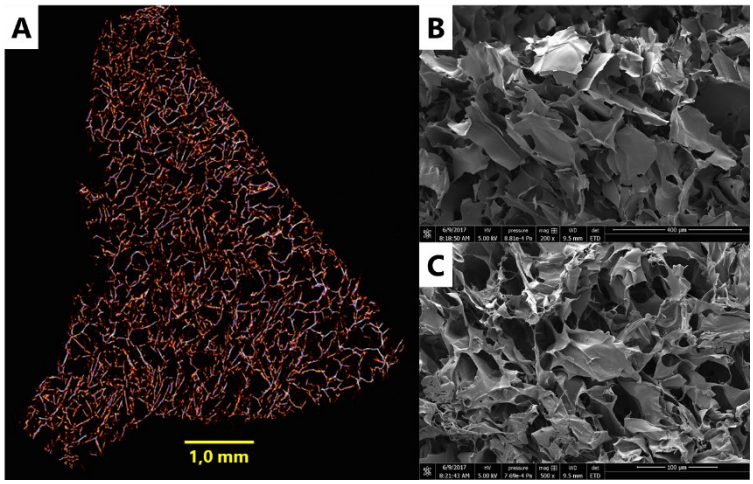

Figura 22: Caracterização estrutural e morfológica do hidrogel de P(EO_2MA-*co*-EO_9MA)$_{90:10}$-*g*-CNC por (A) microtomografia de raios-X e (B) microscopia eletrônica de varredura (MEV).

Para avaliar se esses pontos de adesão poderiam ser desfeitos com solventes, a solubilização do hidrogel de P(EO_2MA-*co*-EO_9MA)$_{90:10}$-*g*-CNC foi testada em diversos solventes orgânicos. Apesar de serem bons solventes para o polímero, nenhum foi capaz de solubilizar e desfazer o hidrogel, mesmo quando aquecidos, evidenciando o emaranhamento das cadeias poliméricas. Os solventes apresentaram a ordem de compatibilidade com o hidrogel:

DMSO > $CHCl_3$ > THF > etanol > éter > acetona > heptano

em que a maior compatibilidade foi indicada pelo intumescimento do hidrogel tornando-o até transparente (DMSO e $CHCl_3$), ao passo que a menor compatibilidade foi indicada pelo sistema inalterado.

Hidrogel formado por adição de eletrólitos

Para compreender o efeito de eletrólitos na formação do hidrogel, realizou-se a adição de uma solução de NaCl em uma solução de POEGMA-*g*-CNC com diferentes composições monoméricas a fim de variar o teor de grupos EO em relação ao grupo metacrilato do *backbone* do polímero. A Figura 23 mostra que o teor de grupos EO presentes no polímero de fato desempenham um papel fundamental na formação do hidrogel e na sua densidade. Sem adição de sal, todas as amostras contendo POEGMA-*g*-CNC estavam homogeneamente dispersas. Com a adição de NaCl ocorreu a precipitação e decantação ou coagulação do POEGMA-*g*-CNC. O aumento da concentração de eletrólito causa a blindagem das cargas superficiais da CNC (devidas ao sulfato residual do seu processo de produção), facilitando a aproximação dos bastões de CNC e a sua coagulação [92]; uma precipitação similar foi também

observada quando se adicionou sal à uma dispersão de CNC. Além disso, a concentração do sistema é também relevante para a formação de coágulos passíveis de formar um hidrogel, como visto nas duas primeiras colunas do diagrama, que contém a mesma relação de POEGMA-*g*-CNC e NaCl, mas um mais diluído que o outro.

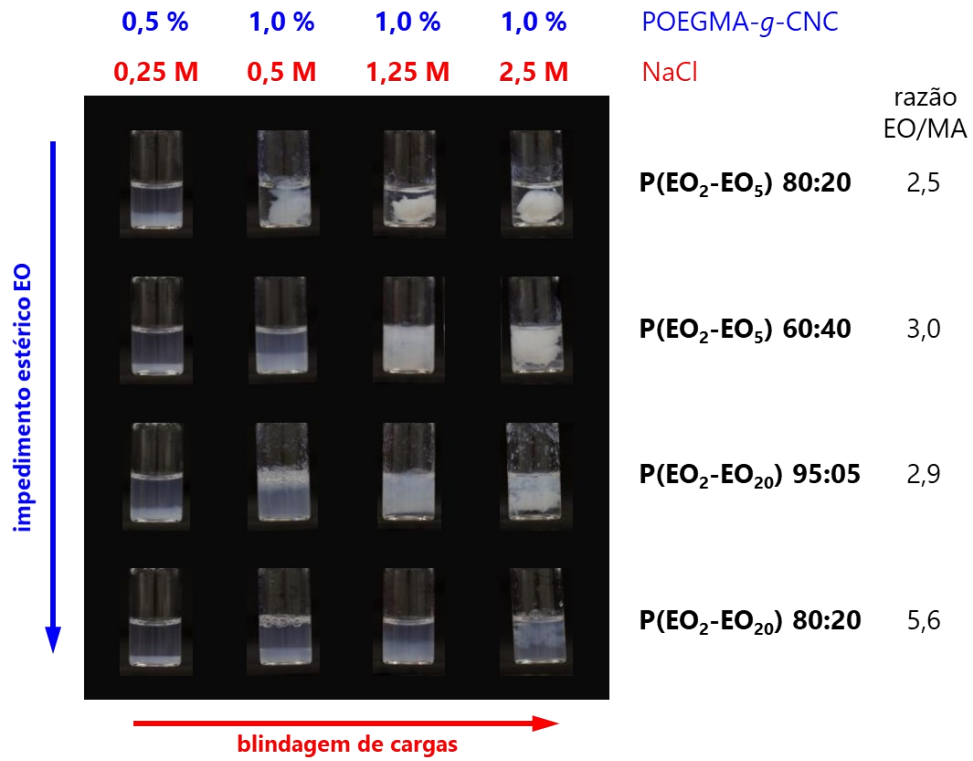

Figura 23: Fotografia de amostras de POEGMA-*g*-CNC (concentração em azul) e em diferentes concentrações de NaCl (indicadas em vermelho). Composição monomérica do POEGMA indicada ao lado, em preto. EO/MA: relação molar entre os grupos óxido de etileno (EO) e metacrilato (MA).

A dispersão aquosa de P(EO_2MA-*co*-EO_9MA)$_{90:10}$-*g*-CNC mantém sua estabilidade coloidal devido ao impedimento estérico das cadeias de POEGMA e pela repulsão eletrostática das cargas negativas devido aos grupos sulfatos residuais presentes na superfície da CNC em virtude do seu processo de obtenção com ácido sulfúrico. A adição de eletrólitos causa o efeito *salting-out* e a neutralização das cargas, favorecendo a aproximação dos bastões de CNC e sua consequente precipitação em um processo reversível, como demonstrado na Figura 24. Alharthi e colaboradores [93] demonstraram que concentrações baixas de sal (KCl, na ordem de 10^{-2} M) são suficientes para reduzir a temperatura de transição do POEGMA enxertado na superfície da CNC devido aos íons cloreto. Similarmente, Mariano e colaboradores [94] formaram hidrogéis supramoleculares a partir de celulose nanofibriladas (CNF) com cargas opostas, identificando que o balanço destas estruturas afeta as propriedades mecânicas do material obtido.

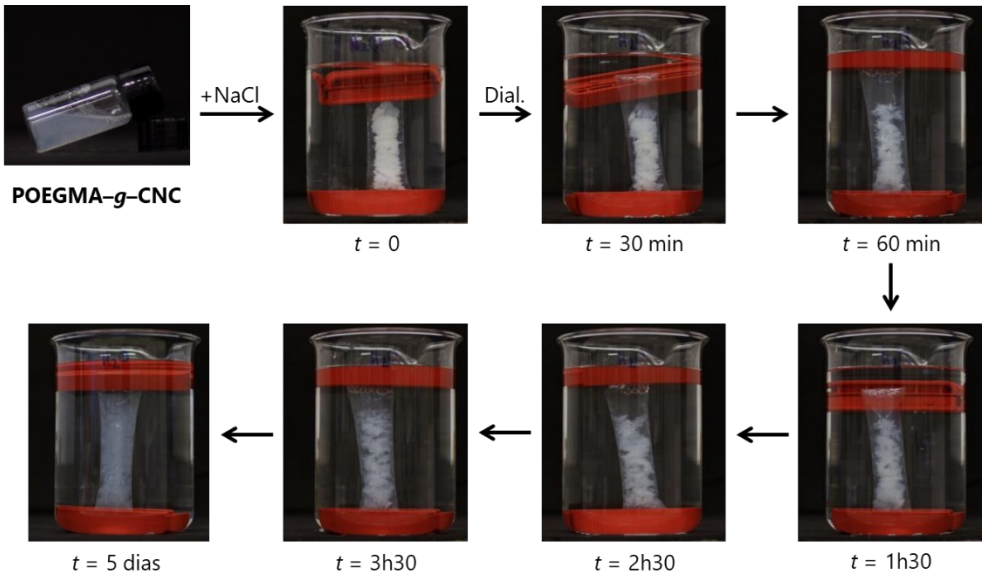

Figura 24: Formação de gel reversível do P(EO_2MA-*co*-EO_5MA)$_{80:20}$-*g*-CNC com a adição de NaCl e sua remoção por diálise.

Hidrogel formado por aquecimento

A formação de hidrogel induzida pela temperatura foi estudada por reologia utilizando uma dispersão aquosa de P(EO_2MA-*co*-EO_{20}MA)$_{95:5}$-*g*-CNC, que apresenta transição de fase por volta de 25–30 °C (Figura 25). O estudo foi realizado em tensão e frequência adequados para este sistema, conforme mostrado nas curvas em vermelho de amplitude e de frequência. A partir da temperatura de transição de fase do polímero, o sistema P(EO_2MA-*co*-EO_{20}MA)$_{95:5}$-*g*-CNC apresentou um aumento nos parâmetros viscoelásticos indicando a formação de uma estrutura e, portanto, o hidrogel, como pode ser visualizado na fotografia.

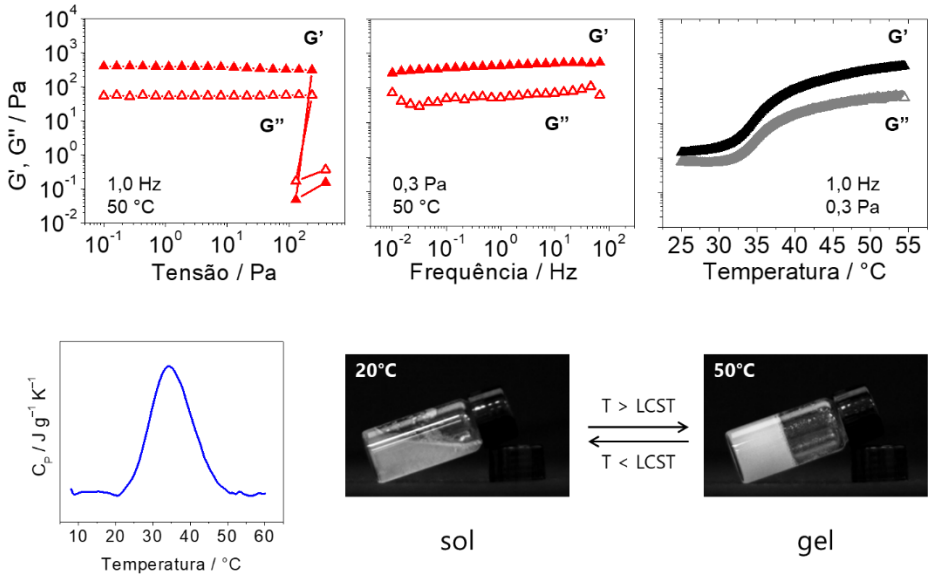

Figura 25: Ensaios reológicos da formação reversível do hidrogel de P(EO_2MA-*co*-EO_{20}MA)$_{95:5}$-*g*-CNC induzida pela temperatura.

Os hidrogéis compostos por POEGMA-*g*-CNC podem ter a sua formação induzida duplamente por eletrólitos e/ou temperatura e o processo de coagulação é dependente da composição monomérica do polímero. Por apresentarem baixa variação de volume com a transição de fase do polímero, o POEGMA nestes sistemas age como uma "cola", adesivando os bastões de CNC através do emaranhamento de suas cadeias poliméricas, formando primeiro precipitados na forma de nanogéis que eventualmente se conectam, gerando a rede tridimensional maior do gel, como um fractal [95], conforme ilustrado na Figura 26.

De acordo com a concentração de sais da solução aquosa e do copolímero enxertado na superfície da CNC, pode-se obter um hidrogel mais ou menos reticulado e com um valor maior ou menor de densidade. Estas diferentes características resultam em propriedades distintas e que podem ser utilizadas em variadas aplicações. Hidrogéis menos densos podem ser formados e aplicados, por exemplo, no solo com o objetivo de reter umidade e/ou nutrientes na região das raízes, permitindo que as raízes consigam penetrar facilmente a sua rede tridimensional. Como outro exemplo, ajustando-se adequadamente a densidade e a estrutura do hidrogel, pode-se desenvolver um material que seja suficientemente transparente para aplicação como lentes de contato, similar ao que foi desenvolvido de forma bastante inovadora pela startup Medella Health Inc. [96], e que possua temperatura de transição de fase próxima à do globo ocular, possibilitando uma melhor e mais confortável acomodação das lentes de contato nos olhos.

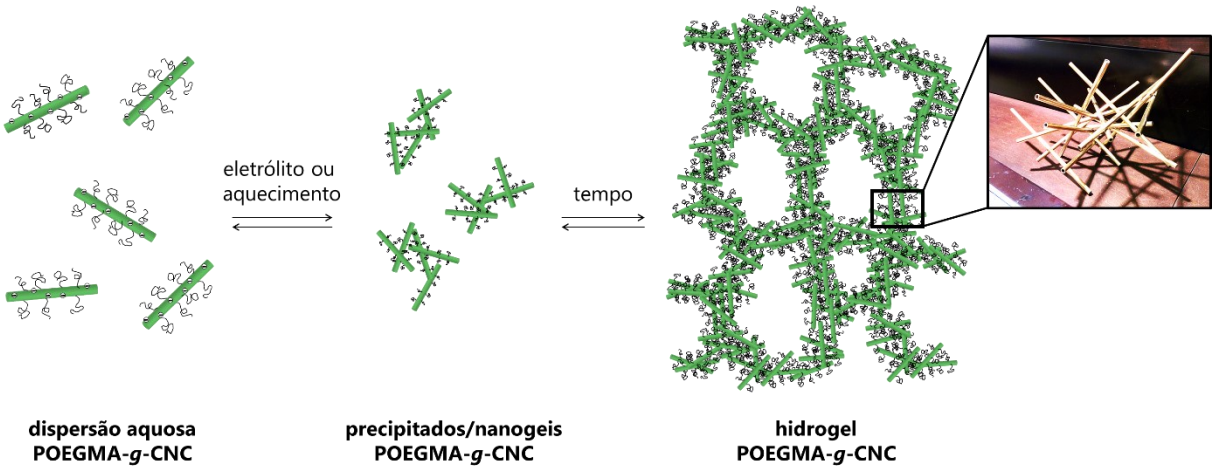

Figura 26: Esquema ilustrando a formação do hidrogel a partir da temperatura ou da adição de eletrólitos.

5.3. Conclusões

A formação do hidrogel foi estudada de forma sistemática variando-se a composição do POEGMA enxertado sobre a CNC e adicionando-se diferentes concentrações de cloreto de sódio. Os hidrogéis de POEGMA-*g*-CNC são formados pela interação das cadeias poliméricas de um objeto coloidal com outro ou adsorção na superfície da CNC, formando uma reticulação física. Estes hidrogéis podem ser obtidos de forma reversível seja pela adição de sal ou pelo aumento da temperatura. A adição de sal neutraliza as cargas negativas da superfície da CNC, o que permite a aproximação dos objetos coloidais e a interação das cadeias poliméricas. A remoção do sal através de diálise faz com que o hidrogel se desfaça, voltando à dispersão de POEGMA-*g*-CNC como inicialmente. Por outro lado, as cadeias laterais mais longas do POEGMA promovem um impedimento estérico, prevenindo a aproximação dos POEGMA-*g*-CNC e a formação da reticulação. Com o aumento da temperatura, o copolímero POEGMA enxertado na superfície da CNC passa por uma transição de fase e se contrai, diminuindo o impedimento estérico e aproximando os objetos que interagem entre si formando o gel. Desta forma, variando-se a quantidade de grupos EO na composição do POEGMA, pode-se controlar a temperatura de formação do hidrogel e a sua densidade. Com tempo de contato suficiente, a formação do sistema pode ser irreversível, gerando um material permanente. Com a conclusão das investigações aqui apresentadas, outros estudos foram positivamente impactados, com a ampliação da pesquisa referente ao uso de outros polímeros enxertados sobre a nanopartícula assim como a variação da nanopartícula em que o polímero está enxertado. Ademais, este trabalho desperta a investigação focada no efeito dos diferentes copolímeros da família POEGMA na formação da estrutura do hidrogel, que pode ser caracterizada, por exemplo, pela

determinação de área superficial, porosidade e densidade aparente, microestrutura, capacidade de retenção de água ou solventes, e propriedades mecânicas.

6. Reticulação supramolecular *host-guest*

Adicionalmente à formação de hidrogel pela coagulação do POEGMA-*g*-CNC com adição de solução aquosa de sais ou pela indução aquecendo a amostra acima da temperatura de transição do POEGMA, foi investigada a aplicação da α-ciclodextrina (α-CD) como agente de reticulação supramolecular através de complexos de inclusão utilizando a cadeia lateral mais longa do POEGMA, conforme ilustrado na Figura 27. A hipótese é que neste caso o aumento da temperatura causa a transição de fase do POEGMA, consequentemente o encolhimento da cadeia polimérica, e a saída da cadeia lateral do POEGMA de dentro da cavidade da α-CD.

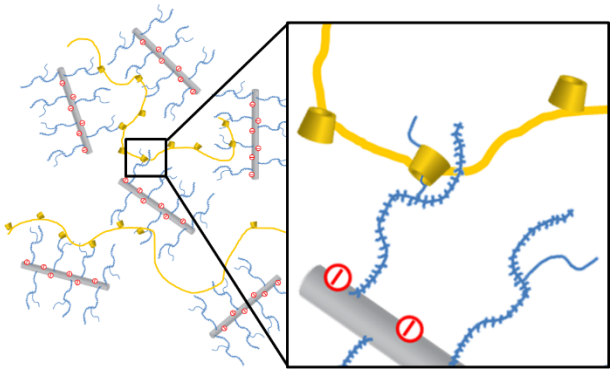

Figura 27: Conceito da reticulação supramolecular promovida pela α-CD em um sistema contendo POEGMA-*g*-CNC, formando um hidrogel *self-healing*.

O objetivo neste capítulo foi investigar a complexação do monômero $EO_{45}MA$, utilizado na composição dos copolímeros POEGMA nos capítulos anteriores desta Tese, com a α-CD. Estes relevantes resultados obtidos (apresentados a seguir) levaram a uma investigação mais focada neste fenômeno, sendo liderada pelo então pesquisador pós-doc do grupo, Dr. Marcos Mariano, e publicamos na revista *ACS Omega* em 2020 o artigo intitulado *Inclusion complexation between α-cyclodextrin and oligo(ethylene glycol) methyl ether methacrylate* [97]. Minha colaboração naquele trabalho foi a ideia original do estudo com os resultados iniciais obtidos e a discussão dos dados obtidos no estudo. Este artigo na íntegra está como anexo.

6.1. Introdução

Ciclodextrinas (CD) são moléculas macrocíclicas que têm uma estrutura em forma de cone truncado com cavidade hidrofóbicas e exterior hidrofílico, conforme ilustrado na Figura 28. Podem formar complexos de inclusão do tipo hospedeiro-hóspede com moléculas

hidrofóbicas e são utilizadas para formar hidrogéis supramoleculares [98–100]. Por exemplo, o grupo de pesquisa do Prof. Akira Harada desenvolveu hidrogéis *self-healing* utilizando ciclodextrinas que formam complexos de inclusão com ferroceno [101], azobenzene [102, 103], derivados do adamantano [104], dentre outros [105]. Não apenas grupos pequenos formam complexo de inclusão com ciclodextrinas: cadeias de PEO podem também entrar espontaneamente na cavidade da α-CD e formar géis supramoleculares [65, 103, 106]. Similar a estes complexos, McKee e colaboradores [107] produziram um hidrogel com elevada propriedade mecânica, devido à CNC, e com propriedades *self-healing*, promovida por complexos de inclusão utilizando cucurbiturilas, uma molécula macrocíclica análoga à CD.

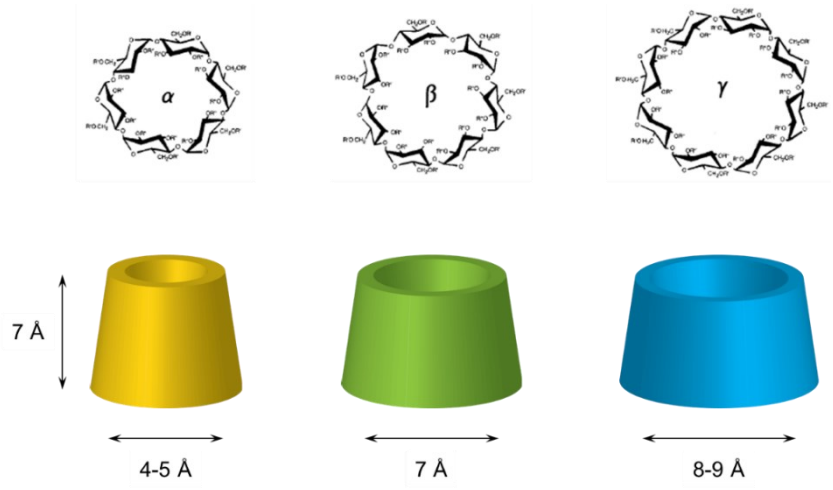

Figura 28: Representação da alfa-, beta- e gama-ciclodextrina, respectivamente.

Com o objetivo de unir as propriedades dos copolímeros da família POEGMA com a propriedade *self-healing* promovida pela CD e com a resistência mecânica promovida pela CNC, pode-se desenvolver um hidrogel com tais características composto por POEGMA-*g*-CNC e reticulado utilizando-se CD. Este capítulo foi um estudo inicial da formação de complexos de inclusão das cadeias laterais de EO presentes no copolímero POEGMA na cavidade da α-CD.

6.2. Experimental

Reagentes

Metacrilato de oligoetileno glicol metil éter ($EO_{45}MA$) (M_n = 2.080 g mol^{-1}) (Sigma-Aldrich) foi purificados passando por uma coluna de alumina básica para remover os inibidores. A α-ciclodextrina (α-CD, Aldrich, ≥99,0%) foi utilizada sem purificação adicional.

Água do sistema Milli-Q® (resistividade de 18,2 MΩ·cm) foi utilizada no preparo de todas as soluções.

Titulação calorimétrica isotérmica

A interação entre a α-CD e o monômero $EO_{45}MA$ foi investigada através de experimentos calorimétricos, realizados em um MicroCal VP-ITC. Soluções aquosas do oligômero $EO_{45}MA$ a 0,2, 0,7, 2,5 e 5,0 mM foram tituladas com uma solução de α-CD a 120 mM. Utilizou-se água como branco. As medições foram realizadas a 25 °C e a velocidade de agitação foi de 394 rpm.

Espalhamento de luz dinâmico

Análises de espalhamento de luz dinâmico (DLS) de soluções aquosas da amostra a 0,1 % (m/m) foram realizadas em um Zetasizer Nano ZS (Malvern Instruments, Reino Unido), equipada com um laser vermelho de He-Ne (λ = 632,8 Nm). As contagens de fótons foram detectadas no ângulo de 173°. Antes das medidas, todas as soluções foram filtradas utilizando um filtro descartável de 0,45 μm. Cada medida foi realizada em triplicata após equilibrar por 120 s.

6.3. Resultados e discussão

A α-CD pode proporcionar a propriedade *self-healing* ao hidrogel formado por POEGMA-*g*-CNC através da reticulação supramolecular pela inclusão na sua cavidade da cadeia lateral mais longa de EO do copolímero POEGMA.

Inclusão da cadeia polimérica EO na α-CD

Para confirmar a inclusão da cadeia $EO_{45}MA$ na cavidade da α-CD foram feitas medições de ITC e DLS. A Figura 29 mostra a energia envolvida na interação da α-CD com o oligômero $EO_{45}MA$. A diluição da α-CD é endotérmica enquanto a interação α-CD–oligômero é exotérmica. Quanto mais concentrada a solução oligomérica, mais exotérmica a energia da interação α-CD–oligômero. A inclinação da região entre 0 e 10 mM de α-CD torna-se mais negativa com a concentração do oligômero. As titulações de α-CD nas soluções de oligômero a 2,5 e 5,0 mM apresentam uma alteração abrupta nesta inclinação na região de concentração da α-CD entre 6 e 10 mM, indicando uma saturação na inclusão do oligômero na sua cavidade.

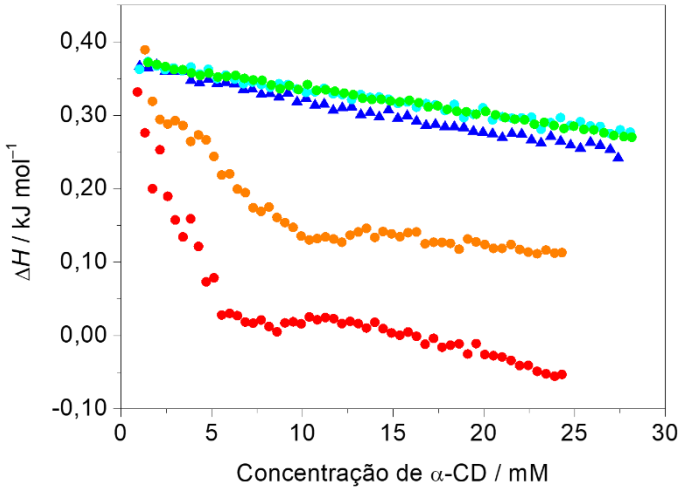

Figura 29: Titulação calorimétrica isotérmica (ITC) de α-CD a 120 mM em (▲) água e em soluções aquosas do oligômero $EO_{45}MA$ a concentrações variadas: (●) 0,2, (●) 0,7, (●) 2,5 e (●) 5,0 mM. T = 25 °C, velocidade de agitação = 394 rpm.

A Figura 30 mostra as curvas de DLS do complexo α-CD–$EO_{45}MA$ em diferentes proporções. O monômero livre em soluções apresenta principalmente um tamanho menor que 10 nm, ao passo que, com a adição de α-CD, os picos em tamanhos maiores (tipicamente 100–500 nm) tornam-se predominantes.

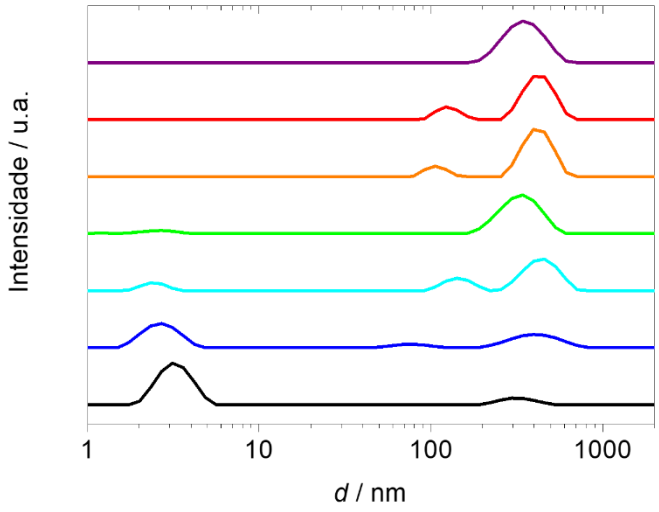

Figura 30: Curvas de DLS para o (■) monômero $EO_{45}MA$ a 5,0 mM e misturas com soluções aquosas nas concentrações finais de α-CD de (■) 50, (■) 100, (■) 150, (■) 200, (■) 300 e (■) 500 mM.

Reticulação supramolecular

A reticulação supramolecular proporcionada pela α-CD traz um brilho especial ao desenvolvimento de hidrogel *self-healing*. Os resultados de ITC e de DLS indicam que ocorre a formação de um complexo de inclusão entre a α-CD e o oligômero $EO_{45}MA$. Os resultados das duas técnicas mostram uma alteração abrupta na mesma região da razão α-CD:$EO_{45}MA$, o que sugere uma estequiometria aproximada do complexo formado instantaneamente de 1,3:1 (α-CD:$EO_{45}MA$). Neste processo de inclusão, apenas uma das extremidades da cadeia de $EO_{45}MA$ está disponível para a entrada da α-CD: o grupo metacrilato impede a incorporação do macrociclo. A incorporação de mais de uma α-CD depende de a primeira percorrer a cadeia deixando a extremidade livre, o que pode levar horas para ocorrer (Figura 31). A formação do complexo de inclusão é dependente da concentração da α-CD, sendo que concentrações maiores induzem a sua formação. Cada um destes complexos de inclusão formado pode atuar como pontos de reticulação no caso POEGMA-*g*-CNC.

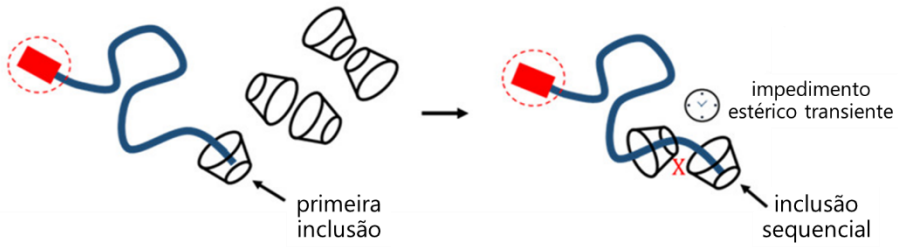

Figura 31: Representação do processo de formação do complexo de inclusão da α-CD com $EO_{45}MA$. Adaptado da referência [97]. © 2020 American Chemical Society.

Foram realizados ensaios de reticulação supramolecular de POEGMA-*g*-CNC com a α-CD. A adição de α-CD livre à solução aquosa de POEGMA-*g*-CNC causa uma precipitação instantânea, o que indica a incorporação das cadeias laterais de EO na cavidade da α-CD. Contudo, em nenhum dos casos foi ainda possível obter um gel. Diversas condições e proporções de misturas foram testadas, mas nenhuma atingiu a formação de um hidrogel supramolecular. Para uma reticulação eficiente é necessário que as α-CD estejam conectadas entre si, formando um polímero contendo grupos pendentes do macrociclo.

6.4. Conclusões

Por duas técnicas diferentes aqui apresentadas foi possível evidenciar a formação de complexos de inclusão do monômero $EO_{45}MA$, que pode ser utilizado como cadeia lateral nos copolímeros da família POEGMA, com a α-CD. A inclusão na α-CD ocorre pela

extremidade da cadeia do monômero contendo o grupo metila enquanto a outra extremidade, contendo o grupo metacrilato, impede a passagem do macrocíclo. Estes complexos de inclusão formados podem atuar como pontos de reticulação em um hidrogel *self-healing*, no entanto, é necessário que os macrociclos estejam conectados em uma cadeia polimérica, podendo ser o grupo pendente disponível para a inclusão das cadeias laterais de EO do POEGMA.

7. Conclusões Gerais

Neste trabalho, investigou-se o efeito da arquitetura molecular nos agregados formados em água por copolímeros biocompatíveis e termorresponsivos da família POEGMA em função da temperatura. A arquitetura molecular destes copolímeros pode ser projetada para atingir um valor determinado de temperatura de transição de fase e uma estrutura de agregação específica, micelar ou agregados com separação de fase macroscópica, com potencial aplicação em encapsulamento e liberação controlada de compostos hidrofóbicos. A incorporação de copolímeros desta família na superfície da CNC pode ser realizada por um procedimento simples, adequando a sua composição para a temperatura de transição desejada, uma vez que a capacidade de resposta térmica do polímero não é alterada; porém, neste caso ocorre apenas separação de fase macroscópica. Uma nova metodologia utilizando-se HSDSC foi utilizada para estimar a quantidade de polímero enxertado na superfície da CNC e abre a possibilidade para esta determinação através de uma técnica mais simples e robusta. A adição de sal e/ou o aumento da temperatura induz de forma reversível a formação de gel, com a aproximação das nanopartículas de celulose. Além disso, a CNC melhora as propriedades mecânicas do hidrogel e diminui a quantidade de polímero necessária para formar gel. Ademais, a cadeia lateral de grupos EO do copolímero POEGMA formam complexos de inclusão com a α-CD, que podem ser utilizados como pontos de reticulação supramolecular para a formação de um hidrogel *self-healing*. Todos estes estudos aqui apresentados influenciaram pesquisas correntes do Grupo de Pesquisa e de outros. O entendimento individual e em conjunto destes complexos sistemas permite a elaboração de sistemas poliméricos funcionais otimizados, beneficiando aplicações em diversas áreas da ciência e possibilitando aumentar a eficiência e racionalização no uso dos materiais poliméricos.

8. Referências

1. H.-G. Elias, R. Mülhaupt. “Plastics, General Survey, 1. Definition, Molecular Structure and Properties”. In: B. Elvers (Ed.). *Ullmann's Polymers and Plastics: Products and Processes*, 4 Volume. Weinheim, Germany Wiley-VCH, 2016.
2. A. Scudo, B. Liebmann, C. Corden, D. Tyrer, J. Kreissig, O. Warwick. “Intentionally added microplastics in products”. *Final report of the study conducted by Amec Foster Wheeler Environment & Infrastructure UK Limited in October 2017 on behalf of the European Commission*, 2017.
3. The Nobel Prize in Chemistry 1953. https://www.nobelprize.org/prizes/chemistry/1953/summary, acessado em 3 de abril de 2021.
4. American Chemical Society (ACS). Chemical Abstracts Service (CAS). SciFinder^{n}. https://scifinder-n.cas.org, acessado em 3 de abril de 2021.
5. PatSnap IP intelligence platform. https://analytics.patsnap.com, acessado em 3 de abril de 2021.
6. World Intellectual Property Organization (WIPO). Classificação Internacional de Patentes (IPC). http://ipc.inpi.gov.br/classifications/ipc/ipcpub, acessado em 3 de abril de 2021.
7. T.S. Galloway, M. Cole, C. Lewis. “Interactions of microplastic debris throughout the marine ecosystem”, *Nature Ecology & Evolution*, **2017**, *1*, 0116.
8. W.R. Waldman, M.C. Rillig. “Microplastic Research Should Embrace the Complexity of Secondary Particles”, *Environmental Science & Technology*, **2020**, *54*, 7751–7753.
9. M.C. Rillig, S.W. Kim, T.-Y. Kim, W.R. Waldman. “The Global Plastic Toxicity Debt”, *Environmental Science & Technology*, **2021**, *55*, 2717–2719.
10. H.S. Auta, C.U. Emenike, S.H. Fauziah. “Distribution and importance of microplastics in the marine environment: A review of the sources, fate, effects, and potential solutions”, *Environment International*, **2017**, *102*, 165–176.
11. A.L. Andrady. “The plastic in microplastics: A review”, *Marine Pollution Bulletin*, **2017**, *119*, 12–22.
12. A. Ragusa, A. Svelato, C. Santacroce, P. Catalano, V. Notarstefano, O. Carnevali, F. Papa, M.C.A. Rongioletti, F. Baiocco, S. Draghi, E. D'Amore, D. Rinaldo, M. Matta, E. Giorgini. “Plasticenta: First evidence of microplastics in human placenta”, *Environment International*, **2021**, *146*, 106274.
13. European Chemicals Agency (ECHA). “Microplásticos”. https://echa.europa.eu/pt/hot-topics/microplastics, acessado em 3 de abril de 2021.
14. A.D. Jenkins, R.G. Jones, G. Moad. “Terminology for reversible-deactivation radical polymerization previously called “controlled” radical or “living” radical polymerization (IUPAC Recommendations 2010)”, *Pure and Applied Chemistry*, **2010**, *82*, 483–491.

15. O. Bertrand, P. Wilson, J.A. Burns, G.A. Bell, D.M. Haddleton. “Cu(0)-mediated living radical polymerisation in dimethyl lactamide (DML); an unusual green solvent with limited environmental impact”, *Polymer Chemistry*, **2015**, *6*, 8319–8324.

16. M. Destarac. “Industrial development of reversible-deactivation radical polymerization: is the induction period over?”, *Polymer Chemistry*, **2018**, *9*, 4947–4967.

17. A. Ding, J. Xu, G. Gu, G. Lu, X. Huang. “PHEA-*g*-PMMA Well-Defined Graft Copolymer: ATRP Synthesis, Self-Assembly, and Synchronous Encapsulation of Both Hydrophobic and Hydrophilic Guest Molecules”, *Scientific Reports*, **2017**, *7*, 12601.

18. A. Kumar, S.V. Lale, S. Mahajan, V. Choudhary, V. Koul. “ROP and ATRP Fabricated Dual Targeted Redox Sensitive Polymersomes Based on pPEGMA-PCL-*ss*-PCL-pPEGMA Triblock Copolymers for Breast Cancer Therapeutics”, *ACS Applied Materials & Interfaces*, **2015**, *7*, 9211–9227.

19. B.E. Woodworth, S. Coca, J.B. O’Dwyer. “Pigment dispersions containing dispersants prepared by controlled radical polymerization and having pendent hydrophilic polymeric segments”, Patente US 6,294,014 B1, 25 de setembro de 2001.

20. C. Farcet. “Gradient copolymer, composition including same and cosmetic make-up or care method”, Patente US 9,827,183 B2, 28 de novembro de 2017.

21. M. Adamy, C. Vernay. “New Dispersant Polymers for the Design of Complex Suspension and Flowable Concentrate Formulations”, *AGROPAGES 2021 Formulation & Adjuvant Technology*, http://news.agropages.com/News/NewsDetail---38842-e.htm, acessado em 22 de abril de 2021.

22. L. Charles, J.-F. Lutz. “Design of Abiological Digital Poly(phosphodiester)s”, *Accounts of Chemical Research*, **2021**, *54*, 1791–1800.

23. K. Matyjaszewski, J. Spanswick. “Controlled/living radical polymerization”, *Materials Today*, **2005**, *8*, 26–33.

24. B. Kronberg, K. Holmberg, B. Lindman. “Surfactants and Polymers Containing Oxyethylene Groups Show a Complex Behavior”. In: B. Kronberg, K. Holmberg, B. Lindman (Eds.). *Surface Chemistry of Surfactants and Polymers*, John Wiley & Sons, Ltd., 2014.

25. M. Kroner, K.-H. Büchner, J. Perner, H.-J. Raubenheimer, D. Faul. “Method for producing water soluble polymer of esters from ethylenically unsaturated carboxylic acids and polyalkylene glycols”, Patente US 6,855,762 B1, 15 de fevereiro de 2005.

26. R.G. Jones, J. Kahovec, R. Stepto, E.S. Wilks, M. Hess, T. Kitayama, W.V. Metanomski. “Definitions of terms relating to the structure and processing of sols, gels, networks and inorganic-organic hybrid materials”. In: R.G Jones, E.S Wilks, W.V. Metanomski, J. Kahovec, M. Hess, R. Stepto, T. Kitayama (Eds.). *Compendium of Polymer Terminology and Nomenclature – IUPAC recommendations 2008*, RSC Publishing, Cambridge, 2009.

27. A. Patel, K. Mequanint. “Hydrogel Biomaterials”. In: R. Fazel-Rezai (Ed.). *Biomedical Engineering - Frontiers and Challenges*, InTech, 2011.

28. D.Y. Ko, U.P. Shinde, B. Yeon, B. Jeong. “Recent progress of in situ formed gels for biomedical applications”, *Progress in Polymer Science*, **2013**, *38*, 672–701.

29. A. Bortolin, F.A. Aouada, L.H.C. Mattoso, C. Ribeiro, “Nanocomposite PAAm/Methyl Cellulose/Montmorillonite Hydrogel: Evidence of Synergistic Effects for the Slow Release of Fertilizers”, *Journal of Agricultural and Food Chemistry*, **2013**, *61*, 7431–7439.

30. N. Annabi, A. Tamayol, J.A. Uquillas, M. Akbari, L.E. Bertassoni, C. Cha, G. Camci-Unal, M.R. Dokmeci, N.A. Peppas, A. Khademhosseini. “25th Anniversary Article: Rational Design and Applications of Hydrogels in Regenerative Medicine”, *Advanced Materials*, **2014**, *26*, 85–124.

31. M.R. Guilherme, F.A. Aouada, A.R. Fajardo, A.F. Martins, A.T. Paulino, M.F.T. Davi, A.F. Rubira, E.C. Muniz. “Superabsorbent hydrogels based on polysaccharides for application in agriculture as soil conditioner and nutrient carrier: A review”, *European Polymer Journal*, **2015**, *72*, 365–385.

32. D. Cheng, Y. Liu, G. Yang, A. Zhang. “Water- and Fertilizer-Integrated Hydrogel Derived from the Polymerization of Acrylic Acid and Urea as a Slow-Release N Fertilizer and Water Retention in Agriculture”, *Journal of Agricultural and Food Chemistry*, **2018**, *66*, 5762–5769.

33. P.W. Livanec, S.A. Klasner. “Hollow hydrogel capsules and methods of using the same”, Patente US 10,662,361 B2. 26 de maio de 2020

34. M. Mahinroosta, Z.J. Farsangi, A. Allahverdi, Z. Shakoori. “Hydrogels as intelligent materials: A brief review of synthesis, properties and applications”, *Materials Today Chemistry*, **2018**, *8*, 42–55.

35. D. Buenger, F. Topuz, J. Groll. “Hydrogels in sensing applications”, *Progress in Polymer Science*, **2012**, *37*, 1678–1719.

36. C.H. Alarcón, S. Pennadam, C. Alexander, “Stimuli responsive polymers for biomedical applications”, *Chemical Society Reviews*, **2005**, *34*, 276–285.

37. M.C. Koetting, J.T. Peters, S.D. Steichen, N.A. Peppas. “Stimulus-responsive hydrogels: Theory, modern advances, and applications”, *Materials Science and Engineering: R: Reports*, **2015**, *93*, 1–49.

38. Y. Habibi, L.A. Lucia, O.J. Rojas. “Cellulose nanocrystals: chemistry, self-assembly, and applications”, *Chemical Reviews*, **2010**, *110*, 3479–3500.

39. R.J. Moon, A. Martini, J. Nairn, J. Simonsen, J. Youngblood. “Cellulose nanomaterials review: structure, properties and nanocomposites”, *Chemical Society Reviews*, **2011**, *40*, 3941–3994.

40. A. Dufresne. “Nanocellulose: a new ageless bionanomaterial”, *Materials Today*, **2013**, *16*, 220–227.

41. M. Jacoby. “Nano From the Forest”, *Chemical & Engineering News*, **2014**, *92*, 9–12.

42. K.J. De France, T. Hoare, E.D. Cranston. “Review of Hydrogels and Aerogels Containing Nanocellulose, *Chemistry of Materials*, **2017**, *29*, 4609–4631.

43. K.J. De France, E.D. Cranston, T. Hoare. “Mechanically Reinforced Injectable Hydrogels”, *ACS Applied Polymer Materials*, **2020**, *2*, 1016–1030.

44. E.S. Ferreira, C.A. Rezende, E.D. Cranston. “Fundamentals of cellulose lightweight materials: bio-based assemblies with tailored properties”, *Green Chemistry*, **2021**, Advance Article.

45. M.S. Reid, M. Villalobos, E.D. Cranston. “Benchmarking Cellulose Nanocrystals: From the Laboratory to Industrial Production”, *Langmuir*, **2017**, *33*, 1583–1598.

46. O.M. Vanderfleet, E.D. Cranston. “Production routes to tailor the performance of cellulose nanocrystals”, *Nature Reviews Materials*, **2021**, *6*, 124–144.

47. B.L. Peng, N. Dhar, H.L. Liu, K.C. Tam. “Chemistry and applications of nanocrystalline cellulose and its derivatives: A nanotechnology perspective”, *The Canadian Journal of Chemical Engineering*, **2011**, *89*, 1191–1206.

48. S. Eyley, W. Thielemans. “Surface modification of cellulose nanocrystals”, *Nanoscale*, **2014**, *6*, 7764–7779.

49. S.P. Akhlaghi, D. Tiong, R.M. Berry, K.C. Tam. “Comparative release studies of two cationic model drugs from different cellulose nanocrystal derivatives”, *European Journal of Pharmaceutics and Biopharmaceutics*, **2014**, *88*, 207–215.

50. N. Lin, A. Dufresne. “Nanocellulose in biomedicine: Current status and future prospect”, *European Polymer Journal*, **2014**, *59*, 302–325.

51. K.J. De France, M. Badv, J. Dorogin, E. Siebers, V. Panchal, M. Babi, J. Moran-Mirabal, M. Lawlor, E.D. Cranston, T. Hoare. “Tissue Response and Biodistribution of Injectable Cellulose Nanocrystal Composite Hydrogels”, *ACS Biomaterials Science & Engineering*, **2019**, *5*, 2235–2246.

52. F.V. Ferreira, C.G. Otoni, K.J. De France, H.S. Barud, L.M.F. Lona, E.D. Cranston, O.J. Rojas. “Porous nanocellulose gels and foams: Breakthrough status in the development of scaffolds for tissue engineering”, *Materials Today*, **2020**, *37*, 126–141.

53. C. Liu, H. Du, L. Dong, X. Wang, Y. Zhang, G. Yu, B. Li, X. Mu, H. Peng, H. Liu, “Properties of Nanocelluloses and Their Application as Rheology Modifier in Paper Coating”, *Industrial & Engineering Chemistry Research*, **2017**, *56*, 8264–8273.

54. R. Nasseri, C.P. Deutschman, L. Han, M.A. Pope, K.C. Tam. “Cellulose nanocrystals in smart and stimuli-responsive materials: a review”, *Materials Today Advances*, **2020**, *5*, 100055.

55. K. Liu, S. Wei, L. Song, H. Liu, T. Wang. “Conductive Hydrogels—A Novel Material: Recent Advances and Future Perspectives”, *Journal of Agricultural and Food Chemistry*, **2020**, *68*, 7269–7280.

56. S.A. Kedzior, V.A. Gabriel, M.A. Dubé, E.D. Cranston. “Nanocellulose in Emulsions and Heterogeneous Water-Based Polymer Systems: A Review”, *Advanced Materials*, **2020**, 2002404

57. X. Yang, E.D. Cranston. “Chemically cross-linked cellulose nanocrystal aerogels with shape recovery and superabsorbent properties”, *Chemistry of Materials*, **2014**, *26*, 6016–6025.

58. Q. Pang, J. Tang, H. Huang, X. Liang, C. Hart, K.C. Tam, L.F. Nazar. “A nitrogen and sulfur dual-doped carbon derived from polyrhodanine@cellulose for advanced lithium–sulfur batteries”, *Advanced Materials*, **2015**, *27*, 6021–6028.

59. X. Yang, K. Shi, I. Zhitomirsky, E.D. Cranston. “Cellulose Nanocrystal Aerogels as Universal 3D Lightweight Substrates for Supercapacitor Materials”, *Advanced Materials*, **2015**, *27*, 6104–6109.

60. J. Tang, P.J. Quinlan, K.C. Tam. “Stimuli-responsive Pickering emulsions: Recent advances and potential applications”, *Soft Matter*, **2015**, *11*, 3512–3529.

61. Yi Liu, Shan-hui Hsu. “Synthesis and Biomedical Applications of Self-healing Hydrogels”, *Frontiers in Chemistry*, **2018**, *6*, 449.

62. S. Talebian, M. Mehrali, N. Taebnia, C. P. Pennisi, F. B. Kadumudi, J. Foroughi, M. Hasany, M. Nikkhah, M. Akbari, G. Orive, A. Dolatshahi-Pirouz. “Self-Healing Hydrogels: The Next Paradigm Shift in Tissue Engineering?”, *Advanced Science*, **2019**, *6*, 1801664.

63. J. Wankar, N. G. Kotla, S. Gera, S. Rasala, A. Pandit, Y. A. Rochev. “Recent Advances in Host–Guest Self-Assembled Cyclodextrin Carriers: Implications for Responsive Drug Delivery and Biomedical Engineering”, *Advanced Functional Materials*, **2020**, *30*, 1909049.

64. L.-H. Fu, C. Qi, M.-G. Ma, P. Wan. “Multifunctional cellulose-based hydrogels for biomedical applications”, *Journal of Materials Chemistry B*, **2019**, *7*, 1541–1562.

65. A. Harada, M. Kamachi. “Complex formation between poly(ethylene glycol) and α-cyclodextrin”, *Macromolecules*, **1990**, *23*, 2821–2823.

66. The Nobel Prize in Chemistry 2016. Prize announcement. https://www.nobelprize.org/-prizes/chemistry/2016/prize-announcement, acessado em 22 de maio de 2021.

67. M. Xue, Y. Yang, X. Chi, X. Yan, F. Huang. “Development of Pseudorotaxanes and Rotaxanes: From Synthesis to Stimuli-Responsive Motions to Applications”, *Chemical Reviews*, **2015**, *115*, 7398–7501.

68. G. Sinawang, M. Osaki, Y. Takashima, H. Yamaguchi, A. Harada. “Supramolecular self-healing materials from non-covalent cross-linking host–guest interactions”, *Chemical Communications*, **2020**, *56*, 4381–4395.

69. J.-F. Lutz, K. Weichenhan, Ö. Akdemir, A. Hoth. “About the phase transitions in aqueous solutions of thermoresponsive copolymers and hydrogels based on 2-(2-

methoxyethoxy)ethyl methacrylate and oligo(ethylene glycol) methacrylate", *Macromolecules*, **2007**, *40*, 2503–2508.

70. R. Pires-Oliveira, J. Tang, A.M. Percebom, C.L. Petzhold, K.C. Tam, W. Loh. "Effect of Molecular Architecture and Composition on the Aggregation Pathways of POEGMA Random Copolymers in Water", *Langmuir*, **2020**, *36*, 15018–15029.

71. C. Brinatti, S.P. Akhlaghi, R. Pires-Oliveira, O.D. Bernardinelli, R.M. Berry, K.C. Tam, W. Loh. "Controlled coagulation and redispersion of thermoresponsive poly di(ethylene oxide) methyl ether methacrylate grafted cellulose nanocrystals", *Journal of Colloid and Interface Science*, **2019**, *538*, 51–61.

72. N. Lin, A. Dufresne. "Supramolecular hydrogels from in situ host–guest inclusion between chemically modified cellulose nanocrystals and cyclodextrin", *Biomacromolecules*, **2013**, *14*, 871–880.

73. J.A. Kelly, A.M. Shukaliak, C.C.Y. Cheung, K.E. Shopsowitz, W.Y. Hamad, M.J. MacLachlan. "Responsive photonic hydrogels based on nanocrystalline cellulose", *Angewandte Chemie International Edition*, **2013**, *52*, 8912–8916.

74. H. Zhu, X. Yang, E.D. Cranston, S. Zhu. "Flexible and Porous Nanocellulose Aerogels with High Loadings of Metal–Organic-Framework Particles for Separations Applications", *Advanced Materials*, **2016**, *28*, 7652–7657.

75. K. Shi, X. Yang, E.D. Cranston, I. Zhitomirsky. "Efficient Lightweight Supercapacitor with Compression Stability", *Advanced Functional Materials*, **2016**, *26*, 6437–6445.

76. X. Yang, E. Bakaic, T. Hoare, E.D. Cranston. "Injectable Polysaccharide Hydrogels Reinforced with Cellulose Nanocrystals: Morphology, Rheology, Degradation, and Cytotoxicity", *Biomacromolecules*, **2013**, *14*, 4447–4455.

77. J.O. Zoppe, M. Österberg, R.A. Venditti, J. Laine, O.J. Rojas. "Surface interaction forces of cellulose nanocrystals grafted with thermoresponsive polymer brushes", *Biomacromolecules*, **2011**, *12*, 2788–2796.

78. A. Hebeish, S. Farag, S. Sharaf, Th.I. Shaheen. "Thermal responsive hydrogels based on semi interpenetrating network of poly(NIPAm) and cellulose nanowhiskers", *Carbohydrate Polymers*, **2014**, *102*, 159–166.

79. U.D. Hemraz, A. Lu, R. Sunasee, Y. Boluk. "Structure of poly (*N*-isopropylacrylamide) brushes and steric stability of their grafted cellulose nanocrystal dispersions", *Journal of Colloid and Interface Science*, **2014**, *430*, 157–165.

80. N. Adams, U.S. Schubert. "Poly(2-oxazolines) in biological and biomedical application contexts", *Advanced Drug Delivery Reviews*, **2007**, *59*, 1504–1520.

81. T.R. Dargaville, B.G. Hollier, A. Shokoohmand, R. Hoogenboom. "Poly(2-oxazoline) hydrogels as next generation three-dimensional cell supports", *Cell Adhesion & Migration*, **2014**, *8*, 88–93.

82. N.M.B. Smeets, E. Bakaic, M. Patenaude, T. Hoare. “Injectable poly(oligoethylene glycol methacrylate)-based hydrogels with tunable phase transition behaviours: Physicochemical and biological responses”, *Acta Biomaterialia*, **2014**, *10*, 4143–4155.

83. C. Gauche, M.I. Felisberti. “Colloidal Behavior of Cellulose Nanocrystals Grafted with Poly(2-alkyl-2-oxazoline)s”, *ACS Omega*, **2019**, *4*, 11893−11905.

84. K.J. De France, K.J.W. Chan, E.D. Cranston, Todd Hoare. “Enhanced Mechanical Properties in Cellulose Nanocrystal–Poly(oligoethylene glycol methacrylate) Injectable Nanocomposite Hydrogels through Control of Physical and Chemical Cross-Linking”, *Biomacromolecules*, **2016**, *17*, 649–660.

85. C. Weber, C.R. Becer, R. Hoogenboom, U.S. Schubert. “Lower Critical Solution Temperature Behavior of Comb and Graft Shaped Poly[oligo(2-ethyl-2-oxazoline)methacrylate]s”, *Macromolecules*, **2009**, *42*, 2965–2971.

86. N. Grishkewich, S.P. Akhlaghi, Z. Yao, R. Berry, K.C. Tam. “Cellulose nanocrystal-poly(oligo(ethylene glycol) methacrylate) brushes with tunable LCSTs”, *Carbohydrate Polymers*, **2016**, *144*, 215–222.

87. C. Weber, R.C. Becer, A. Baumgaertel, R. Hoogenboom, U.S. Schubert. “Preparation of Methacrylate End-Functionalized Poly(2-ethyl-2-oxazoline) Macromonomers”, *Designed Monomers and Polymers*, **2009**, *12*, 149–165.

88. C. Weber, C.R. Becer, W. Guenther, R. Hoogenboom, U.S. Schubert. “Dual Responsive Methacrylic Acid and Oligo(2-ethyl-2-oxazoline) Containing Graft Copolymers”, *Macromolecules*, **2010**, *43*, 160–167.

89. K.H.M. Kan, J. Li, K. Wijesekera, E.D. Cranston. “Polymer-grafted cellulose nanocrystals as pH-responsive reversible flocculants”, *Biomacromolecules*, **2013**, *14*, 3130–3139.

90. S.A. Kedzior, L. Graham, C. Moorlag, B.M. Dooley, E.D. Cranston. “Poly (methyl methacrylate)-grafted cellulose nanocrystals: One-step synthesis, nanocomposite preparation, and characterization”, *The Canadian Journal of Chemical Engineering*, **2016**, *94*, 811–822.

91. J.-F. Lutz, A. Hoth. “Preparation of Ideal PEG Analogues with a Tunable Thermosensitivity by Controlled Radical Copolymerization of 2-(2-Methoxyethoxy)ethyl Methacrylate and Oligo(ethylene glycol) Methacrylate”, *Macromolecules*, **2006**, *39*, 893–896.

92. T. Phan-Xuan, A. Thuresson, M. Skepö, A. Labrador, R. Bordes, A. Matic. “Aggregation behavior of aqueous cellulose nanocrystals: the effect of inorganic salts”, *Cellulose*, **2016**, *23*, 3653–3663.

93. S. Alharthia, N. Grishkewich, R.M. Berry, K.C. Tam. “Functional cellulose nanocrystals containing cationic and thermo-responsive polymer brushes”, *Carbohydrate Polymers*, **2020**, *246*, 116651.

94. M. Mariano, S.F. Souza, A.C. Borges, D.M. do Nascimento, J.S. Bernardes. "Tailoring strength of nanocellulose foams by electrostatic complexation", *Carbohydrate Polymers*, **2021**, *256*, 117547.

95. K.R. Peddireddy, I. Capron, T. Nicolai, L. Benyahia. "Gelation Kinetics and Network Structure of Cellulose Nanocrystals in Aqueous Solution", *Biomacromolecules*, **2016**, *17*, 3298–3304.

96. M. Baig, H. Gao, K.C. Tam, V. Maheshwari, X. Wu. "Artificial sensors and methods of manufacture thereof", Aplicação de Patente US 2016/0235347 A1, 18 de agosto de 2016.

97. M. Mariano, O.D. Bernardinelli, R. Pires-Oliveira, G.A. Ferreira, W. Loh. "Inclusion Complexation between α-Cyclodextrin and Oligo(ethylene glycol) Methyl Ether Methacrylate", *ACS Omega*, **2020**, *5*, 9517−9528.

98. W. Deng, H. Yamaguchi, Y. Takashima, A. Harada. "A chemical-responsive supramolecular hydrogel from modified cyclodextrins", *Angewandte Chemie*, **2007**, *119*, 5236–5239.

99. F. Yuen, K.C. Tam. "Cyclodextrin-assisted assembly of stimuli-responsive polymers in aqueous media", *Soft Matter*, **2010**, *6*, 4613–4630.

100. F. Li, J. He, M. Zhang, K.C. Tam, P. Ni. "Injectable supramolecular hydrogels fabricated from PEGylated doxorubicin prodrug and α-cyclodextrin for pH-triggered drug delivery", *RSC Advances*, **2015**, *5*, 54658–54666.

101. M. Nakahata, Y. Takashima, H. Yamaguchi, A. Harada. "Redox-responsive self-healing materials formed from host–guest polymers", *Nature Communications*, **2011**, *2*, 511.

102. Y. Takashima, T. Nakayama, M. Miyauchi, Y. Kawaguchi, H. Yamaguchi, A. Harada. "Complex Formation and Gelation between Copolymers Containing Pendant Azobenzene Groups and Cyclodextrin Polymers", *Chemistry Letters*, **2004**, *33*, 890–891.

103. S. Tamesue, Y. Takashima, H. Yamaguchi, S. Shinkai, A. Harada. "Photoswitchable Supramolecular Hydrogels Formed by Cyclodextrins and Azobenzene Polymers", *Angewandte Chemie International Edition*, **2010**, *49*, 7461–7464.

104. O. Kretschmann, S.W. Choi, M. Miyauchi, I. Tomatsu, A. Harada, H. Ritter. "Switchable Hydrogels Obtained by Supramolecular Cross-Linking of Adamantyl-Containing LCST Copolymers with Cyclodextrin Dimers", *Angewandte Chemie International Edition*, **2006**, *45*, 4361-4365.

105. A. Harada, Y. Takashima, M. Nakahata. "Supramolecular Polymeric Materials via Cyclodextrin–Guest Interactions", *Accounts of Chemical Research*, **2014**, *47*, 2128–2140.

106. C.A. Dreiss, T. Cosgrove, F.N. Newby, E. Sabadini. "Formation of a Supramolecular Gel between α-Cyclodextrin and Free and Adsorbed PEO on the Surface of Colloidal

Silica: Effect of Temperature, Solvent, and Particle Size", *Langmuir*, **2004**, *20*, 9124–9129.

107. J.R. McKee, E.A. Appel, J. Seitsonen, E. Kontturi, O.A. Scherman, O. Ikkala. "Healable, Stable and Stiff Hydrogels: Combining Conflicting Properties Using Dynamic and Selective Three-Component Recognition with Reinforcing Cellulose Nanorods", *Advanced Functional Materials*, **2014**, *24*, 2706–2713.

9. Anexos

9.1. Artigo publicado no *J. Colloid Interface Sci.* (Referência [71])

Journal of Colloid and Interface Science 538 (2019) 51–61

Contents lists available at ScienceDirect

Journal of Colloid and Interface Science

journal homepage: www.elsevier.com/locate/jcis

Regular Article

Controlled coagulation and redispersion of thermoresponsive poly di(ethylene oxide) methyl ether methacrylate grafted cellulose nanocrystals

César Brinatti [a], Seyedeh Parinaz Akhlaghi [a], Rafael Pires-Oliveira [a], Oigres Daniel Bernardinelli [a], Richard M. Berry [b], Kam Chiu Tam [c], Watson Loh [a,*]

[a] Institute of Chemistry – Universidade Estadual de Campinas (UNICAMP), CP 6154, CEP 13083-970 Campinas, SP, Brazil
[b] CelluForce Inc., 625 Président-Kennedy Avenue, Montreal, Quebec H3A 1K2, Canada
[c] Department of Chemical Engineering, Waterloo Institute for Nanotechnology, University of Waterloo, 200 University Avenue West, Ontario N2L 3G1, Canada

GRAPHICAL ABSTRACT

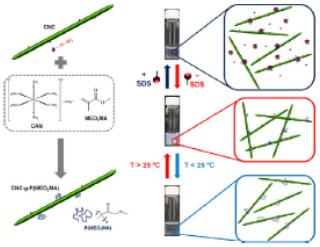

ARTICLE INFO

Article history:
Received 25 September 2018
Revised 15 November 2018
Accepted 16 November 2018
Available online 17 November 2018

Keywords:
Cellulose nanocrystals
PEO-based polymer grafting
Anionic surfactant
Temperature-induced phase transition

ABSTRACT

Hypothesis: Cellulose nanocrystals (CNCs) undergo precipitation in the presence of high concentrations of cationic surfactants in aqueous solutions. To avoid such behavior and/or to promote redispersion of CNC/surfactant mixtures, the CNC surface was grafted with poly di(ethylene oxide) methyl ether methacrylate, P(MEO_2MA).

Experiments: CNC-*g*-P(MEO_2MA) was characterized using the following techniques ^{13}C solid-state nuclear magnetic resonance (^{13}C SSNMR), Fourier-transform infrared spectroscopy – attenuated total reflection spectroscopy (FTIR-ATR) and thermal gravimetric analysis (TGA). Isothermal titration calorimetry (ITC), electrophoretic mobility, light scattering and high sensitivity differential scanning calorimetry (HSDSC) were used to study the interaction between CNC-*g*-P(MEO_2MA) and ionic surfactants, dodecyltrimethylammonium bromide ($C_{12}TAB$, cationic) and sodium dodecylsulfate (SDS, anionic) at temperatures below and above the LCST.

Findings: CNC-*g*-P(MEO_2MA) underwent phase separation above its lower critical solution temperature (LCST ~ 25 °C) and precipitated from solution as seen by HSDSC and transmittance experiments. When $C_{12}TAB$ was added to CNC-*g*-P(MEO_2MA) it induced the precipitation that prevented the redispersion due to strong electrostatic interactions with the negative charges on the CNC surface. With increasing concentrations of SDS, the polymer phase transition temperature was increased, which can be used to redisperse the CNC complexes. By removing SDS from the mixture via dialysis, the CNC-*g*-P(MEO_2MA) underwent subsequent phase transition.

* Corresponding author.
E-mail address: wloh@iqm.unicamp.br (W. Loh).

https://doi.org/10.1016/j.jcis.2018.11.071
0021-9797/

1. Introduction

Cellulose nanocrystals (CNCs) are a class of renewable nanomaterials derived from cellulose, typically via sulfuric acid hydrolysis. The negative sulfate-ester groups promote electrostatic stability of the CNC in aqueous and polar solvents [1–5]. In the presence of oppositely charged molecules, such as cationic alkyltrimethylammonium bromide surfactants (C_nTAB) the electrostatic interaction between CNC and surfactant resulted in the precipitation [6] when the surfactant concentration approaches approximately half its critical micellar concentration (*cmc*) [7]. To negate such behavior, one could alter the amount of cationic surfactants bound to CNC, by surface grafting polymers to the CNC, for instance one that would increase the CNC specific surface area and enhance the number of available binding sites.

Surface modification of cellulose and its derivatives [8], such as CNC with stimuli-responsive polymers – especially pH and temperature responsive systems – has been actively pursued in the past decade [9–13]. Poly (ethylene oxide) (PEO) and its derivatives have the advantages of being water-soluble, biocompatible and thermo-responsive. An important and yet relatively new class of PEO derivatives are those containing a methacrylate segment, whose monomers could be polymerized, and offer new application possibilities in various fields [12,14]. Nho & Kwon [15] modified the surface of cellulose films using the radiation polymerization grafting technique. They prepared poly (ethylene oxide methacrylate) (PEO_nMA) with increasing degree of hydrophilicity where the ethylene oxide units were increased from 2 to 9. The process was followed by amination and heparin immobilization to assess its compatibility with blood. Grishkewich et al. [11] reported that the lower critical solution temperature (LCST) behavior of the CNC-*g*-POEGMA nanoparticles could be varied over a wide temperature range of 24 to 64 °C by adjusting the grafted molar ratio of oligoethylene oxide methyl ether methacrylate units ($OEGMA_{300}$) to di(ethylene oxide) methyl ether methacrylate (MEO_2MA). They also observed a thermal hysteresis during the cool down cycle, denoting a kinetic effect on the nanoparticle's aggregation. Peng et al. [16] studied the interactions between alkyltrimethylammonium bromide C_nTAB series (n = 12, 14 and 16 carbon atoms in the alkyl chain) surfactants and a thermoresponsive copolymer comprised of MEO_2MA-*co*-$PEGMA_{2080}$ at temperatures below (25 °C) and above (30 °C) its LCST, using isothermal titration calorimetry (ITC) and ion-selective electrode (ISE) techniques. In their study, they concluded that hydrophobic forces dominated the interactions between the surfactant's alkyl chain and the hydrophobic polymer backbone. By increasing the temperature of the system beyond its LCST, the interactions with the more hydrophobic surfactant ($C_{16}TAB$ compared to $C_{12}TAB$) presented a larger enthalpy change (exothermic process). In a similar study [17], the interactions between a polymer-grafted CNC (CNC-*g*-M600, a poly (propylene glycol) (PPG) derivative) and different surfactants with alkyl chains containing 12 carbon atoms namely anionic sodium dodecylsulfate (SDS), $C_{12}TAB$ (cationic) and Brij 30 (a nonionic polyethyleneglycol (4) lauryl ether) was reported. No interactions were observed between CNC-*g*-M600 and Brij 30; but SDS interacted with the grafted polymer chains driven by hydrophobic forces, while $C_{12}TAB$ would bind electrostatically to the negatively charged sulfate-ester groups on the CNC surface.

In the present study, we modified the CNC surface by grafting a thermo-responsive polymer, poly di(ethylene oxide) methyl ether methacrylate, P(MEO_2MA) to its surface. We examined the multiple temperature-induced redispersion of the system containing CNC-*g*-P(MEO_2MA) in the presence of ionic surfactants SDS and C_nTAB at a temperature above its LCST of 25 °C. The "switch on/switch off" mechanism over various cycles of addition and removal of surfactant through dialysis was evaluated. The CNC surface modification was characterized by ^{13}C solid-state nuclear magnetic resonance (^{13}C SSNMR), Fourier-transform infrared spectroscopy – attenuated total reflection spectroscopy (FTIR-ATR) and thermal gravimetric analysis (TGA). The interactions between CNC-*g*-P(MEO_2MA) and surfactants were analyzed by ITC, electrophoretic mobility and light scattering measurements and high sensitivity differential scanning calorimetry (HSDSC) with varying SDS concentrations.

2. Experimental section

2.1. Chemicals

Cellulose nanocrystals (CNC) hydrolyzed with sulfuric acid from wood pulp were provided by CelluForce Inc and used as received. The ionic surfactants used were alkyltrimethylammonium bromide (C_nTAB, n = 12 and 16) and sodium dodecylsulfate (SDS) (≥98% purity). All the surfactants were used without purification. The monomer di(ethylene oxide) methyl ether methacrylate (MEO_2MA, 95% purity, M_w = 188.22 g mol^{-1}) was purified by passing it through a basic alumina oxide column to remove inhibitors. Cerium (IV) ammonium nitrate (CAN, purity ≥ 98%) was used without purification. All the chemicals were purchased from Sigma-Aldrich®. The water used to prepare all solutions and dispersions was of Milli-Q grade (18.2 MΩ cm).

2.2. Graft polymerization

In a two-neck round bottom flask 0.5 g of CNC powder was dispersed in 50.0 mL of water by ultrasonication using a Hielscher UP100H (Germany), with a MS3 sonication probe. The dispersion was kept under constant stirring at room temperature (23 °C) for 20 h and purged for 20 min with nitrogen gas. To maximize the amount of grafted polymer on the CNC surface, a ratio of 100:1 (MEO_2MA monomer to –OH groups on the CNC surface) was introduced into the flask. To the CNC dispersion, 1.0 mL of a solution containing 100 mg L^{-1} of cerium (IV) ammonium nitrate was added dropwise – the drops were only added after the yellow color from the cerium (IV) solution had disappeared. After this, the nitrogen purge was stopped, and the two necks of the flask were sealed with a rubber stopper and silicone glue. The final product (white solid agglomerate) was dialyzed against deionized water for 1 week using a membrane with a M_W cut-off of 12,000 g mol^{-1}. The reaction mechanism is described in Scheme 1. The product was then washed and centrifuged at 3,000 rpm during 20 min for 6 times. These procedures were adopted to ensure the complete removal of unreacted MEO_2MA monomers and unbound polymers that might be physically adsorbed to the CNC [18]. The polymer molecular weight should not interfere with the phase separation temperature according to Lutz [14] and therefore, for the purpose of the present study, it was not determined.

2.3. CNC-g-P(MEO_2MA) sample preparation

Stock dispersions of 3.0 wt% CNC-*g*-P(MEO_2MA) were prepared by ultrasonication in an ice bath with a Hielscher UP100H (Germany), using an MS3 sonication probe for at least 20 min and were later stored in the fridge. All the experiments were performed with 1.0 wt% CNC-*g*-P(MEO_2MA) by simply diluting the stock dispersion.

2.4. ^{13}C Solid-state NMR

^{13}C solid-state nuclear magnetic resonance (^{13}C SSNMR) experiments were performed using a Bruker Avance 400 spectrometer,

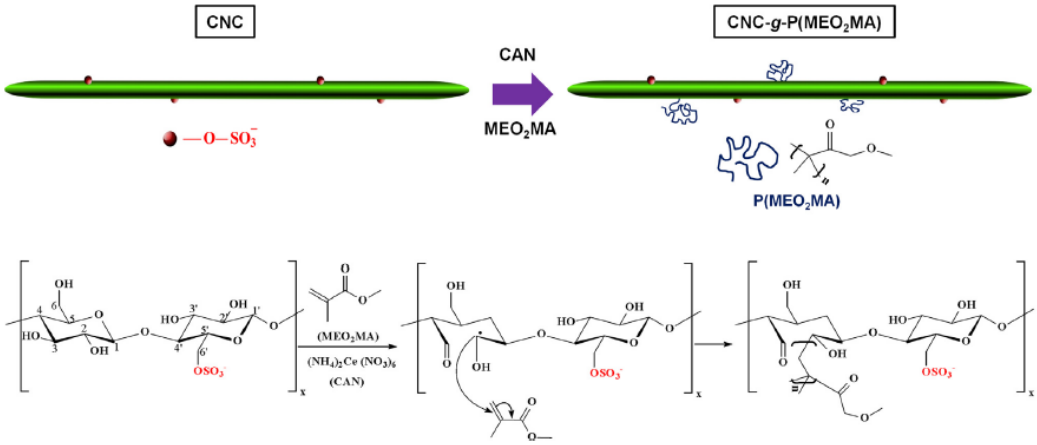

Scheme 1. Reaction mechanism at the CNC surface between MEO_2MA and hydroxyl groups in the presence of the cerium ammonium nitrate initiator.

equipped with a Bruker 4 mm MAS double-resonance probe head, with frequencies of 100.5 and 400.0 MHz for ^{13}C and ^{1}H, respectively. The macroscopic spinning frequencies at 14 kHz were controlled by a pneumatic system that ensures rotation stability higher than ~2 Hz. Typical $\pi/2$ pulse lengths of 3 and 2.7 μs were applied for ^{13}C and ^{1}H, respectively. A proton decoupling field strength of $\gamma B_1/2\pi = 80$ kHz was used. The ^{13}C multiple cross polarization blocks (MultiCP) method described by Johnson and Schmidt-Rohr was used to obtain quantitative spectra [19]. Here, 9 cross-polarization (CP) blocks with 1 ms were implemented, while the last CP before acquisition was executed with 0.8 ms, resulting in a total of 10 CP blocks with a variation of radiofrequency (RF) amplitude increment between 90 and 100%. The recycle delay was 2 s and the duration of the repolarisation period t_z was 0.9 s [20].

2.5. FTIR-ATR spectroscopy

An Agilent Cary 630 FTIR spectrometer (USA) with diamond attenuated total reflectance (ATR) with a ZnSe beamsplitter crystal was used to characterize both the pristine CNC and surface modified CNC-*g*-P(MEO_2MA). Each sample as analyzed over a frequency range of 400–4000 cm^{-1} and with a resolution of 4 cm^{-1}.

2.6. Thermogravimetric analysis (TGA)

Thermogravimetric experiments were conducted using TA 20.50 equipment (USA). The analyzed samples (pristine CNC powder, CNC-*g*-P(MEO_2MA) and P(MEO_2MA) supernatant) were put in a platinum pan and heated from 30 to 800 °C at a rate of 10 °C min^{-1}, under a nitrogen flow rate of 30 mL min^{-1}.

2.7. High sensitivity differential scanning calorimetry (HSDSC)

A MicroCal VP-DSC (Northampton, MA, USA) calorimeter was used for the experiments. CNC-*g*-P(MEO_2MA) dispersions and its mixtures containing SDS (0.1, 1.0, 5.0, 20.0 and 40.0 mmol kg^{-1}) were added in a 0.5 mL reaction cell and were scanned from 20 up to 110 °C. For the "switch on/switch off" studies, a fixed concentration of 5.0 mmol L^{-1} of SDS was used and removed subsequently by dialysis. Scan rates were performed at 60 °C h^{-1}. For all experiments, three consecutive runs were performed and the first one was considered to have erased the grafted-polymer thermal history. Data obtained were treated with the Origin® 7.0 software.

2.8. Transmittance measurements

Transmittance measurements were carried out on an 8453 Spectrophotometer (Hewlett-Packard) (USA), equipped with a Peltier system, at a wavelength of 600 nm under stirring (500 rpm). For the determination of the cloud point of CNC-*g*-P(MEO_2MA) the dispersion was heated from 15 to 40 °C and then cooled to 15 °C at a rate of 1.0 °C min^{-1}. Three consecutive cycles were performed, and the first cycle was intended to erase the thermal history of the grafted polymer.

2.9. Isothermal titration calorimetry (ITC)

A MicroCal VP-ITC (Northampton, MA, USA) was the calorimeter used for these experiments. Aliquots ranging from 3 to 10 μL were added stepwise by an automatic injection syringe containing 270 μL of a concentrated surfactant solution (at least twelve times above its *cmc* value) into the reaction cell of 1.43 mL, containing either water or a CNC-*g*-P(MEO_2MA) dispersion, with a 5 min interval between injections. Two different temperatures were used in the experiments: 15 °C and 40 °C, below and above the CNC-*g*-P(MEO_2MA) LCST, respectively. All the experiments were performed in duplicate. Data obtained were treated with the Origin® 7.0 software.

2.10. Electrophoretic mobility and particle size determination

Electrophoretic measurements were carried out using a Nano ZS Zetasizer (Malvern Instruments) (UK). It uses an M3-PALS technique – a combination of phase analysis light scattering and laser Doppler velocimetry. The CNC-*g*-P(MEO_2MA) concentration was fixed while the surfactant concentration was varied. When measuring highly concentrated surfactant solutions, only the $\mu\zeta$ sign is relevant, for there is a contribution from both the C_nTAB-CNC complex and the bulk micelles [21]. The experiments were performed in triplicate for all the systems.

For particle size determination (wavelength of 632.8 nm and detection angle of 173°), the *apparent* hydrodynamic diameter

($d_{H(app)}$) was measured at 15.0 ± 0.1 °C and at 40 ± 0.1 °C for C_{12}TAB and SDS, respectively. All the experiments were performed in triplicate.

3. Results

3.1. CNC-g-P(MEO$_2$MA) characterization

3.1.1. ^{13}C Solid-state NMR experiments

The MultiCP technique provides quantitative high sensitivity ^{13}C SSNMR spectra, enabling a good signal-to-noise ratio curve with reduced measurement time. Thus, the surface modification on the CNC by polymer grafting could be followed using SSNMR.

Fig. 1a shows the ^{13}C MultiCP SSNMR spectrum of CNC. The peak pattern is similar to the ones presented by Bernardinelli et al. [20], Simmons et al. [22], and Kedzior et al. [18] for cellulose signals, with some minor differences due to the use of CNC and ^{13}C MultiCP sequence. Based on the prior knowledge, the cellulose peaks are assigned at 62.8 ppm (carbon C_6^2 – surface cellulose), 65.3 ppm (carbon C_6^1 – internal cellulose), region between 70 and 78 ppm (carbons $C_{2,3,5}$ surface/internal cellulose), 84.0 ppm (carbon C_4^2 – surface cellulose), 89.0 ppm (carbon C_4^1 – internal cellulose), and 105 ppm (carbon C_1 – surface/internal cellulose) [20,22].

Fig. 1b shows the ^{13}C MultiCP spectrum of the CNC-g-P(MEO$_2$MA). All the peaks were integrated using Gaussians/Lorentzian deconvolutions and the quantity of each chemical group could be determined, except for the chemical shift range between 50 and 75 ppm, where the signal stemming from the CNC and the grafted polymer overlapped and deconvolution was not possible. The CNC-g-P(MEO$_2$MA) spectrum shows a clear contribution from the CNC signals and the presence of the polymer on its surface. It is not possible, however, to assess a specific shift in the spectra caused solely by the polymer grafting and we could not confirm whether or not there is a chemical linkage between CNC and P(MEO$_2$MA) chains [18]. Therefore, it was assumed that any polymer chains that were not bound to CNC would have been removed by washing/dialysis procedures. When comparing the signal ratio from C_4^1/C_4^2 (Fig. 1a) to C4 (Fig. 1b) there is a decrease in its signal from a) to b) that can be related to an increase in the order of the cellulose rings of the CNC by removing amorphous regions in between crystalline domains as seen in other studies [20,23,24]. The crystallinity index was determined in the spectral region in which the signals of the ordered cellulose domains (carbon C_4^1 – internal cellulose) and disordered cellulose domains (carbon C_4^2 – surface cellulose) could be distinguished [20,22]. For this purpose, the peaks at 80–86 and 86–94 ppm were deconvoluted through two Gaussians centered at 84 and 88 ppm in order to compare the disordered and ordered cellulose domains, respectively [20,25]. The crystallinity index value for the CNC was 53% while for the CNC-g-P(MEO$_2$MA) was 58%, which showed a trend of increasing overall order caused by the polymer grafting.

To address the overlap of the spectra in the region 50 to 75 ppm, the subtraction of the CNC-g-P(MEO$_2$MA) spectrum by the CNC spectrum was performed, as showed in Fig. 1c. With this approach it was possible to isolate the peak associated with the P(MEO$_2$MA) polymer chains and a proper assignment of their signals. Their values are labeled as CH_3 (17 ppm), C-backbone (45.3 ppm), OCH_3 (55.6 ppm), OCH_2 (58–75 ppm) and C=O (carbonyl 178 ppm) [18].

The number of carbon atoms in each chemical group for the P(MEO$_2$MA) polymer is shown in Table 1.

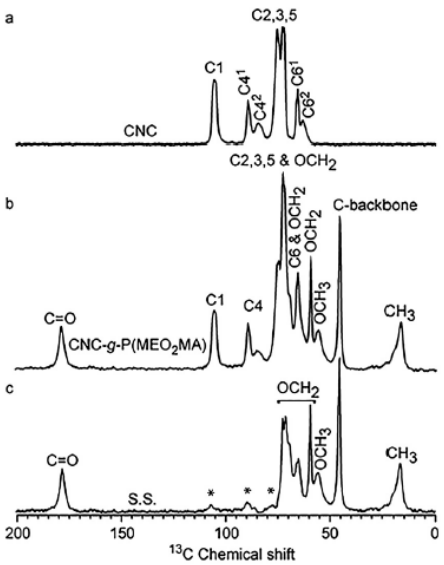

Fig. 1. ^{13}C MultiCP SSNMR spectra for: (a) Pristine CNC; (b) CNC-g-P(MEO$_2$MA); and (c) subtraction of the ^{13}C MultiCP SSNMR spectra "a" and "b". The * symbol represents carbons from anhydroglucose units from the CNC surface.

3.1.2. FTIR-ATR experiments

FTIR-ATR spectra of both pristine CNC and CNC-g-P(MEO$_2$MA) are presented in Fig. 2. Pristine CNC spectrum peaks are in accordance with previous studies [11,18,26]. The presence of a new peak at 1723 cm^{-1} at the CNC-g-P(MEO$_2$MA) spectrum is characteristic of a new C=O bond on the CNC surface agreeing with the proposed ring opening mechanism [15,27].

3.1.3. TGA experiments

Fig. 3 shows the decomposition curves obtained for pristine CNC, CNC-g-P(MEO$_2$MA) and the supernatant comprising mostly of P(MEO$_2$MA) loose polymer chains and unreacted monomers. Analyzing Fig. 3 (inset-derivative weight) we see that the pristine CNC (black curve) and CNC-g-P(MEO$_2$MA) (red curve) profiles were superimposed and displayed a pyrolysis process starting at 275 °C, that is attributed to the presence of sulfate groups on the surface associated with the acid hydrolysis of cellulose [28–30]. The pyrolysis process at higher temperatures of 350 °C and 600 °C is attributed to a slow char residue formation [28,29]. However, CNC-g-P(MEO$_2$MA) displayed an initial peak at a lower temperature of 185 °C. This indicates a reduction in the CNC thermal stability after polymer grafting [30]. In the proposed mechanism for the cerium (IV) ammonium nitrate ion initiated "grafting-from" radical reaction [9,18], it was suggested that the covalent bonds between C2 and C3 on the anhydroglucose units at the surface are broken

Table 1
Number of carbon atoms in each chemical group of the polymer grafted on the CNC surface obtained by ^{13}C MultiCP SSNMR.

Chemical group	Number of carbon atoms
AGU*	1.5 ± 0.3
C=O	1.0 ± 0.1
OCH_2	4.6 ± 0.4
OCH_3	1.2 ± 0.1
C-backbone	1.6 ± 0.2
CH_3	1.2 ± 0.1

* anhydroglucose unit.

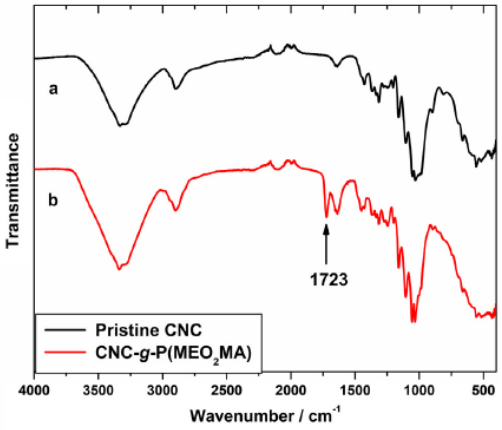

Fig. 2. ATR spectra obtained for (a) pristine CNC and (b) CNC-*g*-P(MEO_2MA).

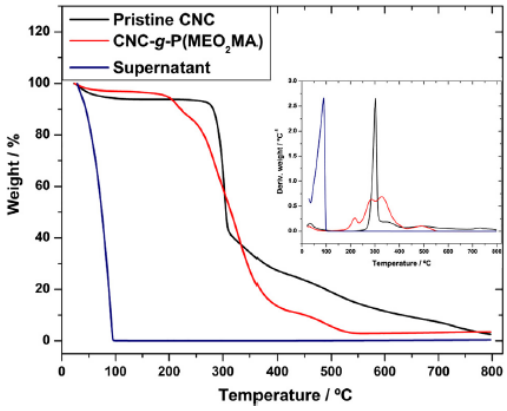

Fig. 3. TGA thermograms obtained for Pristine CNC (—), CNC-*g*-P(MEO_2MA) (—), and Supernatant (—). Inset shows the derivative weight loss thermograms of the three samples.

[18]. The supernatant (blue curve) does not show any significant traces of CNC – there is only one transition temperature starting at 85 °C throughout the entire temperature range.

3.1.4. HSDSC and transmittance experiments

In order to assess the LCST behavior of CNC-*g*-P(MEO_2MA), we performed a series of experiments using HSDSC and transmittance measurements (Fig. 4). The HSDSC results showed a temperature transition in the range of 24.3 to 35.4 °C, with a maximum at 25.0 °C; after this point the curve kept decreasing and did not return to the base line, in a similar way as proteins [31]. These results are in close agreement with the ones obtained by transmittance: a temperature transition in the range of 20.3 to 34.8 °C, with a maximum at 23.0 °C. Similar results were reported by Lutz et al. [14] and Grishkewich et al. [11]. Fig. 4 also shows that the thermoresponsive behavior is reversible and presented some hysteresis that is associated with the dehydration/aggregation (heating, red curve) and rehydration/redispersion (cooling, blue curve) process, the latter being a slower process than the former. Three consecutive runs were performed for each technique and the system showed reversibility after the grafted-polymer thermal history was erased.

3.1.5. Mixtures containing CNC-g-P(MEO_2MA)/surfactants

The polymer-grafted CNC is considered to be completely dispersed in aqueous solution at a temperature below its LCST as confirmed by visual inspection for concentrations up to 1.0 wt%. Increasing the temperature of the system beyond its LCST produced a visual phase separation that could be reversed by the addition of surfactants. By using ionic surfactants with the same alkyl chain length, we could assess both the hydrophobic contributions and their binding affinity, such as to the polymer chain coil/globules and/or the CNC negative charges. This could be achieved using oppositely charged surfactants, cationic C_{12}TAB and anionic SDS.

3.1.6. ITC experiments

To examine the effects of the addition of ionic surfactants with different electrical charges on CNC-*g*-P(MEO_2MA), we performed a series of calorimetric titration experiments with both C_{12}TAB and SDS at 15 and 40 °C, below and above the LCST, respectively (Fig. 5a and b). Electrostatic interactions would not be affected within this temperature range, while hydrophobic interactions are expected to be significantly affected because of the large ΔCp associated with the hydrophobic effect [32]. For C_{12}TAB (Fig. 5a), an interaction with the negative sulfate-ester groups on the CNC surface is expected at both temperatures. However, cationic surfactants are known to present a lower interaction with hydrophilic polymers [33,34] due to their large trimethylammonium headgroup. Therefore, we would expect to see no significant hydrophobic interactions at 15 °C, whereas at 40 °C some binding interaction is expected due to the hydrophobicity of POEGMA above its LCST. At a lower surfactant concentration range, from 0.5 up to 2.0 mmol kg^{-1} (Fig. 5a), there is a small peak in the titration curve of the CNC-*g*-P(MEO_2MA) that is associated with electrostatic interactions, regardless of the temperature [7]. Increasing the surfactant concentration to 7.2 mmol kg^{-1} we observed one peak for the system at 40 °C that is attributed to hydrophobic interactions between the surfactants and the polymer chains. This is associated with the polymer-induced micellization process, and the critical aggregation concentration (*cac*) has been reported previously [35–37].

Comparing the ITC results of C_{12}TAB (Fig. 5a) with SDS (Fig. 5b), our hypothesis of electrostatically bound surfactant was confirmed. SDS can only interact with the grafted polymer chains and this is reflected in the titration curves in the presence of CNC-*g*-P(MEO_2MA). At 15 °C, there is a small exothermic interaction (−1.8 kJ mol^{-1}) at a surfactant concentration of 0.9 mmol kg^{-1}, while at 40 °C there is a much more pronounced interaction (−18.2 kJ mol^{-1}), with both peaks corresponding to a polymer-induced micellization (*cac*). This difference is attributed to the rehydration of the grafted polymer chains for the binding interaction between CNC-*g*-P(MEO_2MA) and SDS. At 40 °C the grafted polymer chains acquire a globular structure and are dehydrated (into the micellar aggregates), a phenomenon similar to (N-isopropylacrylamide), PNIPAM [38,39]. When SDS was added to the system it was responsible for the formation of micellar aggregates around the P(MEO_2MA) chains, and they assumed a coil fashion and were rehydrated (moving to outer regions of the micellar aggregates).

3.1.7. Electrophoretic mobility and particle size measurements

By preparing mixtures containing CNC-*g*-P(MEO_2MA) while varying the surfactant concentration in the same range as studied by ITC, we could gather more information on the interaction between CNC-*g*-P(MEO_2MA) in the presence of C_{12}TAB and SDS at the two temperatures of 15 and 40 °C. Fig. 6 shows elec-

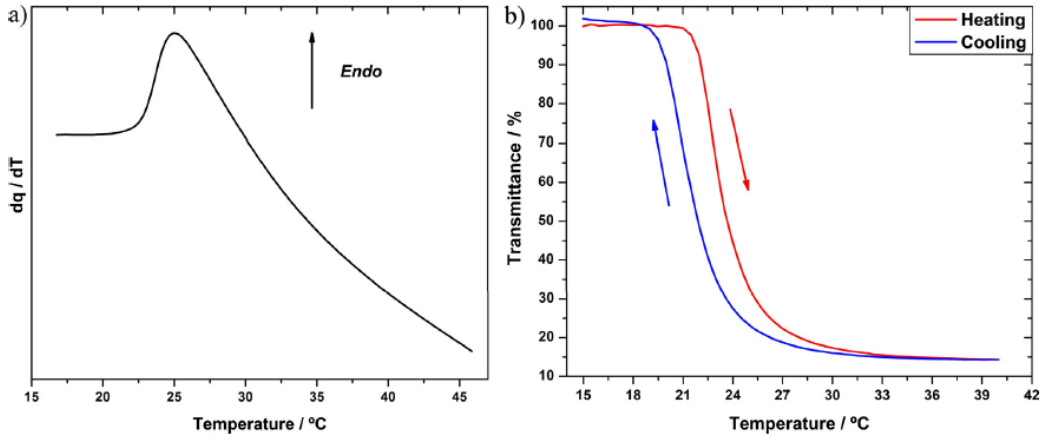

Fig. 4. (a) thermogram obtained at a scan rate of 60 °C h^{-1} for the CNC-g-P(MEO_2MA) dispersion; (b) hysteresis behavior for the second heating and cooling cycles of the CNC-g-P(MEO_2MA) dispersion.

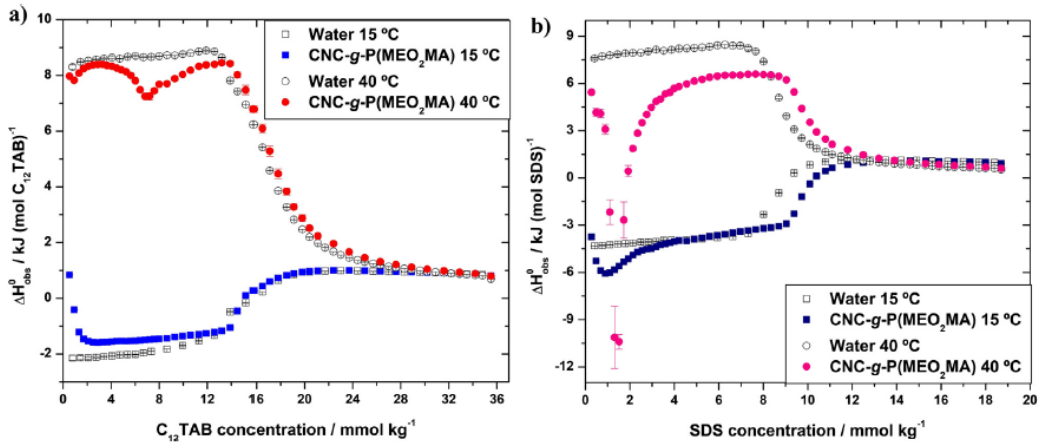

Fig. 5. ITC curves at 15 and 40 °C for the titration of: a) C_{12}TAB into water (empty symbols) and into 1.0 wt% CNC-g-P(MEO_2MA) dispersion; b) SDS into water (empty symbols) and into 1.0 wt% CNC-g-P(MEO_2MA) dispersion.

trophoretic mobility (a and b) and particle size (c and d) results for C_{12}TAB (left) and SDS (right).

For the mixtures containing 1.0 wt% CNC-g-P(MEO_2MA) and increasing C_{12}TAB concentrations (0, 0.5, 4.0, 7.0, 16.0 and 32.0 mmol kg^{-1})(Fig. 6a), there is a sign inversion for their surface charge from negative to positive values at low surfactant concentration that corresponds to the first small ITC peak (0.5 mmol kg^{-1}) and which can be associated to the charge neutralization on the CNC surface. Increasing the surfactant concentration led to more positive electrophoretic mobility values, with values obtained at 40 °C more positive than the ones obtained at 15 °C. For the first two concentration points (0.5 and 4.0 mmol kg^{-1}) it was not possible to measure the particle size (Fig. 6c), which are correlated to the small ITC peak observed. The CNC-g-P(MEO_2MA)/C_{12}TAB mixtures were turbid and agglomerated (Figs. S1 and S2 in Supplementary Material). This is why there is a dashed line connecting the points for pure CNC-g-P(MEO_2MA) to the point related to a surfactant concentration of 7.0 mmol kg^{-1}, where we have the second peak at 40 °C in the ITC experiments (Fig. 5a). It shows how large the particles became (>2 μm) especially at 15 °C because of the aggregation/agglomeration of the CNC-g-P(MEO_2MA) particles. At high surfactant concentration the particle size at both temperatures decreased to values of 610 ± 50 nm and the mixtures became transparent again (Fig. S2 in Supplementary Material). We can assume that the binding of C_{12}TAB to the CNC-g-P(MEO_2MA) particles at high temperature occurs in a sequential manner: it first binds to the negatively charged sulfate-ester groups as was observed for pristine CNC [6,7], followed by a polymer-induced micellization (*cac*) because of its interaction with the polymer, which causes the now C_{12}TAB decorated CNC-g-P(MEO_2MA) particles to repel each other and to remain dispersed in solution [16]. At 15 °C the cationic surfactant binds solely to the negative electrostatic charge on the grafted CNC surface, providing some steric hindrance along with the surface grafted hydrophilic polymer chains that would prevent the CNC rods from agglomerating. This contrasts with what we have previously reported for pristine CNC

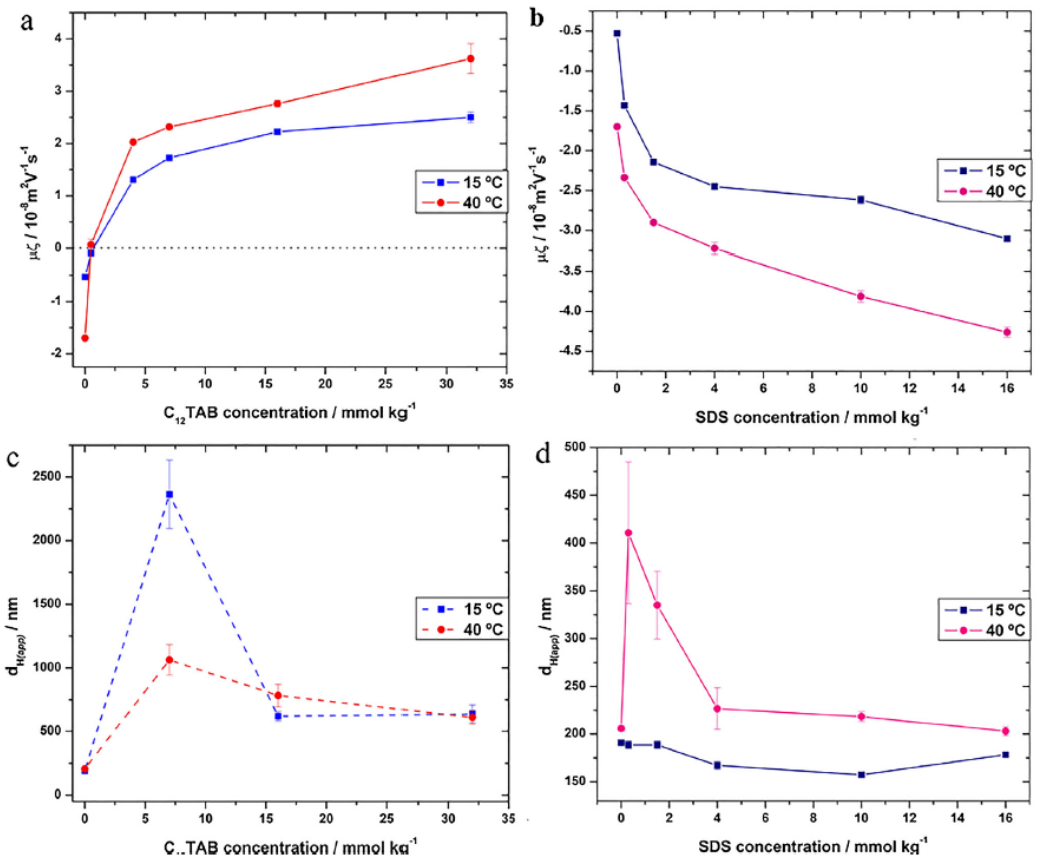

Fig. 6. Results for electrophoretic mobility of 1.0 wt% CNC-g-P(MEO_2MA) dispersion with $C_{12}TAB$ (a) and SDS (b) and hydrodynamic diameters ($d_{H(app)}$) obtained for mixtures with $C_{12}TAB$ (c) and SDS (d) as a function of surfactant concentration.

[7]. Additionally, at 15 °C the surfactant-decorated CNC-g-P(MEO_2MA) particles are more hydrophilic when compared to pristine CNC, therefore preventing agglomeration.

For the mixtures containing 1.0 wt% CNC-g-P(MEO_2MA) and varying SDS concentrations (0, 0.3, 1.5, 4.0, 10.0 and 16.0 mmol kg^{-1}), the electrophoretic mobility (Fig. 6b) became more negative with increasing surfactant concentration. Analyzing the particle size results (Fig. 6d) at 15 °C, there is only a slight variation at all SDS concentrations. With the mixtures at 40 °C there was a considerable increase in the particle size (from 206 ± 1 to 410 ± 70 nm) at a surfactant concentration of 0.3 mmol kg^{-1} that is associated with the polymer-induced micellization process (*cac*) as indicated by the peak in the ITC results (Fig. 5). Increasing the SDS concentration caused the particle size of the mixtures to decrease to 230 ± 20 nm. Within this latter size range, these mixtures became transparent and did not display any visual agglomeration and/or aggregation (Figs. S3 and S4 in Supplementary Material). At 40 °C, the increase in the particle size at low surfactant concentration may be related to the aggregation of SDS/CNC-g-P(MEO_2MA) complexes. As SDS concentration increases, the polymer-induced micellization between SDS and P(MEO_2MA) chains produces a physical network of several SDS/CNC-g-P(MEO_2MA) aggregates. When the SDS concentration was further increased, these aggregates began to repel each other, causing a reduction in the particle size. This phenomenon is identical to the one reported for the interaction of surfactants with hydrophobically-modified polymers, where a peak in viscosity was observed at intermediate surfactant concentration, that was ascribed to the formation of a physical polymer network [40].

3.1.8. "Switch on/switch off" mechanism for CNC-g-P(MEO_2MA)/SDS mixture

As described earlier, depending on the concentration of $C_{12}TAB$ surfactant in the CNC-g-P(MEO_2MA) (ca. 16.0 mmol kg^{-1}, Fig. S2, Supplementary Material), it was possible to reverse the phase separation above its LCST of 40 °C, by activating the "switch on" mechanism with the removal of the surfactant. Our next step is to remove the added surfactant by dialysis, where the CNC-g-P(MEO_2MA) dispersion could undergo phase transition once again, hence producing a "switch off" mechanism. However, the $C_{12}TAB$ surfactant could not be removed from the mixture even after dialysing 3 times/day for 1 week, due to its strong electrostatic interactions with the sulfate-ester groups on the CNC surface – some flocs would still remain in solution (Fig. S5 in Supplementary Material), as observed previously [7].

To avoid such strong electrostatic interactions, we decided to study the mixture containing CNC-g-P(MEO_2MA)/SDS, where hydrophobic interaction occurs between the polymer chains and surfactant alkyl chains. We further investigated the LCST behavior in the presence at various SDS concentrations. From the HSDSC measurements, the polymer dehydration associated with the critical temperature was observed as an endothermic peak [11]; these results are shown in Fig. 7.

At the lowest SDS concentration added to the system (0.1 mmol kg^{-1}), a shoulder appeared at around 25 °C, while the peak related to the P(MEO2MA) phase transition was shifted to a higher temperature at around 29 °C – the phase separation was centered at 25 °C for pure P(MEO_2MA). This increase in phase separation temperature is ascribed to the charges associated with the surfactant-polymer complex as reported for other systems on the increase of charged groups in the copolymers [41] or interaction with surfactant [42].

Beyond the surfactant concentration of 1.0 mmol kg^{-1}, two distinct peaks appeared in the DSC curves: a large one at lower temperatures, and a broader one at higher temperatures. This behavior was observed up to a concentration of 20.0 mmol kg^{-1}, above which the phase transition was beyond the detectable limit of the instrument. The interesting consequence of these results is the deconvolution of the phase transition to a two-stage dehydration process when SDS concentration exceeds 1.0 mmol kg^{-1}. This phenomenon has not been reported until now. The same process was observed previously by our group when studying PNIPAM in the presence of increasing SDS concentrations (see Supplementary Material for further information).

Table 2 shows the values of T_m (°C) at various SDS concentrations. A plot of T_m obtained for the first peaks as a function of SDS concentration (Fig. S6 in Supplementary Material) shows that the LCST presented an exponential growth, much similar to what was found by Schild & Tirrell [39] when studying sodium n-alkyl sulfates in the presence of poly (N-isopropylacrylamide), PNIPAM.

The SDS concentration of 5.0 mmol kg^{-1} was chosen to verify the concept of a "switch on/switch off" mechanism in the following manner (images are shown in Fig. 8 top and their HSDSC curves in the bottom). To a pure dispersion of CNC-g-P(MEO_2MA) at a temperature above its LCST (**1**) we added SDS and the system became clear (**2, "switch on"**), with the two expected peaks appearing in the HSDSC curve. Dialysis was performed on the final mixture by replacing the dialysis medium three times within 24 h – the system was turbid at higher temperature. Another HSDSC measurement was performed and it confirmed that the SDS surfactant was removed from the mixture, which was indicated by the presence of only one transition peak at 25.0 °C (**3, "switch off"**) related to the pure CNC-g-P(MEO_2MA) dispersion. SDS was added again to the dispersion, which became clear even at high temperature (**4**), and its HSDSC curve resembles that of system **2**. We repeated the dialysis procedure and yet again obtained a pure CNC-g-P(MEO_2MA) dispersion (**5, "switch on"**), with a smaller peak this time due to dilution effects caused by handling during dialysis.

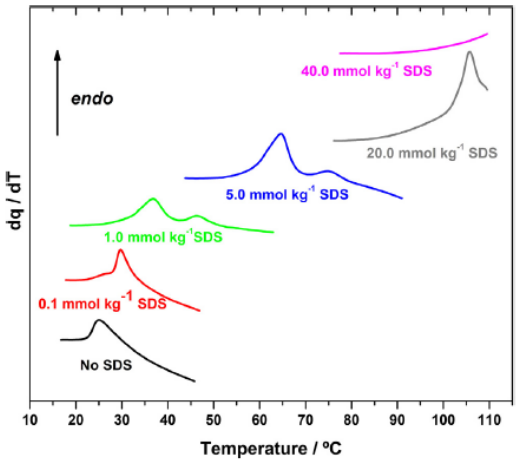

Fig. 7. HSDSC curves for 1.0 wt% CNC-g-P(MEO_2MA) in the presence of increasing SDS concentrations.

Table 2
Phase separation temperature, T_m (°C), obtained from HSDSC curves as a function of SDS concentration.

SDS concentration/mmol kg^{-1}	T_m/°C	
0.0	25.0	
0.1	25.2	28.9*
1.0	36.7	46.3*
5.0	64.7	74.8*
20.0	105.8	—
40.0	—	
Dialyzed	25.0	

* T_m obtained at the maximum of the second peak (using 1st derivative).

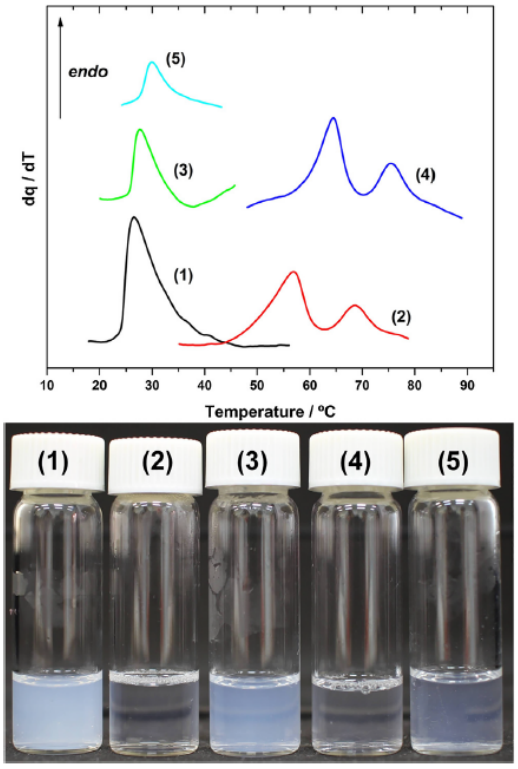

Fig. 8. Pictures taken at around 40 °C, showing the switch on/ switch off mechanism applied to dispersions containing 1.0 wt% CNC-g-P(MEO_2MA) (samples 1, 3 and 5) and 1.0 wt% CNC-g-P(MEO_2MA) in the presence of 5.0 mmol kg^{-1} SDS (samples 2 and 4), as explained in the text.

4. Discussion

Although C_{12}TAB is able to bind and decorate pristine CNC and alter its surface charge characteristics, precipitation still occurred with particles displaying high surface charge. This was previously reported and associated with the cross-linking effect of surfactant aggregates bound to different CNC particles [7]. The presence of P(MEO_2MA) polymer chains provides more binding sites for the surfactant. When additional C_{12}TAB is added it can bind to the polymer chains as well, which enhances the stability of the CNC in solution. In addition, when temperature is raised above its critical solubility temperature, the polymer becomes hydrophobic, enhancing the surfactant affinity and binding. Using a thermo-responsive polymer with a phase transition near room temperature (starting at 23.6 °C, Fig. 4), we were able to visualize this phenomenon. Below the LCST, C_{12}TAB surfactant initially binds to the negative sulfate-ester groups on the CNC. C_{12}TAB will only bind to P(MEO_2MA) chains at higher surfactant concentrations, at half the *cmc*. Above the LCST there are sufficient hydrophobic domains brought about by the dehydration of the polymer chains, which promotes the intermolecular interactions between the CNC rods. The cationic surfactant can now bind to aggregated CNC rods as revealed by a peak associated with an exothermic process (Fig. 5a) and by the large particle size observed (Fig. 6c). These hydrophobic interactions with the polymer chains are reversible and the bound surfactant molecules could be removed by dialysis, while the surfactant bound to the negative charges cannot be removed (see Fig. S5, Supplementary Material). Overall, the remaining surfactant prevents the full redispersion of this system even after extensive dialysis.

As SDS possesses the same electrical charge as CNC, the only possible interaction between them is via the binding to P(MEO_2-MA) chains. This can be seen by the presence of an exothermic peak in the ITC results (Fig. 5b) regardless of the temperature and it becomes more prominent at 40 °C (above LCST). As observed for PEO in the presence of SDS, the polymer chains of P(MEO_2MA) at a temperature above LCST can be rehydrated and incorporated into micellar aggregates [43,44]. This causes a continuous decrease of the electrophoretic mobility (Fig. 6b) and the formation of larger aggregates (Fig. 6d), at a surfactant concentration where only one peak is showed in ITC results (Fig. 5b).

As revealed by HSDSC results (Fig. 7) the presence of an increasing amount of SDS caused a shift in the phase transition temperature to higher values. In addition, the SDS bound to the polymer chains enhanced the negative charges on the CNC-*g*-P(MEO_2MA)/SDS complexes (lower temperature peak in Fig. 7) [39,45,46]. It is interesting to note that at intermediate SDS concentrations (Fig. 7), two endothermic peaks were observed, a phenomenon that is nor clearly understood at the moment. Increasing the SDS concentration, from 1.0 to 5.0 mmol kg^{-1} did not lead to an increase in any of the two peaks, suggesting that the probable formation of two different populations arising from an unequal distribution of SDS monomers bound to the polymer grafted CNC. It seems that at higher SDS concentrations these two peaks merged, although our instrument could not assess the highest phase transition temperatures. This could be illustrated by comparing the HSDSC curve at 5.0 mmol kg^{-1} SDS (Fig. 7) with the ITC curves obtained at 40 °C (Fig. 5b). At 40 °C, the ITC results indicated that SDS aggregation on the polymer-grafted CNC surface commenced at a very low concentration (the ITC curves in the presence and absence of surfactant are diverging from each other at the very first few injections). The maximum of interaction between SDS and CNC-*g*-P(MEO_2MA) occurred at a concentration of 1.0 mmol kg^{-1} (lowest ΔH^0_{obs} values observed) and it continued up to 6.0–7.0 mmol kg^{-1}.

Because the interactions between SDS and CNC-*g*-P(MEO_2MA) are purely hydrophobic, they could be removed by dialysis. This was not possible with an oppositely charged surfactant because the electrostatic interaction is much stronger. With this procedure, a reversible phase transition corresponding to a "switch on/switch off" mechanism (Fig. 8) was demonstrated by adding and removing surfactant by dialysis. This finding not only confirms the dual nature of surfactant interactions with polymer grafted CNC (electrostatic and hydrophobic) but serves as a proof of concept for the observed switch on/switch off process. For practical applications, this could be further improved in order to allow a faster and more efficient surfactant removal or extended with the use of surfactant scavenger molecules such as cyclodextrins.

5. Conclusions

The surface modification of CNC with a thermo-responsive polymer P(MEO_2MA) was confirmed by NMR, FTIR-ATR and TGA techniques, and its reversible phase transition was demonstrated by performing DSC and transmittance experiments that suggests that polymer grafting onto CNC did change its thermal behavior. ITC was used to study the interactions between CNC-*g*-P(MEO_2MA) and two oppositely charged ionic surfactants with the same alkyl chain length, the cationic C_{12}TAB and the anionic SDS. With DSC measurements we were able to assess the changes in the temperature of phase transition of CNC-*g*-P(MEO_2MA) in the presence of increasing concentration of SDS. We could also verify the concept of "switch on/switch off mechanism" for a mixture containing 1.0 wt% CNC-*g*-P(MEO_2MA) and 5.0 mmol kg^{-1} of SDS by simple dialysis.

By grafting a thermo-responsive polymer on the CNC surface and with the addition of ionic surfactants to the system above its phase transition temperature, we were able to redisperse C_nTAB/CNC-*g*-P(MEO_2MA) mixtures. In the case of cationic C_{12}TAB surfactant, not only it was able to bind to the P(MEO_2MA) polymer chains at temperatures above its LCST due to hydrophobic interactions between the polymer chains and the surfactant alkyl chains, it could also strongly be bound electrostatically to the CNC negative charges, preventing its complete removal even after one week of dialysis. Anionic SDS surfactant was bound to the polymer chains regardless of the temperature; however, a more intense binding occurred above the LCST, in a similar fashion as for C_{12}TAB, and the SDS molecules could be completely removed from the CNC-*g*-P(MEO_2MA)/SDS complexes after dialysis. Increasing the SDS concentration increases the phase transition temperature of CNC-*g*-P(MEO_2MA). Dialysis can remove the SDS surfactant from the mixture, which could be used to tune the phase transition behavior.

The findings from this work provide new insights on the surfactant binding to polymer-grafted CNC. Surface modification is one way of tuning the number of binding sites [47] and it also demonstrates that CNC derivatives in the presence of surfactants could be applied in various systems such as, drug delivery [48,49], emulsion stabilizers [50], water remediation [51], bacterial imaging [52], as well as many other applications presented in recent reviews by Xie et al. [12], Klemm et al. [53] and Grishkewich et al. [54] to list a few, where nanoparticle coagulation and redispersion might be desirable.

Acknowledgments

We acknowledge the Brazilian agencies FAPESP (2016/25406-5) for financial support. W.L. thanks CNPq for a productivity research grant. C.B would like to thank CAPES for the Ph.D. scholarship. S. P.A acknowledges a postdoctoral grant (2014/24305-8) from the FAPESP. R.P-O would like to thank CNPq for the Ph.D. scholarship (159080/2013-4). W.L. and K.C.T. also thank CAPES for a visiting

professor grant (CAPES-PVE 71/2013) that allowed visits between Campinas and Waterloo.

Conflict of Interest

There are no conflicts of interest to declare.

Appendix A. Supplementary material

Supplementary data to this article can be found online at https://doi.org/10.1016/j.jcis.2018.11.071.

References

[1] M.M. De Souza Lima, R. Borsali, Rodlike cellulose microcrystals: structure, properties, and applications, Macromol. Rapid Commun. 25 (2004) 771–787, https://doi.org/10.1002/marc.200300268.

[2] Y. Habibi, L.A. Lucia, O.J. Rojas, Cellulose nanocrystals: chemistry, self-assembly, and applications, Chem. Rev. 110 (2010) 3479–3500, https://doi.org/10.1021/cr900339w.

[3] A. Dufresne, Nanocellulose: a new ageless bionanomaterial, Mater. Today 16 (2013) 220–227, https://doi.org/10.1016/j.mattod.2013.06.004.

[4] T. Abitbol, E. Kloser, D.G. Gray, Estimation of the surface sulfur content of cellulose nanocrystals prepared by sulfuric acid hydrolysis, Cellulose 20 (2013) 785–794, https://doi.org/10.1007/s10570-013-9871-0.

[5] R.J. Moon, A. Martini, J. Nairn, J. Simonsen, J. Youngblood, Cellulose nanomaterials review: structure, properties and nanocomposites, Chem. Soc. Rev. 40 (2011) 3941–3994, https://doi.org/10.1039/c0cs00108b.

[6] N. Dhar, D. Au, R.C. Berry, K.C. Tam, Interactions of nanocrystalline cellulose with an oppositely charged surfactant in aqueous medium, Colloid Surf. A 415 (2012) 310–319, https://doi.org/10.1016/j.colsurfa.2012.09.010.

[7] C. Brinatti, J. Huang, R.M. Berry, K.C. Tam, W. Loh, Structural and energetic studies on the interaction of cationic surfactants and cellulose nanocrystals, Langmuir 32 (2016) 689–698, https://doi.org/10.1021/acs.langmuir.5b03893.

[8] B.L. Tardy, S. Yokota, M. Ago, W. Xiang, T. Kondo, R. Bordes, O.J. Rojas, Nanocellulose–surfactant interactions, Curr. Opin. Colloid Interface Sci. 29 (2017) 57–67, https://doi.org/10.1016/j.cocis.2017.02.004.

[9] K.H.M. Kan, J. Li, K. Wijesekera, E.D. Cranston, Polymer-grafted cellulose nanocrystals as pH-responsive reversible flocculants, Biomacromolecules 14 (2013) 3130–3139, https://doi.org/10.1021/bm400752k.

[10] S.P. Akhlaghi, M. Zaman, N. Mohammed, C. Brinatti, R. Batmaz, R. Berry, W. Loh, K.C. Tam, Synthesis of amine functionalized cellulose nanocrystals: optimization and characterization, Carbohydr. Res. 409 (2015) 48–55, https://doi.org/10.1016/j.carres.2015.03.009.

[11] N. Grishkewich, P. Akhlaghi, Y. Zhaoling, R. Berry, K.C. Tam, Cellulose Nanocrystal-poly(oligo(ethylene glycol) methacrylate) brushes with tunable LCSTs, Carbohydr. Polym. 144 (2016) 215–222, https://doi.org/10.1016/j.carbpol.2016.02.044.

[12] S. Xie, X. Zhang, M.P. Walcott, H. Lin, Applications of cellulose nanocrystals: a review, Eng. Sci. 2 (2018) 4–16, https://doi.org/10.30919/es.1803302.

[13] A. Boujemaoui, S. Mongkhontreerat, E. Malmström, A. Carlmark, Preparation and characterization of functionalized cellulose nanocrystals, Carbohydr. Polym. 115 (2015) 457–464, https://doi.org/10.1016/j.carbpol.2014.08.110.

[14] J.F. Lutz, Polymerization of oligo(ethylene glycol) (meth)acrylates: toward new generations of smart biocompatible materials, J. Polym. Sci. A 1 (46) (2008) 3459–3470, https://doi.org/10.1002/pola.22706.

[15] Y.C. Nho, O.H. Kwon, Blood compatibility of AAc, HEMA, and PEGMA-grafted cellulose film, Radiat. Phys. Chem. 66 (2003) 299–307, https://doi.org/10.1016/S0969-806X(02)00387-0.

[16] B. Peng, X. Han, H. Liu, K.C. Tam, Binding of cationic surfactants to a thermo-sensitive copolymer below and above its cloud point, J. Colloid. Interface Sci. 412 (2013) 17–23, https://doi.org/10.1016/j.jcis.2013.09.012.

[17] B. Peng, X. Han, H. Liu, R.C. Berry, K.C. Tam, Interactions between surfactants and polymer-grafted nanocrystalline cellulose, Colloid Surface A 421 (2013) 142–149, https://doi.org/10.1016/j.colsurfa.2012.12.059.

[18] S.A. Kedzior, L. Graham, C. Moorlag, B.M. Dooley, E.D. Cranston, Poly(methyl methacrylate)-grafted cellulose nanocrystals: one-step synthesis, nanocomposite preparation, and characterization, Can. J. Chem. Eng. 94 (2016) 811–822, https://doi.org/10.1002/cjce.22456.

[19] R.L. Johnson, K. Schmidt-Rohr, Quantitative solid-state ^{13}C NMR with signal enhancement by multiple cross polarization, J. Magn. Reson. 239 (2014) 44–49, https://doi.org/10.1016/j.jmr.2013.11.009.

[20] O.D. Bernardinelli, M.A. Lima, C.A. Rezende, I. Polikarpov, E.R. DeAzevedo, Quantitative ^{13}C MultiCP solid-state NMR as a tool for evaluation of cellulose crystallinity index measured directly inside sugarcane biomass, Biotechnol. Biofuels 8 (2015) 1–11, https://doi.org/10.1186/s13068-015-0292-1.

[21] E. Fegyver, R. Mészáros, Fine-tuning the nonequilibrium behavior of oppositely charged macromolecule/surfactant mixtures via the addition of nonionic amphiphiles, Langmuir 30 (2014) 15114–15126.

[22] T.J. Simmons, J.C. Mortimer, O.D. Bernardinelli, A.C. Pöppler, S.P. Brown, E.R. DeAzevedo, R. Dupree, P. Dupree, Folding of xylan onto cellulose fibrils in plant cell walls revealed by solid-state NMR, Nat. Commun. 7 (2016) 1–9, https://doi.org/10.1038/ncomms13902.

[23] F.V. Ferreira, M. Mariano, S.C. Rabelo, R.F. Gouveia, L.M.F. Lona, Isolation and surface modification of cellulose nanocrystals from sugarcane bagasse waste: from a micro- to a nano-scale view, Appl. Surf. Sci. 436 (2018) 1113–1122, https://doi.org/10.1016/j.apsusc.2017.12.137.

[24] C. Dong, Y. Ye, L. Qian, G. Zhao, B. He, H. Xiao, Antibacterial modification of cellulose fibers by grafting β-cyclodextrin and inclusion with ciprofloxacin, Cellulose 21 (2014) 1921–1932, https://doi.org/10.1007/s10570-014-0249-8.

[25] C.G. Otoni, A.S. Carvalho, M.V.C. Cardoso, O.D. Bernardinelli, M.V. Lorevice, L.A. Colnago, W. Loh, L.H.C. Mattoso, High-pressure microfluidization as a green tool for optimizing the mechanical performance of all-cellulose composites, ACS Sustain. Chem. Eng. 6 (2018) 12727–12735, https://doi.org/10.1021/acssuschemeng.8b01855.

[26] S.P. Akhlaghi, R.M. Berry, K.C. Tam, Surface modification of cellulose nanocrystal with chitosan oligosaccharide for drug delivery applications, Cellulose 20 (2013) 1747–1764, https://doi.org/10.1007/s10570-013-9954-y.

[27] S. Belfer, R. Fainchtain, Y. Purinson, O. Kedem, Surface characterization by FTIR-ATR spectroscopy of polyethersulfone membranes-unmodified, modified and protein fouled, J. Membr. Sci. 172 (2000) 113–124, https://doi.org/10.1016/S0376-7388(00)00316-1.

[28] M. Roman, W.T. Winter, Effect of sulfate groups from sulfuric acid hydrolysis on the thermal degradation behaviour of bacterial cellulose, Biomacromolecules 5 (2004) 1671–1677.

[29] N. Wang, E. Ding, R. Cheng, Thermal degradation behaviors of spherical cellulose nanocrystals with sulfate groups, Polymer 48 (2007) 3486–3493, https://doi.org/10.1016/j.polymer.2007.03.062.

[30] N. Bitinis, R. Verdejo, J. Bras, E. Fortunati, J.M. Kenny, L. Torre, M.A. López-Manchado, Poly(lactic acid)/natural rubber/cellulose nanocrystal bionanocomposites Part I. Processing and morphology, Carbohydr. Polym. 96 (2013) 611–620, https://doi.org/10.1016/j.carbpol.2013.02.068.

[31] P.L. Privalov, A.I. Dragan, Microcalorimetry of biological macromolecules, Biophys. Chem. 126 (2007) 16–24, https://doi.org/10.1016/j.bpc.2006.05.004.

[32] C. Brinatti, L.B. Mello, W. Loh, Thermodynamic study of the micellization of zwitterionic surfactants and their interaction with polymers in water by isothermal titration calorimetry, Langmuir 30 (2014) 6002–6010, https://doi.org/10.1021/la5012346.

[33] W. Loh, L.A.C. Teixeira, L.-T. Lee, Isothermal calorimetric investigation of the interaction of poly (n-isopropylacrylamide) and ionic surfactants, J. Phys. Chem. B 108 (2004) 3196–3201.

[34] G. Wang, G. Olofsson, Ethyl(hydroxyethyl)cellulose and ionic surfactants in dilute solution. calorimetric and viscosity study of the interaction with sds and some cationic surfactants, J. Phys. Chem. B. 99 (1995) 5588–5596, https://doi.org/10.1021/j100015a049.

[35] W. Loh, C. Brinatti, K.C. Tam, Use of isothermal titration calorimetry to study surfactant aggregation in colloidal systems, Biochim. Biophys. Acta – Gen. Subj. 2015 (1860) 999–1016, https://doi.org/10.1016/j.bbagen.2015.10.003.

[36] S. Courdec-Azouani, J. Sidhu, T.K. Georgiou, D.C. Charalambous, M. Vamvakaki, C.S. Patrickios, D.M. Bloor, J. Penfold, J.F. Holzwarth, E. Wyn-Jones, Binding of sodium dodecyl sulfate to linear and star homopolymers of the nonionic poly (methoxyhexa(ethylene glycol) methacrylate) and the polycation poly(2-(dimethylamino)ethyl methacrylate): electromotive force isothermal titration calorimetry, surface tension, and small-anlge neutron scattering measurements, Langmuir 20 (2004) 6458–6469, https://doi.org/10.1021/la049450l.

[37] J. Sidhu, D.M. Bloor, S. Couderc-Azouani, J. Penfold, J.F. Holzwarth, E. Wyn-Jones, Interactions of Poly(amidoamine) dendrimers with the surfactants SDS, DTAB, and C12EO6: an equilibrium and structural study using a SDS selective electrode isothermal titration calorimetry, and small angle neutron scattering, Langmuir 20 (2004) 9320–9328.

[38] H. Schild, D. Tirrell, Microcalorimetric detection of lower critical solution temperatures in aqueous polymer solutions, J. Phys. Chem. 94 (1990) 4352–4356, https://doi.org/10.1021/j100373a088.

[39] H.G. Schild, D.A. Tirrell, Interaction of poly(N-isopropylacrylamide) with sodium n-alkyl sulfates in aqueous solution, Langmuir 7 (1991) 665–671, https://doi.org/10.1021/la00052a013.

[40] L. Piculell, M. Egermayer, J. Sjöström, Rheology of mixed solutions of an associating polymer with a surfactant. Why are different surfactants different?, Langmuir 19 (2003) 3643–3649, https://doiorg/10.1021/la020912.

[41] M.J. Tiera, G.R. Dos Santos, V.A. de O Tiera, N.A.B. Vieira, E. Frolini, R.C. Da Silva, W. Loh, Aqueous solution behavior of thermosensitive (N-isopropylacrylamide-acrylic acid-ethyl methacrylate) terpolymers, Colloid Polym. Sci. 283 (2005) 662–670.

[42] R. Cardoso, G. Olofsson, K. Schille, Influence of Ionic surfactants on the aggregation of poly (ethylene oxide)-poly (propylene oxide)-poly (ethylene oxide) block copolymers studied by differential scanning and isothermal titration calorimetry, J. Phys. Chem. B 106 (2002) 1239–1246.

[43] S. Dai, K.C. Tam, Isothermal titration calorimetry studies of binding interactions between polyethylene glycol and ionic surfactants, J. Phys. Chem. B 105 (2001) 10759–10763.

[44] R.C. Da Silva, W. Loh, G. Olofsson, Calorimetric investigation of temperature effect on the interaction between poly(ethylene oxide) and sodium dodecylsulfate in water, Thermochim. Acta. 417 (2004) 295–300, https://doi.org/10.1016/j.tca.2003.07.025.
[45] E.I. Tiktopulo, V.E. Bychkova, J. Ricka, O.B. Ptitsyn, Cooperativity of the coil-globule transition in a homopolymer: microcalorimetric study of poly (n-isopropylacrylamide), Macromolecules 27 (1994) 2879–2882, https://doi.org/10.1021/ma00088a031.
[46] Y. Mylonas, G. Staikos, P. Lianos, Investigation of the poly(n -isopropylacrylamide)-sodium dodecyl sulfate complexation with viscosity dialysis, and time-resolved fluorescence-quenching measurements, Langmuir 15 (1999) 7172–7175, https://doi.org/10.1021/la990155o.
[47] S. Lombardo, W. Thielemans, Thermodynamics of the interactions of positively charged cellulose nanocrystals with molecules bearing different amounts of carboxylate anions, Phys. Chem. Chem. Phys. 20 (2018) 17637–17647, https://doi.org/10.1039/c8cp01532e.
[48] S. Dong, H.J. Cho, Y.W. Lee, M. Roman, Synthesis and cellular uptake of folic acid-conjugated cellulose nanocrystals for cancer targeting, Biomacromolecules 15 (2014) 1560–1567, https://doi.org/10.1021/bm401593n.
[49] A.B. Seabra, J.S. Bernardes, W.J. Fávaro, A.J. Paula, N. Durán, Cellulose nanocrystals as carriers in medicine and their toxicities: a review, Carbohydr. Polym. 181 (2018) 514–527, https://doi.org/10.1016/j.carbpol.2017.12.014.
[50] I. Kalashnikova, H. Bizot, B. Cathala, I. Capron, Modulation of cellulose nanocrystals amphiphilic properties to stabilize oil/water interface, Biomacromolecules 13 (2012) 267–275, https://doi.org/10.1021/bm201599j.
[51] R. Batmaz, N. Mohammed, M. Zaman, G. Minhas, R.M. Berry, K.C. Tam, Cellulose nanocrystals as promising adsorbents for the removal of cationic dyes, Cellulose 21 (2014) 1655–1665, https://doi.org/10.1007/s10570-014-0168-8.
[52] J. Zhou, N. Butchosa, H.S.N. Jayawardena, J. Park, Q. Zhou, M. Yan, O. Ramström, Synthesis of multifunctional cellulose nanocrystals for lectin recognition and bacterial imaging, Biomacromolecules 16 (2015) 1426–1432, https://doi.org/10.1021/acs.biomac.5b00227.
[53] D. Klemm, E.D. Cranston, D. Fischer, M. Gama, S.A. Kedzior, D. Kralisch, F. Kramer, T. Kondo, T. Lindström, S. Nietzsche, K. Petzold-Welcke, F. Rauchfuß, Nanocellulose as a natural source for groundbreaking applications in materials science: today's state, Mater. Today 21 (2018) 720–748, https://doi.org/10.1016/j.mattod.2018.02.001.
[54] N. Grishkewich, N. Mohammed, J. Tang, K.C. Tam, Recent advances in the application of cellulose nanocrystals, Curr. Opin. Colloid Interface Sci. 29 (2017) 32–45, https://doi.org/10.1016/j.cocis.2017.01.005.

9.2. Artigo publicado na *ACS Omega* (Referência [97])

ACS OMEGA

http://pubs.acs.org/journal/acsodf

Article

Inclusion Complexation between α-Cyclodextrin and Oligo(ethylene glycol) Methyl Ether Methacrylate

Marcos Mariano,* Oigres Daniel Bernardinelli, Rafael Pires-Oliveira, Guilherme A. Ferreira, and Watson Loh*

Cite This: *ACS Omega* 2020, 5, 9517−9528

Read Online

ACCESS | Metrics & More | Article Recommendations | Supporting Information

ABSTRACT: The preparation of inclusion complexes based on α-cyclodextrin (α-CD) and oligo(ethylene glycol) methyl ether methacrylate (OEGMA) was investigated aiming to reveal complexation particularities and thermodynamic and kinetic aspects as a function of the oligomer architecture. Small-angle X-ray scattering and isothermal titration calorimetry measurements revealed that oligomer molecular weight controls both the kinetics and thermodynamics of inclusion. Unlike linear ethylene glycol polymers, OEGMA groups possess a methacrylate group, which seems to act as a stopper, affecting their mode of complexation. Nuclear magnetic resonance spectra and relaxation measurements support the fact that methacrylate groups lie outside the α-CD ring and that a full sequential complexation of the oligomer ethylene oxide groups is not observed. These results allied to the temperature sensitivity of these oligomers and enable possible routes for chemical modifications and design of new stimuli-responsive materials.

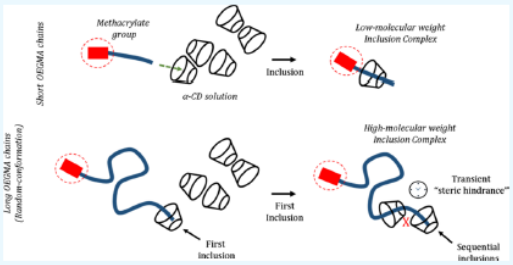

1. INTRODUCTION

Supramolecular interactions have been used as a tool to create systems that are not based on covalent bonds, and, as a consequence, can assemble into reversible structures. Nowadays, thermoresponsive and self-healing gels are common examples of this approach. Earlier investigations on the topic are focused on the most basic phenomena and inclusion complexation (IC), which ultimately lead to the fabrication of fundamental molecular machines.[1,2] The achievement of the so-called inclusion complexes is based on host−guest interactions, where a macrocycle motif is able to thread specific molecules inside its cavity.

Both chemical affinity and adequate size affect the thermodynamic parameters that govern the formation of such complexes. As frequently discussed in the literature, van der Waals and hydrophobic interactions are the main factors involved in this complexation phenomenon, although hydrogen bonding and steric effects can also influence this process.[3] Several host−guest combinations have been used to prepare, for instance, polyrotaxanes (and pseudorotaxanes), which have been proposed as biomimetic systems to study different biologically relevant processes, such as drug delivery and other uses of colloidal systems.[4,5]

After pioneer work published by Harada and co-workers,[6,7] who used polyethyleneglicol (PEG) as guest molecules to be included into cyclodextrin (CD) hosts, the association of macrocycles with polymers proved to be useful to control their molecular properties in solution. Recently, IC of thermoresponsive polymers has sparked a great deal of interest because of the possibility of controlling their lower critical solution temperature (LCST) through the complexation of their responsive moieties.[8,9] Formed by the cyclization of six glucose units, α-cyclodextrin (α-CD) possesses a truncated cone ring shape with an inner cavity, displaying a maximum diameter of 0.53 nm and height of 0.78 nm. These dimensions are compatible with the size of stretched ethylene oxide (EO) units present in different polymers and oligomers, among which one is oligo(ethylene glycol) methyl ether methacrylate (OEGMA).

This oligomer and its derived polymers were extensively studied by Lutz and collaborators[10,11] because of their biocompatible and thermoresponsive properties, ideal to be used in sustainable drug release[12] and injectable hydrogels[13] or even to preserve protein structures.[14] Unlike PEG, the EO moieties present in poly oligo(ethylene glycol) methyl ether methacrylate (POEGMA) are not in the polymer backbone but appear as side chains, and their size can be used to control polymer LCST by tuning the EO chain length.[15] Despite the great potential of POEGMA in the preparation of smart gels

Received: February 19, 2020
Accepted: April 1, 2020
Published: April 17, 2020

https://dx.doi.org/10.1021/acsomega.0c00741
ACS Omega 2020, 5, 9517−9528

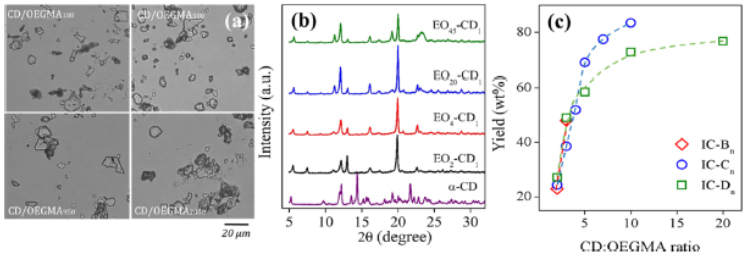

Figure 1. Analyses of solid IC through optical microscopy (a), XRD patters of 1:1 IC complexes (b), and mass yield of ICs as a function of CD/OEGMA ratio (c). Dashed lines are guides to the eyes.

Table 1. Composition of Samples and Characteristics of the Resulting Precipitates

composition[a] (OEGMA-M_w)	EO units in OEGMA	complex ID	CD/OEGMA[b] ratio (n)	yield[c] range (wt %)	phase separation time[d]	complex aspect
$OEGMA_{188}$/α-CD	2	EO_2-CD_n	1	30	minutes/hours	powder
$OEGMA_{300}$/α-CD	4−5	EO_4-CD_n	1−2	23−48	hours	powder
$OEGMA_{950}$/α-CD	20	EO_{20}-CD_n	1−10	25−84	days	powder/gel
$OEGMA_{2050}$/α-CD	45	EO_{45}-CD_n	1−20	28−77	weeks/no separation	gel

[a]Subscript values on OEGMA represent its nominal molecular weight (g·mol^{-1}). [b]Minimum and maximum mole ratio between α-CD and the OEGMA chain used to prepare different ICs. This is also represented as the subscript in the complex ID, as EO_x-CD_n. [c]Referring to different CD/OEGMA ratios, calculated as $Y\% = \frac{W_{IC}}{W_{OEGMA} + W_{CD}}$. [d]Dependent on sample composition. Pictures of the suspensions and more comprehensive data can be found in the Supporting Information, Figure S1 and Table S1.

and other biomedical materials, few information is available about its complexation with macrocycles (such as α-CD). Systems based on cyclodextrins and POEGMA are until now limited to the preparation of some hydrogels based on di-block polymers.[16,17]

Besides the presence of EO groups, OEGMA behavior is also influenced by the presence of a methacrylate group which occupies one end of the oligomer chain. Because the formation of pseudorotaxanes is dependent on macrocycle−polymer end group interactions, the role played by the methacrylate group is essential to understand the IC of these oligomers. In this paper, we will discuss the complexation mechanism of POEGMA monomers (*i.e.*, OEGMAs) and their potential application in polymer synthesis and in modulation of thermal properties. For this purpose, we present results from different experimental techniques to demonstrate the importance of oligomer molecular weight and the OEGMA to α-CD ratio during inclusion to form OEGMA/α-CD complexes.

2. RESULTS

2.1. Characterization of Solid Complexes. One of the first signs of IC is an increase of sample turbidity, which usually (but not always) is followed by the appearance of a white solid precipitate. In this study, the obtained solids were isolated through water removal and analyzed by optical microscopy, X-ray diffraction (XRD), and gravimetry.

Figure 1a shows isolated particles observed by optical microscopy. Despite their wide range of sizes, particles present a plate-like aspect with an approximate size of around 10 μm. Previous studies revealed that the layer of individual PEG/α-CD inclusion complexes normally present a thickness of 10 nm, which indicates that particles observed are probably formed as a laminated structure.[18] The crystalline character of such solids could be probed by XRD (Figure 1b), showing some complex diffraction patterns, as described by He *et al* (2005).[19] The formation of an inclusion complex is characterized by the appearance of a new peak at 2θ = 19.9°, which is observed for all IC samples, independent of oligomer molecular weight. According to Bragg's Law, this peak indicates d = 4.5 Å and may be ascribed to a tubular structure of the formed crystals. At the same time, fading of the peak at 2θ = 21.6° suggests the absence of pristine cyclodextrin in these solid samples.[20]

It can also be observed that samples EO_{20}-CD_1 and EO_{45}-CD_1 display a new secondary peak at 2θ = 19.2°. The same peak was previously observed by Zou *et al.*,[21] studying a copolymer containing an OEGMA block (M_w 450 g·mol^{-1}) complexed with α-CD. The position of such a peak is consistent with the diffraction pattern of PEG crystals, suggesting the presence of free EO (1:1 samples) units that can form crystalline domains upon drying.[22] Similarly, Travelet *et al.*[23] reported that the crystallinity of free EO moieties is affected by the amount of α-CD present.

For all samples, free EO groups seem to be present. As observed in Figure 1c, an increase in the amount of α-CD (higher CD/OEGMA ratio) leads to higher mass yield of the complex, with maximum yields around 70−80 wt % being achieved (Table 1). These values are almost twice those described in the literature for ICs based on star-poly(ethylene glycol) molecules[24] but very similar to those reported for long PEG-based molecules containing a bulk end group, where a plateau is described at high CD concentration.[25] If precipitate washing is not fully efficient in removing free CD, these values may be slightly biased toward higher CD/OEGMA ratios.

Longer EO moieties lead to an increase in IC mass yield, suggesting that the oligomer size affects complexation efficiency, indicating that the exclusion of high-energy water molecules from the CD cavity may not be the only force driving this process, as previously proposed by Takahashi *et al* (2016).[18] Besides, the size of the oligomer also modifies the kinetics of incorporation, as established from visual observation of mixtures. The arising cloudiness and, in some cases, complex

https://dx.doi.org/10.1021/acsomega.0c00741
ACS Omega 2020, 5, 9517−9528

precipitation can vary from minutes to weeks depending on OEGMA molecular weight. These phase separation phenomena seem to be related to the ability of longer molecules to produce nonstoichiometric complexes (*i.e.*, complexes whose composition differs from the expected EO/CD ratio). Earlier literature describes the sequential complexation of α-CD units along linear polymer chains to form "necklace" structures called pseudorotaxanes (PRs).[26] A ratio of 1 unit of α-CD for each 2 units of EO (2:1) is usually described in the literature as the value of oligomer saturation during the formation of such complexes.[27]

To further explore such multiple complexations, different ratios between α-CD and OEGMA were used in order to obtain saturated PRs. The visual inspection of these samples follows the same tendency previously described here and in the literature.[24] Solutions containing longer oligomers take longer times to display cloudiness. Concerning the CD/EO ratio, higher amounts of α-CD lead to a faster increase of suspension turbidity. However, longer oligomers (EO_{20}-CD_n and EO_{45}-CD_n) do not present the formation of a well-defined solid precipitate at the investigated compositions. For these ICs, after following certain samples for 5 weeks, the formation of a consistent white gel-like material is observed. Here, it is worth to note that visual observations (*e.g.*, turbidity and precipitations) are related to the aggregation of formed complexes because early stages of threading cannot be verified by the visual aspect of the samples.[28]

2.2. Nuclear Magnetic Resonance Techniques. In order to understand IC structures and the role of different moieties in complexation, several nuclear magnetic resonance (NMR) techniques were explored.

2.2.1. ^{1}H Nuclear Magnetic Resonance. Initially, the spectra of pristine components were obtained. As observed in Figure S2, the α-CD spectrum shows characteristic glucose peaks at 3.4 ppm (m, H-3), 3.8 ppm (m, H-5), 3.9 ppm (m, H-2), and 5.0 ppm (s, H-1), similar to those described by Schneider *et al.*[29] The oligomers (*e.g.*, EO_2) present peaks at 1.9 ppm (s, CH_3), 3.2 ppm (s, CH_3), 3.6 ppm (m, $-CH_2$), 4.2 ppm (t, $-CH_2$), 5.6 ppm (s, CH), and 6.1 ppm (s, CH). As also demonstrated in Figure S2, ICs spectra are found to be very similar to the superposition of α-CD and OEGMA peaks.

Furthermore, sample stoichiometry was complementarily determined by ^{1}H NMR and gravimetric methods. Such a complementary approach was necessary because of limitations of each method. Gravimetry fails to predict sample composition at lower α-CD concentration because an unknown amount of oligomers and macrocycles can be lost during sample washing. On the other hand, the ^{1}H NMR approach leads to a deviation of nominal expected composition in samples containing higher amounts of α-CD. This can be related to its inefficient washing as medium viscosity increases (gel phases), as previously discussed in the literature.[6,30] Furthermore, at these compositions, larger experimental errors are related to the decrease of signal/noise ratio in longer ICs (related to the low intensity OEGMA peak), which can vary up to 25%. Figure 2 exhibits the relationship between the expected (nominal) and experimental composition of the complexes estimated from both techniques.

As can be observed, experimental and nominal compositions are similar at lower CD/OEGMA ratios (*i.e.*, until 5:1 values), independent of the oligomer size, following the expected 2:1 (EO/CD) ratio. At higher CD/OEGMA ratios, both techniques present the expected deviations. This disagreement

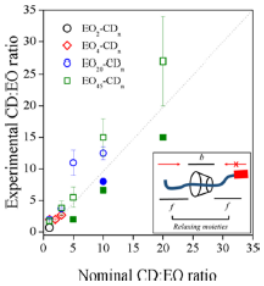

Figure 2. Relationship between nominal and experimental values of the CD/OEGMA ratio (line is added to aid visualization). Open symbols are estimated from ^{1}H NMR data, and closed ones are obtained from gravimetric experiments. Error bars are related to the signal/noise ratio of ^{1}H NMR analysis. The inset represents free and bonded oligomer moieties together with the possible "one-side" complexation mechanism.

between nominal and real sample compositions was previously observed and discussed in the literature for linear molecules.[31] Furthermore, we use the relaxation of the oligomer in low-field NMR to investigate this observation in the present system, as discussed in the next section.

2.2.2. Low-Field NMR. Once threaded inside the macrocycle cavity, oligomers present different molecular dynamics. Such a property can be followed in order to obtain valuable information about host−guest complexation. NMR is applied to obtain the spin−spin relaxation time (also named transverse relaxation) of protons present in the system (^{1}H-T_2). Such relaxation times can be related to material mobility and structure.[32,33]

The addition of α-CD units to an oligomer solution restrains, at first, molecule diffusion because of steric limitations arising in a crowded environment. With time and advancement of oligomer inclusion, EO groups are stretched and threated in a different chemical environment.[31,34] These new conditions lead protons present in OEGMA to exhibit new spin−spin relaxation times (T_2), which can be expressed in terms of relaxation times of free (T_{2f}) and bonded (T_{2b}) protons, according to eq 1 and as illustrated in Figure 3.[35]

$$\frac{1}{T_2} = \frac{1}{T_{2f}}(1 - p) + \frac{1}{T_{2b}}p \quad (1)$$

where p is the probability to find a bonded molecule. This equation suggests that two different contributions can be observed in relaxation time spectra if the difference between individual contributions of each term is large enough.

As observed in Figure 3a−c, the distributions of relaxation times from α-CD and oligomers are modified after inclusion, eventually reaching intermediate values. This behavior can be clearly observed for EO_4-CD_n samples (M_w 300 g·mol^{-1}). Because of its rigid structure, relaxation times of α-CD are short, around 85 ms. For bulky oligomers, T_2 varies from 150 to 800 ms according to the sample molecular weight, as shown in Figure 3d. Intermediary values found for different samples (200−600 ms) are related to relaxation of α-CD after exclusion of high-energy water molecules from its internal cavity. Such an effect is combined with the reduction of oligomer mobility after inclusion. These results show that inner cavity interactions among the host and guest are not strictly rigid,

https://dx.doi.org/10.1021/acsomega.0c00741
ACS Omega 2020, 5, 9517−9528

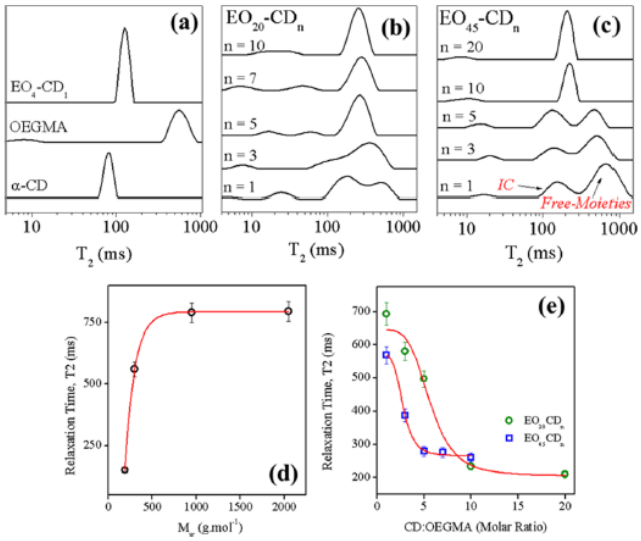

Figure 3. Relaxation time distribution (T_2) for different inclusion complexes (a–c), OEGMA-T_2 at different molecular weights (d), and examples of T_2-decay for EO_{20}-CD_n and EO_{45}-CD_n (e). Red lines in figures (d,e) are exponential fits. A complete list of relaxation times calculated in this work can be found in the Supporting Information (Table S2).

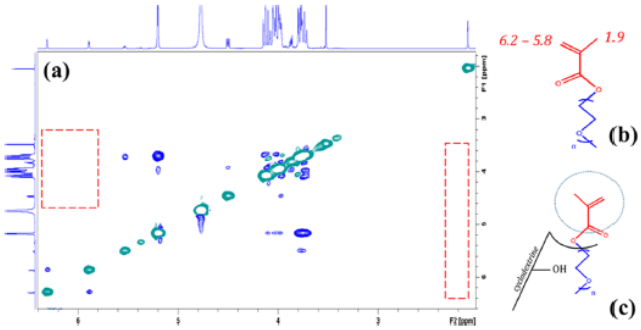

Figure 4. 2D-NOESY spectra of IC-A (a), OEGMA methacrylate peaks (b), and proposed position of the methacrylate group with respect to the cyclodextrin ring (c). H^1 NMR spectra of the individual oligomer, α-CD, and IC can be found in Figure S2.

which fits the expectations of necklace formation (where a certain level of flexibility is necessary). The decay in OEGMA-T_2 is much smaller than the one previously reported in the literature for EO groups trapped inside TiO_2 nanotubes, where molecule relaxation decreases almost 40 times.[36] Again, this difference indicates some malleability of molecules in the ICs investigated in the present work.

2.2.3. NOESY. During this study, we attempted to prepare inclusion complexes between α-CD and similar methacrylic acid but no change in appearance or turbidity was observed. Furthermore, the position of OEGMA methacrylic groups was analyzed by NMR techniques which did not reveal signs of complexation. Figure 4 shows the NOESY–H^1 NMR spectrum of a CD/OEGMA complex. The spectrum shows some interactions between OEGMA protons (*e.g.*, 4.25 ppm) with internal protons of the macrocycle (around 3.8 ppm) but very weakly with its external ones (*e.g.*, 5 ppm). It corroborates the results presented by Takahashi *et al.*[18] In addition, spatial proximity between methacrylate protons (Figure 4b) and internal hydroxyl groups of cyclodextrin (mostly between 3 and 4 ppm) is not observed, which indicates the absence of interaction between these molecules. Overall, these results suggest that methacrylate protons are spatially distant, probably in the external part of the cavity, as illustrated in Figure 4c. As a consequence, it seems that methacrylate groups do not participate in IC, despite their influence on neighbor protons, as shown in low-field NMR results discussed above.

2.3. ITC Experiments. Because many properties of the complex are dependent on oligomer molecular weight, inclusion kinetics and thermodynamics was studied as a function of oligomer size. Isothermal titration calorimetry (ITC) was used in order to measure the heat involved in the addition of α-CD to an aqueous solution of OEGMA, which could provide information about the kinetics and energetics of this incorporation.[37]

https://dx.doi.org/10.1021/acsomega.0c00741
ACS Omega 2020, 5, 9517–9528

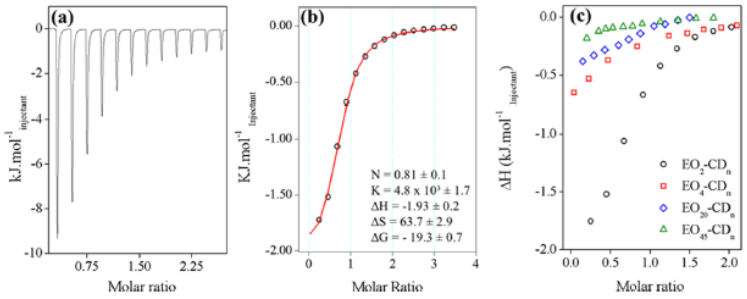

Figure 5. Measured heat of interaction obtained from ITC from sequential α-CD injections into an $OEGMA_{188}$ solution (a); fitting of heat mathematical integration as a function of molar ratio for the EO_2-CD_1 inclusion complex (b) and for longer oligomers (c).

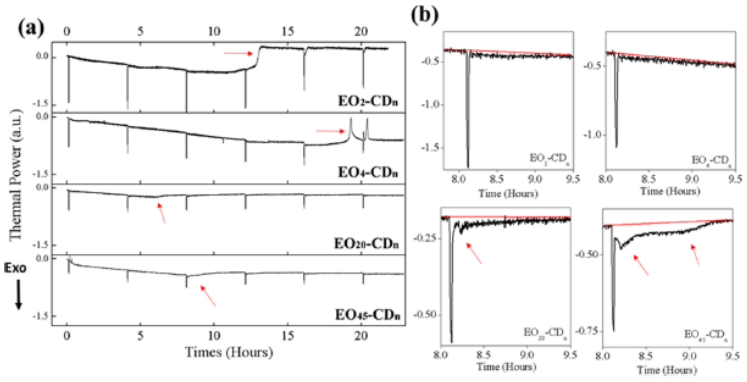

Figure 6. ITC curves with longer injection times (a); closeup in the injection peaks for different oligomers (b).

ITC curves associated with the formation of these inclusion complexes vary significantly with the molecular weight of the OEGMA used. In general, the peaks associated with this interaction (after discounting the heats of dilution of CD) are all exothermic, indicating a favorable enthalpic interaction involved in the inclusion of EO groups into the CD cavity. For the measurements with small OEGMA ($n = 2$), the interaction is fast, as confirmed by the quick return to the baseline. However, as the molecular weight of OEGMA increases (as discussed below), the process becomes slower and intervals between injections were increased from minutes to hours. This finding agrees with the visual observation of time scales for the appearance of precipitates resulting from IC discussed above. It is noteworthy that more sensitive ITC is capable of monitoring early processes involved in the incorporation of EO groups into CD, while visual observation is less sensitive and detects only macroscopic phase separation.

2.3.1. Fitting ITC Data for IC. The complexation of $OEGMA_{188}$ and α-CD presents the simplest ITC data, as shown in Figure 5a. Because the endothermic heat of dilution of cyclodextrin in water was subtracted, the resulting negative enthalpy values can be ascribed to be related to the formation of the EO_2-CD_1 complex.

The observed decrease in heat exchanged as titration advances is a consequence of the oligomer saturation, giving rise to a sigmoidal curve, as shown in Figure 5b. Using experimental heat of interaction (ΔH) and different binding models, the fitting of such a curve allows the determination of parameters such as association constants (K), stoichiometry of inclusion (N), entropy (ΔS), and Gibbs energy (ΔG) of EO_2-CD_1 formation. Equations 2−4 show these relations.

$$K = \frac{[\alpha - \text{CD}\cdot\text{OEGMA}]}{[\alpha - \text{CD}]\cdot[\text{OEGMA}]} \quad (2)$$

$$\Delta G = RT \ln K \quad (3)$$

$$\Delta G = \Delta H - T\Delta S \quad (4)$$

In the case of $OEGMA_{188}$, it was possible to fit the experimental ITC data using a model that assumes only one set of binding sites (the CD cavity), as shown in Figure 5c, producing a stoichiometry of CD/OEGMA for the complex close to 1:1.

However, as shown in Figure 5c, the profile of interaction enthalpy values as a function of CD/OEGMA mole ratio varies with the oligomer molecular weight. Not only this but also the shape of heat peaks becomes more complex with the increase of oligomer size (as can be observed in Figures S3 and S4). Clearly, the simple model that accounted for the formation of EO_2-CD_1 was not suitable to describe these more complex interaction processes, especially for the earlier indications, suggesting the absence of defined stoichiometry for this IC. These inclusion processes were therefore re-investigated by running ITC experiments with longer intervals between injections to account for the slow incorporation kinetics. Results for these experiments are shown in Figure 6a that

https://dx.doi.org/10.1021/acsomega.0c00741
ACS Omega 2020, 5, 9517−9528

contains different titration profiles according to the oligomer nature.

In the case of EO_2-CD_1 and EO_4-CD_n systems, heat peaks are narrow and no sign of secondary processes is observed. However, curves associated to these two samples show strong perturbations (abrupt changes in the baseline) around 10−20 h, which is probably related to the precipitation of solid particles. Moreover, Figure 6b shows in detail the aspect of the third injection peak (prior to any sign of precipitation) for different oligomers. These peaks clearly show that for EO_{20} and EO_{45}, secondary events occur following the oligomer inclusion, leading to broader peaks that are consistent with slow processes. This confirms the observations obtained with other techniques in the present study, suggesting a slow incorporation of oligomers with longer EO chains.

2.4. Small-Angle X-ray Scattering. Self-assembly of cyclodextrin complexes can lead to the formation of different structures. Simpler organizations such as channel tube and cage-like ones are well reported in the literature, but the formation of complex morphologies at the mesoscopic scale was recently described as a function of the different guest molecule headgroups.[38] Here, the study of the formed ICs by small-angle X-ray scattering (SAXS) reveals some interesting features of the obtained rod-like complex and its formation mechanism.

2.4.1. IC Suspensions. Figure 7 shows the SAXS curves of pristine α-CD and its complexes with oligomers of different

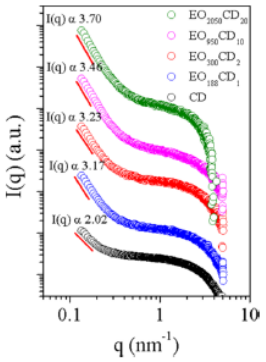

Figure 7. Scattering profiles of the obtained pseudo-rotaxanes in different compositions with the correspondent power law exponents for the low q-range.

molecular weights for EO-saturated compositions. These samples were prepared after complex isolation, that is, after drying and redispersion in water. Considering the α-CD sample, it presents an upturn in the low-q region, which suggests some level of aggregation.[39] All presented curves could be fitted to a power law, $I(q) \propto q^n$, behavior at low q values, as represented in Figure 7, with n values that increase from 2.02 for the pristine α-CD solution to 3.70 for the $EO_{45}CD_{20}$ sample. Assuming the formation of a fractal object, such an increase in Porod exponents indicates the modification of shape and size of the scattering objects. In fact, n increases from pristine α-CD to EO_{45}-CD_{20}, which indicates that large and loose aggregates are being formed, presenting low colloidal stability and tendency toward phase separation. Because of the size of these objects and the q range available during these experiments, further detailed information about such objects could not be obtained.

2.4.2. In Situ Complexation. The progressive formation of ICs and aggregates was followed for the longer complexes (*i.e.*, EO_{20}-CD_n and EO_{45}-CD_n) through *in situ* SAXS measurements. In this case, α-CD and OEGMA solutions were mixed shortly before injection into the sample holder, and scattering profiles were acquired during 1 h. As shown in Figure 8, the SAXS curves show distinct profiles for the two oligomers investigated and for the longest EO chain (EO_{45}), features that evolve during the acquisition time. For the IC of EO_{20}, the SAXS profiles remained, basically, unchanged during this period of time, suggesting that complexation was accomplished before the first minute after mixing (before data collection), although intensity modification with time is observed. The curves for IC with EO_{45}, however, display a broad peak centered at 0.5 nm^{-1}, whose intensity increases with time, along with the intensity of scattering at lower q values. Scattering data obtained for EO_{20}-CD_5 present a power law behavior with an exponent of 3.6 that remains almost constant with time, suggesting that the structure is already present in the first measurement (after 1 min of sample preparation). On the other hand, EO_{45}-CD_5 samples initially display a power law exponent of 2.2 (close to that present by pristine α-CD samples, Figure S5), which progressively increases to a value of 3.4 after 60 min. The appearance of a second peak at higher q values (around 3.5 nm^{-1}) is also observed in Figure 8c,d. This peak is promptly observed in the $EO_{20}CD_5$ sample, remaining constant during the measurements, but it is barely observed after 60 min in sample $EO_{45}CD_5$.

Based on the visualization of pseudopolyrotaxanes structures reported in the literature,[40] we attempted to fit these SAXS curves to a pearl-necklace model, producing the solid lines represented along the scattering data in Figure S6, with good agreement, as discussed in the next section. Concerning α-CD units present on PRs, the dimensions obtained by the fits are similar to those found in pristine α-CD suspensions (*i.e.*, 0.8 nm), fitted using the cylinder model, which also agree with CD dimensions.

3. DISCUSSION

Based on the obtained results, we propose that OEGMA complexation by α-CD follows the same general mechanism demonstrated for PEG molecules. It means that PR formation should takes place by the accommodation of stretched EO units into the macrocycle cavity. However, several particularities arise for OEGMA monomers, mostly because of the role of the methacrylate group as a stopper at one end of the oligomer chain. Further details on IC derived from the current experimental data are discussed below.

3.1. Mechanism of Inclusion Complex Formation. As illustrated in Figure 9a, the α-CD structure possesses an internal cavity that can be filled with different molecules. In aqueous solutions, simulations indicates that pristine α-CD units can include around 2−4 water molecules in their inner cavity.[41] The hydrogen bonds created between the α-CD structure and trapped water creates an environment where these molecules are kept in highly restricted orientations. Because of this confinement effect, such molecules present high energy and their release determines a final entropic gain, similar to that associated with the hydrophobic effect. It is proposed that this provides an initial complexation driving force for these systems.[41,42]

https://dx.doi.org/10.1021/acsomega.0c00741
ACS Omega 2020, 5, 9517−9528

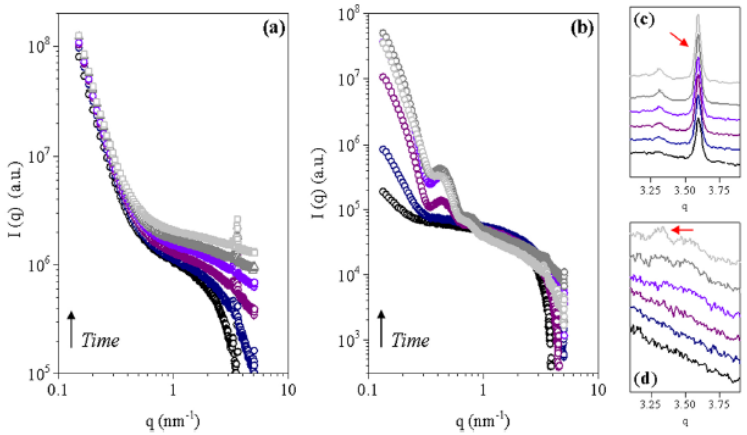

Figure 8. Time evolution of SAXS scattering profiles for (a) IC-C_5 and (b) IC-D_5 systems. Figures (c,d) contain a zoom at a higher q region (3−4 nm^{-1}) for same samples. Curves were recorded at times 1, 5, 10, 20, and 60 min after mixing.

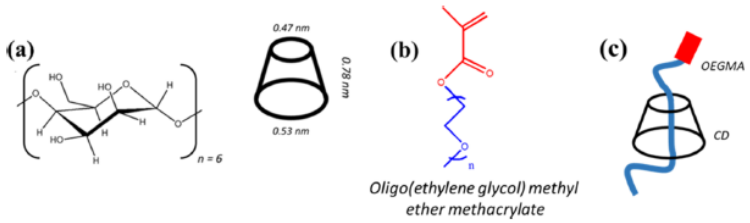

Figure 9. Structure of the α-CD monomer and molecular dimensions (a), structure of the OEGMA monomer (b), and inclusion complex representation of the OEGMA oligomer inside the α-CD cavity (c).

EO moieties that are present in OEGMA molecules (Figure 9b) possess an adequate size to be included into the α-CD cavity. Along with the formation of inclusion complexes (Figure 9c), the solution becomes turbid and complexes tend to precipitate as a crystalline white solid in the case of short oligomers. By modifying oligomer size, their ability to form solid precipitates, complexation yield, and initial clouding times are modified.

The ability of longer oligomers to form gels fits well with the description of Sabadini *et al*[43] about partially threaded PEG chains, which are able to form a supramolecular gel through the interaction of complex α-CDs. The presence of soluble structures consistent with pseudopolyrotaxanes and necklace structure formation is also suggested by these authors.

An important difference in the present study is the influence of the methacrylate end group over the incorporation into α-CD and the complexation mechanism. Most of the inclusion complexes are based on PEG-OH, which can be included *via* both edges of the polymeric chain. In addition, there are no rigid groups in the PEG structure in temperatures above 280 K, providing enough chain mobility to adopt different conformations during inclusion.[30,44] This seems fundamental during α-CD complexation, where PEG chains possess two times the length of relaxed ones because of the stretching effect imposed by cavity restrictions. Such flexibility seems unlikely to be found in methacrylate groups because of their sp^2 bonds. Furthermore, the methacrylate group is also larger than the EO groups and may act as a stopper in one of the extremities of the oligomer chain. We found no evidence to suggest that these bulkier end groups enter the α-CD cavity. In this case, IC should be formed by on-side inclusion into α-CD, as illustrated in Figure 2. Together with oligomer size, this behavior can alter the oligomer chain dynamics and influence inclusion efficiency. Some calculations reported by Serres-Gómes *et al*[25] suggest that one-side complexes can be even more thermodynamically favorable.

The role played by small nonlabile sp^2 molecules as stoppers for α-CD polyrotaxanes has not been reported in the literature, to the best of our knowledge. However, there are reports suggesting that methacrylate makes the threading of a PEG-*b*-PDMAEMA block copolymer into α-CD difficult.[45] In early 2000s, a series of papers described the synthesis of methacrylate-based polymers prepared through an IC methodology.[46−48] As a general rule, these publications are based on the preparation of IC between β-CD and methyl methacrylate monomers (usually resulting in a yellow solution[47]) which are polymerized by ATRP. Some of these studies suggest that methacrylate groups are included in the β-CD cavity and show the interactions between internal β-CD protons and $=CH_2$ from methacrylate through 2D-NMR (NOESY) measurements.[46,49] Such an interaction is not observed here because methacrylate groups are too rigid and bulky to fit inside the smaller α-CD cavity.

3.2. Complex Stoichiometry. As exhibited in Figure 3, complexes based on longer oligomers, where sequential inclusion of α-CD is allowed, present bimodal distribution of

https://dx.doi.org/10.1021/acsomega.0c00741
ACS Omega 2020, 5, 9517−9528

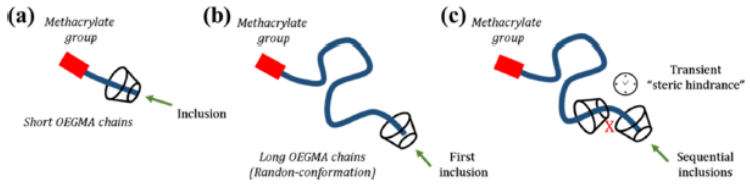

Figure 10. Representation of short (a) and long inclusion complexes (b) in comparison to sequential complexation displayed by longer EO oligomers (c).

T_2 values at average CD/OEGMA ratios. In these samples, both free and bonded species coexist and are associated with two values of T_2. At higher CD/OEGMA ratios, most of the EO groups are inside (or near to) the α-CD cavity and only IC T_2 is observed. Figure 3e also shows that long oligomers (M_w > 300 g·mol^{-1}) display T_2 values reaching a *plateau* after the inclusion of a certain number of α-CDs. This behavior indicates the saturation of the oligomer chains or, at least, that α-CD units are equally distributed along the OEGMA chain, restricting its relaxation. These saturation values are similar to those shown in Figures 1c and 2 for higher amounts of α-CD as determined by gravimetry, corroborating that saturation of oligomer chains occurs with a smaller number of α-CD units than expected (or that would be physically achievable). Similar observation was previously discussed by Joseph *et al*[31] for PEO grafted onto polystyrene particles, where only one extremity of the EO chains is free in solution and, hence, available for interaction. Altogether, these results corroborate the proposed role of the methacrylate group as a stopper, when present at one extremity of the oligomer chain.

During the present experiments, varied T_2 values were observed for oligomers with different molecular weights. An exponential growth (Figure 3d) of relaxation times with an increase in molecular weight suggests that the methacrylate group affects mostly closer EO units, causing short oligomers to present smaller T_2 values. With the increase of molecular weight, longer oligomers escape from this influence for being further apart. As a consequence, the methacrylate group becomes isolated at one chain extremity and cannot affect the majority of EO groups, as illustrated in Figure 2.

3.3. Inclusion Thermodynamics. Calorimetric measurements were performed in order to assess this inclusion thermodynamics. Results shown in Figure 5a,b reveal that data for the formation of the EO_2CD1 inclusion compound could be fitted using a simple binding model that assumes one type of sites. The obtained value of N (0.81) is similar to the one found by H^1-NMR (around 0.7), suggesting that such a model successfully describes the 1:1 (CD/OEGMA) IC ratio between the macrocycle and the simplest oligomer. Model data also reveal that IC is a spontaneous (ΔG < 0) and entropically driven process, associated with displacement of water solvation models from the CD cavity ($|\Delta H| < T|\Delta S|$).[50]

Data presented in Figure 5c show the modification of the measured heat profile according to oligomer molecular weight upon α-CD addition. Assuming full complexation for the first α-CD injections (first points in Figure 5c), average ΔH values for inclusion vary from −1.9 to −0.3 kJ·mol^{-1} as EO molecular weight increases from 188 to 2050 g·mol^{-1}. Such values are in the same range of values reported for other inclusion complexes described in the literature for similar molecules, as some alcohols, determined by calorimetric methods.[3] The observed enthalpy dependency on oligomer size can be a result of incomplete binding for longer EO chains.

The coexistence of different calorimetric events along the observed process can be associated with the changes observed in the shape of the peaks.[51] Here, along with a decrease in peak intensity, secondary events are observable (red arrows) for longer OEGMA chains (EO_{20}-CD_n and EO_{45}-CD_n, Figure 6b) after α-CD injection. These secondary peaks (indicated in Figure 6b) are broader than the main ones and appear in earlier injections for EO_{20}-CD_n in comparison to EO_{45}-CD_n samples. For shorter oligomers (EO_2-CD_1 and EO_4-CD_n), complete inclusion occurs in the first minutes after each injection. On the other hand, longer EO chains display longer inclusion times, sometimes over 1 h. The formation of new complexes per time is reduced for these longer samples, and no complete inclusion (consumption of all species to form PRs) is observed. This occurs because the threading of new α-CDs units depends on the sliding of previously threated ones along the molecular chain. A proposed mechanism is illustrated in Figure 10, agreeing with the previous description of the threading process put forward by Lo Nostro *et al*[52] and reinforcing the effect of oligomer molecular weight on the inclusion process.

In the described scenario, random coil conformations (typical of long segments in solution) make complexation difficult, decreasing the resulting exchanged heat at short periods. Further studies should be performed in order to corroborate or refuse such an effect.

3.4. Pearl-Necklace Structure. The structure of the obtained ICs was investigated by SAXS in order to understand the influence of oligomer size and number of CD units available to complex during complexation and on the final structure of the obtained complex. As observed in Figure 7, scattering profiles change progressively as a function of sample composition. Data analyses reveal a power law behavior associated with the formation of large structures. Samples' n index ($I(q)$ *vs* q^n) increases from pristine α-CD to EO_{45}-CD_{20}, which could indicate that these particles are progressively becoming more anisotropic. This explanation agrees with the model of longer PRs being formed as a function of OEGMA size at a time scale which possibly could not be determined because of the experimental conditions.

A pearl-necklace model was used to estimate the number of pearls per chain for both complexes after 60 min (Figure S6). According to this model, we have found that not only pearl-to-pearl distances are larger at EO_{45}-CD_5 (longer chain) but also that EO_{20}-CD_5 displays around 6 CD units per chain (at complete complexation), while EO_{45}-CD_5 contains only 3 CD units per OEGMA chain.

These results suggest that PRs based on EO_{20} are able to form, align, and self-assemble more rapidly than those based on the longer oligomer, corroborating the rapid aggregation

https://dx.doi.org/10.1021/acsomega.0c00741
ACS Omega 2020, 5, 9517−9528

and precipitation mechanisms revealed by ITC experiments and the slower kinetics of complexation of the longer oligomer. Moreover, the formation of larger structures (lower q values, around 0.5 nm^{-1}) is observed in the EO_{45}-CD_n complex (Figure 8b). Such an observation is probably related to the rapid formation of α-CD self-assembled structure, which potentially follows a cage-like to tubular structure described in earlier studies.[26,53,54] SAXS time evolution shown in Figure 8b also reveals that the 0.5 nm^{-1} peak reaches a maximum in intensity before decreasing. It suggests that equilibration of the samples can lead to scattering patterns similar to those observed in Figure 7 for all samples, after the appropriate time. It is also possible to observe that the time scale where this maximum is reached depends on the concentration of α-CD present in the suspension, as observed in Figure S7. As expected, the process is faster in samples containing higher CD/OEGMA ratios. The same behavior was reported by Serres-Gómez *et al.*[25]

Finally, the peak observed at higher q values (around 3.5 nm^{-1}) should be related to the oligomer threading (as suggested by XRD results, Figure 1b). Notably, it appears earlier and displays better definition for shorter oligomers than for longer ones (arrows in Figure 8c,d, respectively). As EO_{20}-CD_5 complexes show a well-defined peak in the first measurement (less than 1 min after sample preparation), the EO_{45}-CD_5 system only exhibits the same peak position 30 min after OEGMA-CD mixing. Such a difference in complexation times corroborates kinetic observation based on ITC results, where longer inclusion times are clearly observed for larger oligomers. This seems to be a consequence of the random coil formation of longer chains in solution, which hinders the prompt sequential inclusion of different α-CDs in the same oligomer chain.

4. CONCLUSIONS

Besides the large amount of data available about PEG/CDs inclusion complexes, this is the first study which investigates the complexation mechanisms between OEGMA chains and this macrocycle. Here, we demonstrate that IC formation and characteristics are highly dependent on the EO oligomer molecular weight and α-CD concentration. These parameters strongly influence complex appearance and formation kinetics, leading to solids or gel-like materials according to sample composition.

Larger amounts of α-CD accelerate complex formation and aggregation. Calorimetric experiments (ITC) corroborate the visual observations which suggest that longer complexation times are required for inclusion of high M_W oligomers and also reveal that complexation close to 1:1 (EO/CD) is attained only for the shortest EO chain. Structural analyses suggest that threading proceeds to the formation of pearl-necklace structures which vary with the oligomer EO chain, confirming their close relationship to PEG pseudopolyrotaxanes.

SAXS experiments indicate a modification in ordered α-CD structures, already present prior to oligomer inclusion, in the presence of longer *guest* molecules. This is probably related to the progressive accommodation of new α-CD units at long oligomer chains, taking place after certain time intervals.

Although these complexes present several similarities with traditional PEG-based structures, mostly because of EO characteristics, the influence of methacrylate groups leads to certain particularities. The obtained results suggest that the methacrylate group lies outside the α-CD cavity after complexation, acting as a stopper and favoring a one-side complexation mechanism. The availability of such a functional group can be interesting for some applications because it can be used to tune oligomer polymerization in the presence of inclusion complexes, allowing for LCST control and the creation of potentially thermoresponsive molecular machines.

5. MATERIALS AND METHODS

5.1. Materials. OEGMA (with nominal molecular weights of 188, 300, 950, and 2050 $g{\cdot}mol^{-1}$) and α-CD were purchased from Sigma-Aldrich. In this work, OEGMA oligomers were purified by passing them through a basic alumina oxide column to remove inhibitors and α-CD was used as received. All solutions were prepared with Milli-Q grade water (18.2 MΩ cm).

5.1.1. Inclusion Complex Preparation. In a typical procedure, two equal parts of aqueous solutions containing α-CD (50 ± 5 $mg{\cdot}mL^{-1}$) and the desired oligomer (variable concentration) are mixed together at ambient conditions (around 25 °C). After system stabilization, the precipitate was thoroughly washed with water in order to remove non-complexed molecules. Typical equilibration times for these samples depend on oligomer molecular weight. Short ones lead to complete solid precipitation in some minutes, while longer ones lead to the formation of a white suspension stable for several days. At least 24 h after washing, the supernatant is removed and the system is dried in an oven at 60 °C. Samples are weighted and kept in a desiccator. Finally, the dry mass of precipitates was used to determine gravimetric yield. Complex stoichiometry was estimated by assuming that only α-CD is lost during sample washing, resulting in a sample composed of the initial amount of oligomers and a measurable mass of CD.

Herein, the samples used are represented by the following nomenclature: EO_x-CD_n, where x represents the average number of EO units in the oligomer side chain and n represents the mole ratio of α-CD to OEGMA chain used for sample preparation. For example, sample EO_{45}-CD_1 contains 1 mol of α-CD to 1 mol of the OEGMA oligomer with an M_w of 2050 $g{\cdot}mol^{-1}$. All samples are listed in Table 1.

5.1.2. Optical Microscopy. The observation of solid particles was performed in a NIKON H550S microscope under environmental conditions. The particles were simply collected over a glass plate and directly observed.

5.1.3. X-ray Diffraction. The XRD patterns were recorded on a Shimadzu XRD 7000 X-ray diffractometer at 40 kV and 30 mA with Cu Kα radiation (λ = 0.154 nm) in the range of 2θ = 5−35° for samples using a fixed time mode at a scan speed of $2°{\cdot}min^{-1}$ in steps of 0.02°.

5.1.4. Isothermal Titration Calorimetry. Experiments were conducted in a MicroCal VP-ITC (Northampton, MA, USA) at 25 °C. Aliquots ranging from 10 to 40 μL (typically for short and long experiments, respectively) were added stepwise by an automatic injection syringe containing 270 μL of a concentrated α-CD (50 $mmol{\cdot}L^{-1}$) solution into the reaction cell of 1.43 mL, containing either water or OEGMA solutions (25 $mmol{\cdot}L^{-1}$). Injections were performed with intervals varying from 5 to 270 min, which were previously checked to ensure appropriate baselines. ITC data were treated with the associated Origin 7.0 software.

5.1.5. High-Field NMR. ^{1}H-NMR measurements were performed at 40 °C on a Bruker ADVANCE 500 spectrometer with a proton frequency of 499.87 MHz. Accumulations of 16 spectra were used with D_2O as the solvent. 2D NOESY

https://dx.doi.org/10.1021/acsomega.0c00741
ACS Omega 2020, 5, 9517−9528

measurements were performed at 40 °C on a Bruker ADVANCE 400 spectrometer with a proton frequency of 400.18 MHz, using the standard three-pulse sequence.[55] For all the samples, mixing times (T_m) of 200 ms and 1 s were used with 16 accumulations in order to allow better discrimination between intra- and intermolecular interactions.

5.1.6. Relaxation NMR (TD-NMR). Water holding was performed on a Bruker Minispec mq20 NMR analyzer (Bruker Company, USA) with a proton resonance frequency of 20 MHz. The samples prepared with D_2O (20 mg/mL) were placed in an 8 mm-diameter glass tube and inserted into the NMR probe, and a temperature of 39.8 ± 0.2 °C was stabilized for 15 min. The spin−spin relaxation time, T_2, was measured using the Carr−Purcell−Meiboom−Gill sequence, with 90 and 180 proton pulses of 8.4 and 16.7 μs, respectively, and an echo time of 160 μs. The data were recorded in triplicate, in which 30,000 echoes were acquired with 32 scan repetitions with intervals between subsequent scans. The fitting of the CPMG decay curves was performed using multi-exponentials.[33,56,57]

5.1.7. Small-Angle X-ray Scattering. SAXS measurements were taken at the SAXS1 beamline of the Brazilian Synchrotron Light Laboratory, LNLS, in Campinas, Brazil. The samples were positioned in a cell with two flat mica windows, and a thermal bath connected to the sample holder was used for temperature control (at 25.0 ± 0.5 °C). The X-ray wavelength was 1.608 Å, and the sample-to-detector distance was around 0.6 m, calibrated using silver behenate diffraction. The obtained charge-coupled device images were integrated and treated with Fit2D software[58] to obtain the scattering function $I(q)$, where $q = (4\pi/\lambda)\sin(\theta/2)$, with λ being the wavelength and θ being the scattering angle. In typical kinetic experiments, scattering profiles were obtained along 60 min. However, because of apparatus limitation, the first measurement (zero point) was obtained around 1 min after solution preparation and injection into the equipment. SASView software was used to fit experimental data to the "pearl-necklace model" for samples named EO_{20}-CD_5 and EO_{45}-CD_5 and the "cylinder model" for the sample named CD, which are described in detail in refs 59−63, respectively. Additionally, a power law model was used to fit the experimental data of sample EO_{45}-CD_5 at $q > 2$ nm^{-1}. To fit these curves, the scattering length density values were set to 9.4×10^{-6} Å^{-2} for water, 0.135×10^{-6} Å^{-2} for the pearls (cyclodextrin), and 7.8×10^{-6} Å^{-2} for the strings (OEGMA oligomers), calculated using SASView software. Extra information can be found in the SAXS section of the Supporting Information.

■ ASSOCIATED CONTENT

Supporting Information

The Supporting Information is available free of charge at https://pubs.acs.org/doi/10.1021/acsomega.0c00741.

Images and qualitative information about physical aspects of the described systems, NMR, extra calorimetric data, and SAXS curves (PDF)

■ AUTHOR INFORMATION

Corresponding Authors

Marcos Mariano − *Institute of Chemistry, University of Campinas (UNICAMP), 13083-970 Campinas, São Paulo, Brazil;* orcid.org/0000-0003-2374-5198; Email: marcos.mariano1@outlook.com

Watson Loh − *Institute of Chemistry, University of Campinas (UNICAMP), 13083-970 Campinas, São Paulo, Brazil;* orcid.org/0000-0002-8049-3321; Email: wloh@unicamp.br

Authors

Oigres Daniel Bernardinelli − *Institute of Chemistry, University of Campinas (UNICAMP), 13083-970 Campinas, São Paulo, Brazil*

Rafael Pires-Oliveira − *Institute of Chemistry, University of Campinas (UNICAMP), 13083-970 Campinas, São Paulo, Brazil;* orcid.org/0000-0003-1855-5322

Guilherme A. Ferreira − *Institute of Chemistry, University of Campinas (UNICAMP), 13083-970 Campinas, São Paulo, Brazil;* orcid.org/0000-0002-4932-3666

Complete contact information is available at: https://pubs.acs.org/10.1021/acsomega.0c00741

Notes

The authors declare no competing financial interest.

■ ACKNOWLEDGMENTS

M.M. and W.L. thank the Brazilian Agency CNPq for postdoctoral and research productivity grants. This project was also financed by FAPESP (2015-25406-5) and INCT-Catálise (CNPq). We gratefully acknowledge the Brazilian Synchrotron Light Laboratory, LNLS, for SAXS beamtime and for its staff support.

■ REFERENCES

(1) Harada, A. Cyclodextrin-Based Molecular Machines. *Acc. Chem. Res.* **2001**, *34*, 456−464.

(2) Zhu, K.; Baggi, G.; Loeb, S. J. Ring-Through-Ring Molecular Shuttling in a Saturated [3] Rotaxane. *Nat. Chem.* **2018**, *10*, 625−630.

(3) Rekharsky, M. V.; Inoue, Y. Complexation Thermodynamics of Cyclodextrins. *Chem. Rev.* **1998**, *98*, 1875−1918.

(4) Chen, L.; Chen, J.; Ren, J.; Zhao, M. Modifications of Soy Protein Isolates Using Combined Extrusion Pre-Treatment and Controlled Enzymatic Hydrolysis for Improved Emulsifying Properties. *Food Hydrocolloids* **2011**, *25*, 887−897.

(5) Li, J.; Loh, X. Cyclodextrin-Based Supramolecular Architectures: Syntheses, Structures, and Applications for Drug and Gene Delivery. *Adv. Drug Delivery Rev.* **2008**, *60*, 1000−1017.

(6) Harada, A.; Li, J.; Kamachi, M. Formation of Inclusion Complexes of Monodisperse Oligo(ethylene Glycol)s with α-Cyclodextrin. *Macromolecules* **1994**, *27*, 4538−4543.

(7) Harada, A.; Li, J.; Kamachi, M. Preparation and Properties of Inclusion Complexes of Poly(ethylene Glycol) with α-Cyclodextrin. *Macromolecules* **1993**, *26*, 5698−5703.

(8) Yuen, F.; Tam, K. C. Cyclodextrin-Assisted Assembly of Stimuli-Responsive Polymers in Aqueous Media. *Soft Matter* **2010**, *6*, 4613.

(9) De La Rosa, V. R.; Woisel, P.; Hoogenboom, R. Supramolecular Control over Thermoresponsive Polymers. *Mater. Today* **2016**, *19*, 44−55.

(10) Lutz, J.-F.; Hoth, A. Preparation of Ideal PEG Analogues with a Tunable Thermosensitivity by Controlled Radical Copolymerization of 2-(2-Methoxyethoxy)ethyl Methacrylate and Oligo(ethylene Glycol) Methacrylate. *Macromolecules* **2006**, *39*, 893−896.

(11) Lutz, J.-F. Thermo-Switchable Materials Prepared Using the OEGMA-Platform. *Adv. Mater.* **2011**, *23*, 2237−2243.

(12) Teixeira, F.; Popa, A. M.; Guimond, S.; Hegemann, D.; Rossi, R. M. Synthesis of Poly(oligo(ethylene Glycol)methacrylate)-Functionalized Membranes for Thermally Controlled Drug Delivery. *J. Appl. Polym. Sci.* **2013**, *129*, 636−643.

https://dx.doi.org/10.1021/acsomega.0c00741
ACS Omega 2020, 5, 9517−9528

(13) De France, K. J.; Chan, K. J. W.; Cranston, E. D.; Hoare, T. Enhanced Mechanical Properties in Cellulose Nanocrystal-Poly(oligoethylene Glycol Methacrylate) Injectable Nanocomposite Hydrogels through Control of Physical and Chemical Cross-Linking. *Biomacromolecules* **2016**, *17*, 649−660.
(14) Panganiban, B.; Qiao, B.; Jiang, T.; Delre, C.; Obadia, M. M.; Nguyen, T. D.; Smith, A. A. A.; Hall, A.; Sit, I.; Crosby, M. G.; et al. Random Heteropolymers Preserve Protein Function in Foreign Environments. *Science* **2018**, *359*, 1239−1243.
(15) Dalgakiran, E.; Tatlipinar, H. Atomistic Insights on the LCST Behavior of PMEO $_2$ MA in Water by Molecular Dynamics Simulations. *J. Polym. Sci., Part B: Polym. Phys.* **2018**, *56*, 429−441.
(16) Li, T.; Kumru, B.; Al Nakeeb, N.; Willersinn, J.; Schmidt, B. Thermoadaptive Supramolecular α-Cyclodextrin Crystallization-Based Hydrogels via Double Hydrophilic Block Copolymer Templating. *Polymers* **2018**, *10*, 576.
(17) Li, Y.; Guo, H.; Zheng, J.; Gan, J.; Wu, K.; Lu, M. Thermoresponsive and Self-Assembly Behaviors of Poly(oligo(ethylene Glycol) Methacrylate) Based Cyclodextrin Cored Star Polymer and Pseudo-Graft Polymer. *Colloids Surf., A* **2015**, *471*, 178−189.
(18) Takahashi, S.; Yamada, N. L.; Ito, K.; Yokoyama, H. Inclusion Complex of α-Cyclodextrin with Poly(ethylene Glycol) Brush. *Macromolecules* **2016**, *49*, 6947−6952.
(19) He, L.; Huang, J.; Chen, Y.; Liu, L. Inclusion Complexation between Comblike PEO Grafted Polymers and α-Cyclodextrin. *Macromolecules* **2005**, *38*, 3351−3355.
(20) Li, J.; Li, X.; Toh, K. C.; Ni, X.; Zhou, Z.; Leong, K. W. Inclusion Complexation and Formation of Polypseudorotaxanes between Poly[(ethylene Oxide)-Ran-(Propylene Oxide)] and Cyclodextrins. *Macromolecules* **2001**, *34*, 8829−8831.
(21) Zou, H.; Guo, W.; Yuan, W. Supramolecular Hydrogels from Inclusion Complexation of Alpha-Cyclodextrin with Densely Grafted Chains in Micelles for Controlled Drug and Protein Release. *J. Mater. Chem. B* **2013**, *1*, 6235−6244.
(22) Radhakrishnan, S.; Venkatachalapathy, P. D. Effect of Casting Solvent on the Crystallization in PEO/PMMA Blends. *Polym* **1996**, *37*, 3749−3752.
(23) Travelet, C.; Schlatter, G.; Hébraud, P.; Brochon, C.; Lapp, A.; Anokhin, D. V.; Ivanov, D. A.; Gaillard, C.; Hadziioannou, G. Multiblock Copolymer Behaviour of a-CD/PEO-Based Polyrotaxanes: Towards Nano-Cylinder Self-Organization of a-CDs. *Soft Matter* **2008**, *4*, 1855−1860.
(24) Sabadini, E.; Cosgrove, T. Inclusion Complex Formed between Star-Poly (Ethylene Glycol) and Cyclodextrins. *Langmuir* **2003**, *19*, 9680−9683.
(25) Serres-Gómez, M.; González-Gaitano, G.; Kaldybekov, D. B.; Mansfield, E. D. H.; Khutoryanskiy, V. V.; Isasi, J. R.; Dreiss, C. A. Supramolecular Hybrid Structures and Gels from Host−Guest Interactions between α-Cyclodextrin and PEGylated Organosilica Nanoparticles. *Langmuir* **2018**, *34*, 10591−10602.
(26) He, Y.; Fu, P.; Shen, X.; Gao, H. Cyclodextrin-Based Aggregates and Characterization by Microscopy. *Micron* **2008**, *39*, 495−516.
(27) Harada, A. Preparation and Structures of Supramolecules between Cyclodextrins and Polymers. *Coord. Chem. Rev.* **1996**, *148*, 115−133.
(28) Puig-Rigall, J.; Serra-Gómez, R.; Stead, I.; Grillo, I.; Dreiss, C. A.; González-Gaitano, G.; Serra-go, R.; Gonza, G. Pseudo-Polyrotaxanes of Cyclodextrins with Direct and Reverse X - Shaped Block Copolymers : A Kinetic and Structural Study. *Macromolecules* **2019**, *52*, 1458−1468.
(29) Schneider, H.-J.; Hacket, F.; Rüdiger, V.; Ikeda, H. NMR Studies of Cyclodextrins and Cyclodextrin Complexes. *Chem. Rev.* **1998**, *98*, 1755−1786.
(30) Girardeau, T. E.; Leisen, J.; Beckham, H. W. Chain Dynamics of Poly(oxyethylene) in Nanotubes of α-Cyclodextrin by Solid-State 2H-NMR. *Macromol. Chem. Phys.* **2005**, *206*, 998−1005.
(31) Joseph, J.; Dreiss, C. A.; Cosgrove, T.; Dreiss, A. Stretching a Polymer Brush by Making in Situ Cyclodextrin Inclusion Complexes. *Langmuir* **2008**, *24*, 10005−10010.
(32) Rubinstein, M.; Taylor, P. C. Nuclear Quadrupole Resonance in Amorphous and Crystalline As2S3. *Phys. Rev. B: Solid State* **1974**, *9*, 4258−4276.
(33) Carr, H. Y.; Purcell, E. M. Effects of Diffusion on Free Precession in Nuclear Magnetic Resonance Experiments. *Phys. Rev.* **1954**, *94*, 630.
(34) Clop, E. M.; Perillo, M. A.; Chattah, A. K. 1H and 2H NMR Spin-Lattice Relaxation Probing Water: PEG Molecular Dynamics in Solution. *J. Phys. Chem. B* **2012**, *116*, 11953−11958.
(35) Oguzlu, H.; Boluk, Y. Interactions between Cellulose Nanocrystals and Anionic and Neutral Polymers in Aqueous Solutions. *Cellulose* **2017**, *24*, 131−146.
(36) Volel, M.; Armand, M.; Gorecki, W.; Saboungi, M.-L. Threading Polymer into Nanotubes: Evidence of Poly(ethylene Oxide) Inclusion in Titanium Oxide. *Chem. Mater.* **2005**, *17*, 2028−2033.
(37) Loh, W.; Brinatti, C.; Tam, K. C. Use of Isothermal Titration Calorimetry to Study Surfactant Aggregation in Colloidal Systems. *Biochim. Biophys. Acta, Gen. Subj.* **2016**, *1860*, 999−1016.
(38) Yang, S.; Yan, Y.; Huang, J.; Petukhov, A. V.; Kroon-Batenburg, L. M. J.; Drechsler, M.; Zhou, C.; Tu, M.; Granick, S.; Jiang, L. Giant Capsids from Lattice Self-Assembly of Cyclodextrin Complexes. *Nat. Commun.* **2017**, *8*, 15856.
(39) Messner, M.; Kurkov, S. V.; Jansook, P.; Loftsson, T. Self-Assembled Cyclodextrin Aggregates and Nanoparticles. *Int. J. Pharm.* **2010**, *387*, 199−208.
(40) Jia, Y.-G.; Malveau, C.; Mezour, M. A.; Perepichka, D. F.; Zhu, X. X. A Molecular Necklace : Threading B -Cyclodextrins onto Polymers Derived from Bile Acids. *Angew. Chem.* **2016**, *128*, 12158−12162.
(41) Biedermann, F.; Nau, W. M.; Schneider, H.-J. The Hydrophobic Effect Revisited - Studies with Supramolecular Complexes Imply High-Energy Water as a Noncovalent Driving Force. *Angew. Chem., Int. Ed.* **2014**, *53*, 11158−11171.
(42) Nau, W. M.; Florea, M.; Assaf, K. I. Deep inside Cucurbiturils: Physical Properties and Volumes of Their Inner Cavity Determine the Hydrophobic Driving Force for Host-Guest Complexation. *Isr. J. Chem.* **2011**, *51*, 559−577.
(43) Sabadini, E.; do Carmo Egídio, F.; Cosgrove, T. More on Polypseudorotaxanes Formed between Poly(ethylene Glycol) and α-Cyclodextrin. *Langmuir* **2013**, *29*, 4664−4669.
(44) Taneda, H.; Shundo, A.; Matsuno, H.; Tanaka, K. Design of a Well-Defined Polyrotaxane Structure on a Glassy Polymer Surface. *Langmuir* **2018**, *34*, 709−714.
(45) Sui, K.; Shan, X.; Gao, S.; Xia, Y.; Zheng, Q.; Xie, D. Dual-Responsive Supramolecular Inclusion Complexes of Block Copolymer Poly(ethylene Glycol)-Block-Poly[(2-Dimethylamino)ethyl Methacrylate] Witha-Cyclodextrin. *J. Polym. Sci., Part A: Polym. Chem.* **2010**, *48*, 2143−2153.
(46) Jeromin, J.; Ritter, H. Cyclodextrins in Polymer Synthesis: Free Radical Polymerization of a N -Methacryloyl-11-Aminoundecanoic Acid/β-Cyclodextrin Pseudorotaxane in an Aqueous Medium. *Macromolecules* **1999**, *32*, 5236−5239.
(47) Glöckner, P.; Ritter, H. Cyclodextrins in Polymer Chemistry. Influence of Methylated β-Cyclodextrin as Host on the Free Radical Copolymerization Reactivity Ratios of Isobornyl Acrylate and Butyl Acrylate as Guest Monomers in Aqueous Medium. *Macromol. Rapid Commun.* **1999**, *20*, 602−605.
(48) Storsberg, J.; Ritter, H. Cyclodextrins in Polymer Synthesis: Free Radical Polymerization of Cyclodextrin Host-Guest Complexes of Methyl Methacrylate or Styrene from Homogenous Aqueous Solution. *Macromol. Rapid Commun.* **2000**, *21*, 236−241.
(49) Schmitz, S.; Ritter, H. Unusual Solubility Properties of Polymethacrylamides as a Result of Supramolecular Interactions with Cyclodextrin. *Angew. Chem., Int. Ed.* **2005**, *44*, 5658−5661.

https://dx.doi.org/10.1021/acsomega.0c00741
ACS Omega 2020, 5, 9517−9528

(50) Bouchemal, K.; Mazzaferro, S. How to Conduct and Interpret ITC Experiments Accurately for Cyclodextrin-Guest Interactions. *Drug Discovery Today* **2012**, *17*, 623−629.
(51) Löf, D.; Schillén, K.; Loh, W.; Olofsson, G. A Calorimetry and Light Scattering Study of the Formation and Shape Transition of Mixed Micelles of EO20PO68EO20 Triblock Copolymer (P123) and Nonionic Surfactant (C12EO6). *J. Phys. Chem. B* **2007**, *111*, 5911−5920.
(52) Nostro, P. L.; Giustini, L.; Fratini, E.; Ninham, B. W.; Ridi, F.; Baglioni, P. Threading, Growth, and Aggregation of Pseudopolyrotaxanes. *J. Phys. Chem. B* **2008**, *112*, 1071−1081.
(53) Saenger, W.; Jacob, J.; Gessler, K.; Steiner, T.; Hoffmann, D.; Sanbe, H.; Koizumi, K.; Smith, S. M.; Takaha, T. Structures of the Common Cyclodextrins and Their Larger Analogues - beyond the Doughnut. *Chem. Rev.* **1998**, *98*, 1787−1802.
(54) Travelet, C.; Hébraud, P.; Perry, C.; Brochon, C.; Hadziioannou, G.; Lapp, A.; Schlatter, G. Temperature-Dependent Structure of a-CD/PEO-Based Polyrotaxanes in Concentrated Solution in DMSO: Kinetics and Multiblock Copolymer Behavior. *Macromolecules* **2010**, *43*, 1915−1921.
(55) Wider, G.; Macura, S.; Kumar, A.; Ernst, R. R.; Wüthrich, K. Homonuclear Two-Dimensional ' H NMR of Proteins. Experimental Procedures. *J. Magn. Reson.* **1984**, *56*, 207−234.
(56) Bernardinelli, O. D.; Novotny, E. E.; Azevêdo, E. R.; Colnago, L. A. Analyses of Biomass Products by Nuclear Magnetic Resonance Spectroscopy. In *Analytical Techniques and Methods for Biomass*; Springer: Cham, 2016; pp 143−172.
(57) Vidal, V. A. S.; Bernardinelli, O. D.; Paglarini, C. S.; Sabadini, E.; Pollonio, M. A. R. Understanding the Effect of Different Chloride Salts on the Water Behavior in the Salted Meat Matrix along 180 Days of Shelf Life. *Food Res. Int.* **2019**, *125*, 108634.
(58) Hammersley, A. FIT2D: An Introduction and Overview. *European Synchrotron Radiation Facility Internal Report*, 1997.
(59) Schweins, R.; Huber, K. Particle Scattering Factor of Pearl Necklace Chains. *Macromol. Symp.* **2004**, *211*, 25−42.
(60) SASView. Pearl Necklace Model. http://www.sasview.org/docs/user/models/pearl_necklace.html (accessed Jan, 2020).
(61) Feigin, L. A.; Svergun, D. I. *Structure Analysis by Small-Angle X-Ray and Neutron Scattering*; Plenum Press: New York, 1987.
(62) SASView. Cylinder Model. http://www.sasview.org/docs/user/models/cylinder.html (accessed Jan, 2020).
(63) Pedersen, J. S. Analysis of Small-Angle Scattering Data from Colloids and Polymer Solutions : Modeling and Least-Squares Fitting. *Adv. Colloid Interface Sci.* **1997**, *70*, 171−210.

https://dx.doi.org/10.1021/acsomega.0c00741
ACS Omega 2020, 5, 9517−9528

9.3. Termos de permissão de uso das referências

Order Summary

Licensee: Mr. Rafael Pires-Oliveira
Order Date: May 23, 2021
Order Number: 5074630038801
Publication: Materials Today
Title: Nanocellulose: a new ageless bionanomaterial
Type of Use: reuse in a thesis/dissertation
Order Total: 0.00 USD

Order Summary

Licensee: Mr. Rafael Pires-Oliveira
Order Date: May 23, 2021
Order Number: 5074631168452
Publication: Materials Today
Title: Controlled/living radical polymerization
Type of Use: reuse in a thesis/dissertation
Order Total: 0.00 USD

Order Summary

Licensee: Mr. Rafael Pires-Oliveira
Order Date: May 23, 2021
Order Number: 5074631464642
Publication: Nature Reviews Materials
Title: Production routes to tailor the performance of cellulose nanocrystals
Type of Use: Thesis/Dissertation
Order Total: 0.00 USD

Royal Society of Chemistry - License Terms and Conditions

This is a License Agreement between Rafael Pires-Oliveira ("You") and Royal Society of Chemistry ("Publisher") provided by Copyright Clearance Center ("CCC"). The license consists of your order details, the terms and conditions provided by Royal Society of Chemistry, and the CCC terms and conditions.

All payments must be made in full to CCC.

Order Date	24-May-2021	**Type of Use**	Republish in a thesis/dissertation
Order license ID	1121090-1		
ISSN	1364-548X	**Publisher**	ROYAL SOCIETY OF CHEMISTRY
		Portion	Chart/graph/table/figure

LICENSED CONTENT

Publication Title	Chemical communications	**Country**	United Kingdom of Great Britain and Northern Ireland
Author/Editor	Royal Society of Chemistry (Great Britain)	**Rightsholder**	Royal Society of Chemistry
Date	01/01/1996	**Publication Type**	e-Journal
Language	English		

NEW WORK DETAILS

Title	Poli[(etileno glicol) metil éter metacrilato] (POEGMA): comportamento térmico em solução aquosa e formação de hidrogéis com celulose nanocristalina (CNC)	**Institution name**	UNICAMP
		Expected presentation date	2021-06-20
Instructor name	UNICAMP		

ADDITIONAL DETAILS

Order reference number	N/A	**The requesting person / organization to appear on the license**	Rafael Pires-Oliveira

REUSE CONTENT DETAILS

Title, description or numeric reference of the portion(s)	Fig 1	**Title of the article/chapter the portion is from**	Supramolecular self-healing materials from non-covalent cross-linking host–guest interactions
Editor of portion(s)	NA	**Author of portion(s)**	Royal Society of Chemistry (Great Britain)
Volume of serial or monograph	NA	**Issue, if republishing an article from a serial**	N/A
Page or page range of portion	NA	**Publication date of portion**	1996-01-01

PUBLISHER SPECIAL TERMS AND CONDITIONS

Permission is granted as long as the figure is fully acknowledged and a link is given back to the article on our Platform. Please go to rsc.li/permissions for details. Please note that if the material specified above or any part of it appears with credit or acknowledgement to a third party then you must also secure permission from that third party before reproducing that material.